To the Graduate Council:

I am submitting herewith a dissertation written by Russell David Bingham entitled "A Quasi-Cusp Digital Filter for Gamma-Ray Spectroscopy." I have examined the final copy of this dissertation for form and content and recommend that it be accepted in partial fulfillment of the requirements for the degree of Doctor of Philosophy, with a major in Electrical Engineering.

T. V. Blalock

T. V. Blalock, Major Professor

We have read this dissertation
and recommend its acceptance:

James Rochelle

Robert E Bodenheimer

David B Koch

Lee L. Riedinger

Accepted for the Council:

C W Minkel

Associate Vice Chancellor and
Dean of The Graduate School

A QUASI-CUSP DIGITAL FILTER FOR GAMMA-RAY SPECTROSCOPY

A Dissertation
Presented for the
Doctor of Philosophy
Degree
The University of Tennessee, Knoxville

Russell David Bingham
December 1996

Acknowledgments

I would like to thank a number of people who have made this work possible. At the University of Tennessee, I am grateful to my Dissertation Committee, T.V. Blalock, Bob Bodenhiemer, Dan Koch, Jim Rochelle, and Lee Riedinger. I have benefitted greatly from their instruction and advice over the years.

There are a number of people at EG&G ORTEC whose assistance should be recognized. I am grateful to Rex Trammell who put me in charge of this project and provided aide and encouragement along the way. I am grateful to Doyle Cole for designing the Digital Controller Board. I am grateful to Jesse Ursery who authored the control program for the Digital Controller and provided hours of stimulating discussion on how the spectrometer should operate. I am thankful for advice and encouragement from Tom Becker, Jeff Peck, Dale Gedcke, Marshall Spencer and T.J. Paulus. I am especially grateful to Linh Le who helped assemble and test the prototypes.

Finally, I am thankful for my wife, Stephanie, whose encouragement and persistence kept this work moving when I was ready to quit.

Abstract

In this research project, a quasi-cusp digital filter for use with high-purity germanium detectors was developed to provide optimal resolution at long and short pulse width settings while eliminating errors due to ballistic deficit. The implementation allows the filter to operate in real-time with 32 programmable pulse width settings and throughput rates as high as 70,000 counts per second. A cusp factor adjustment allows the pulse shape to be optimized to match the characteristics of the particular detector which is connected to the spectrometer. Furthermore, a digital gated baseline restorer is included in the filter to eliminate peak shifts due to changing DC levels in the detector and the electronics. A digital peak detecting circuit which uses a pattern matching algorithm applied to the slope of the filtered pulse selects the peak of the digital pulses to histogram.

Table of Contents

List of Figures

Chapter I

Introduction

When an unstable nucleus disintegrates, radiation is emitted from the nucleus in several forms including alpha particles, beta particles, neutrons, x-rays and gamma-rays. A gamma-ray spectrometer is an instrument that measures the energy of the gamma-rays emitted from the nucleus. Usually the spectrometer forms a histogram which indicates the frequency of a gamma-ray at a particular energy level as a function of gamma-ray energy. These histograms are analyzed to determine not only which radio-nuclides are present in a sample, but the amount of the nuclide in a sample. Gamma-ray spectrometers have a number of practical applications, ranging from determination of the quantity and type of radioactive contamination in foodstuffs, to monitoring shipments of plutonium products for nuclear arms treaty verification, to analysis of the electromagnetic radiation emitted by bombarded atoms in nuclear physics experiments.

The detector determines the dynamic range, efficiency and resolution of the spectrometer. High-purity germanium detectors offer very high resolution and a wide dynamic range. Figure 1 is a histogram which resulted when beach sand was placed near the detector of a gamma-ray spectrometer with a germanium detector. As shown in the figure, the spectrometer can cover a very wide energy range (6 keV to 3 MeV), and the peaks are very narrow indicating that the resolution is very fine. The low energy peaks are less then 1 keV wide at half of the maximum peak amplitude.

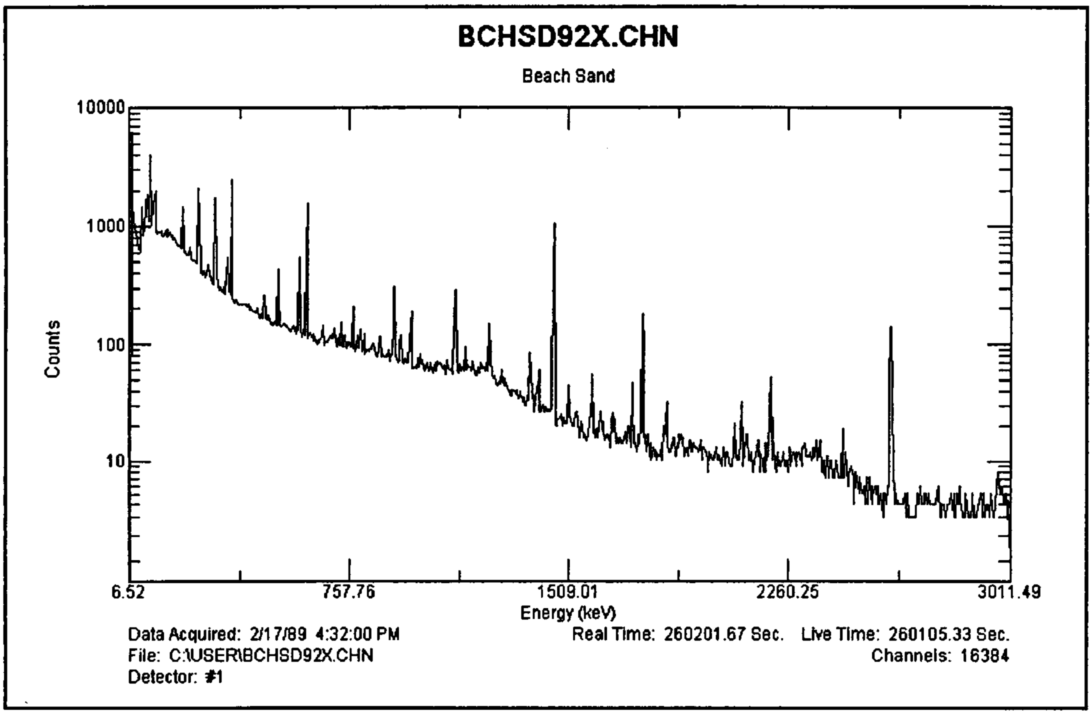

Figure 1. Sample Spectrum of Beach Sand.

This chapter begins with a description of the classical analog germanium gamma-ray spectrometer. It continues with a description of the weighting function method of noise analysis, a description of pile-up losses and concludes with a literature survey of the application of digital techniques to analyze germanium detector signals.

Classical Spectrometer

In a high-purity germanium (HPGe) detector, an electric field is created inside a germanium diode by applying a reverse bias. When incident radiation strikes the diode, electron-hole pairs are created in the depletion region of the diode. The electric field in the depletion region forces the electrons and holes to be collected at the electrodes of the diode. A charge-sensitive preamplifier integrates the charge arriving at the electrodes creating a voltage step with an amplitude proportional to the energy of the incident radiation. This signal is amplified, and then filtered to improve the signal-to-noise ratio. The output of the filter is typically analyzed with a pulse height sensing analog-to-digital converter which creates a pulse height distribution spectrum. Figure 2 shows the block diagram of such a system.

Detector

A high-purity germanium detector is a large single crystal of germanium with impurity concentrations as low as 10^{10} atoms/cm^3. Most modern detectors are of the coaxial variety shown in Figure 3. If the detector is p-type (acceptor impurities dominate), a lithium contact is formed on the outer surface. This creates an n^+-p junction at the outer surface of the crystal. An boron contact is implanted on the inner surface to connect to the preamplifier. If the detector is n-type (donor impurities dominate), the two contacts are reversed creating a p^+-n junction. Because

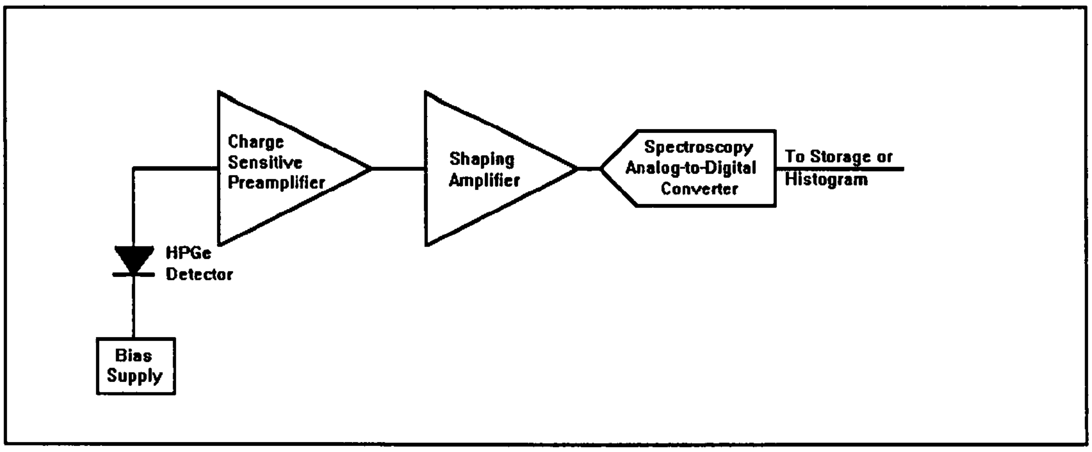

Figure 2. HPGe Detector System Block Diagram.

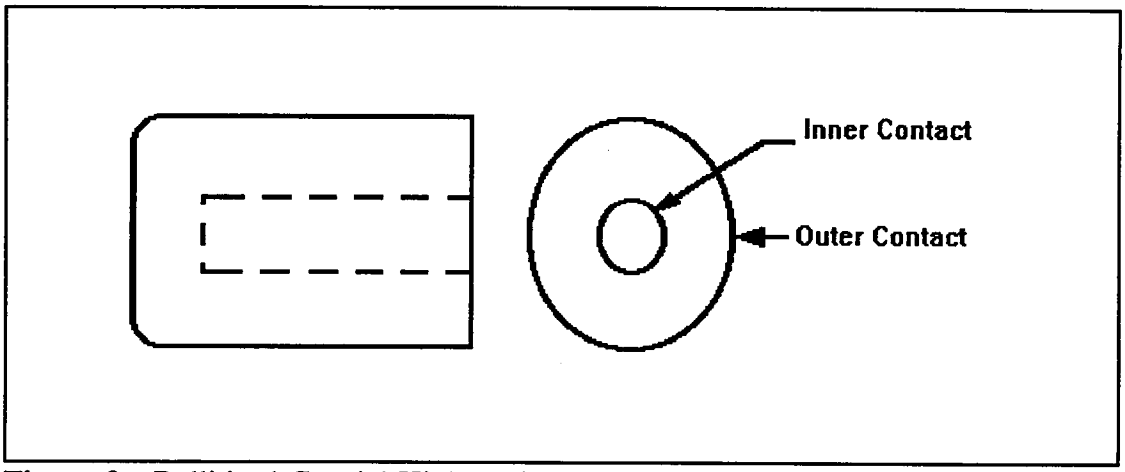

Figure 3. Bullitized Coaxial High-Purity Germanium Detector

the boron implant can be made very thin, the n-type detector can detect lower energy gamma-rays, since the gamma-ray is able to penetrate the contact. A positive bias is placed on the n^+ contact of the p-type detector to fully deplete the crystal, and a negative bias is placed on the p^+ contact to deplete the n-type detector. The bias is usually set above the value required to just deplete the detector in order to increase the electric field. Since germanium has a bandgap of only 0.7 eV, a large number of thermally induced carriers are present in the crystal at room temperature. These carriers create a large leakage current which adds excessive noise. For this reason, HPGe detectors are cooled to 77 K with liquid nitrogen.

Preamplifier

Two types of preamplifiers are typically used with HPGe detectors, resistive feedback preamplifiers (RFP) and transistor reset preamplifiers (TRP). As Figure 4 indicates, the typical RFP consists of two stages. The first stage is connected to the

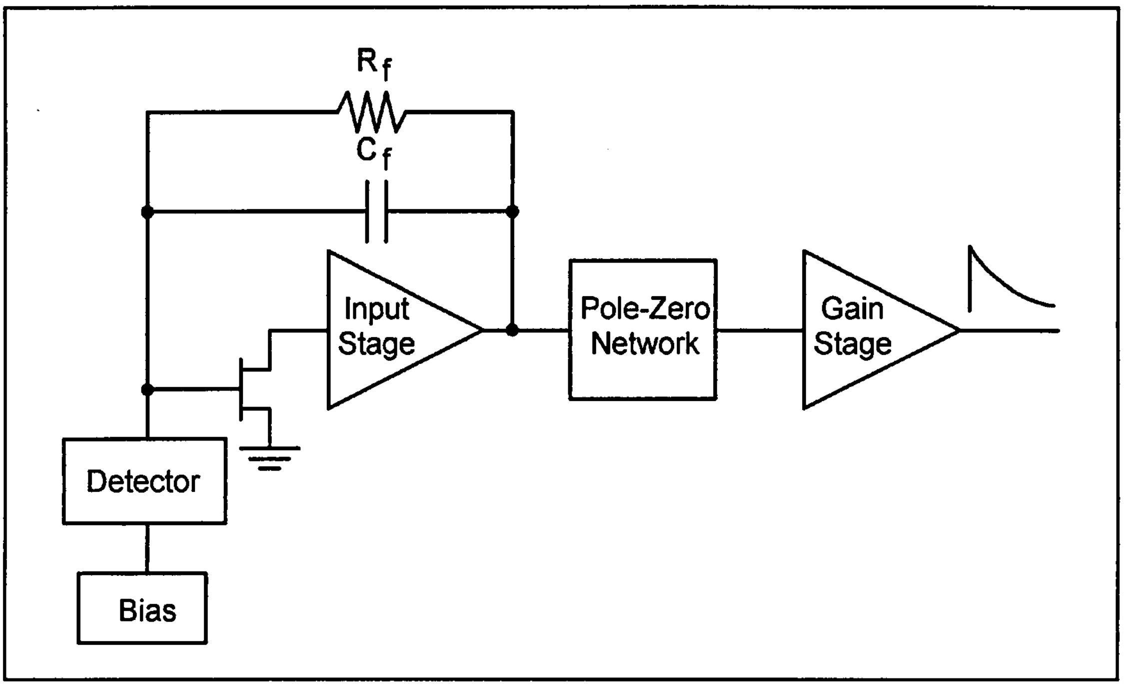

Figure 4. Resistor Feedback Preamplifier Block diagram

detector with a low-noise field-effect transistor (FET). A feedback capacitor (C_f) integrates the charge collected from the detector generating a voltage step at the output of the first stage. Resistor R_f discharges the capacitor to return the output of the first stage to its original DC level. In order to get optimum noise performance from the detector, the feedback capacitor must be kept quite small (<1 pf) and the resistor quite large ($\sim 2{,}000$ M ohms). As a result, the time constant of the output exponential is quite long (1-2 mS). The second stage consists of a pole-zero network and a gain stage. The pole-zero network reduces the time constant of the exponential to approximately 50 μs, by applying a filter with the following transfer function:

$$H(s)=\frac{s+\frac{1}{R_f C_f}}{s+\frac{1}{\tau_{new}}} \tag{1}$$

where τ_{new} is the desired output time constant. Since the Laplace Transform of the exponential pulse from the first stage of the preamplifier is

$$X(s)=\frac{1}{s+\frac{1}{R_f C_f}} \tag{2}$$

the output of the filter is

$$Y(s)=X(s)H(s)=\frac{1}{s+\frac{1}{\tau_{new}}} \tag{3}$$

Taking the inverse Laplace Transforms results in an exponential pulse with a time constant equal to τ_{new}. This shorter time constant allows a larger gain without requiring a large dynamic range form the preamplifier output.

At high input signal rates, the RFP is overloaded and no pulses come out of the preamplifier. Landis et al.[1] invented the TRP to overcome this disadvantage. The TRP shown in Figure 5 does not have a feedback resistor. As a result, each pulse causes the output of the preamplifier to step up and stay at the new output level. Once the output reaches a predefined level, the reset circuit turns on the reset

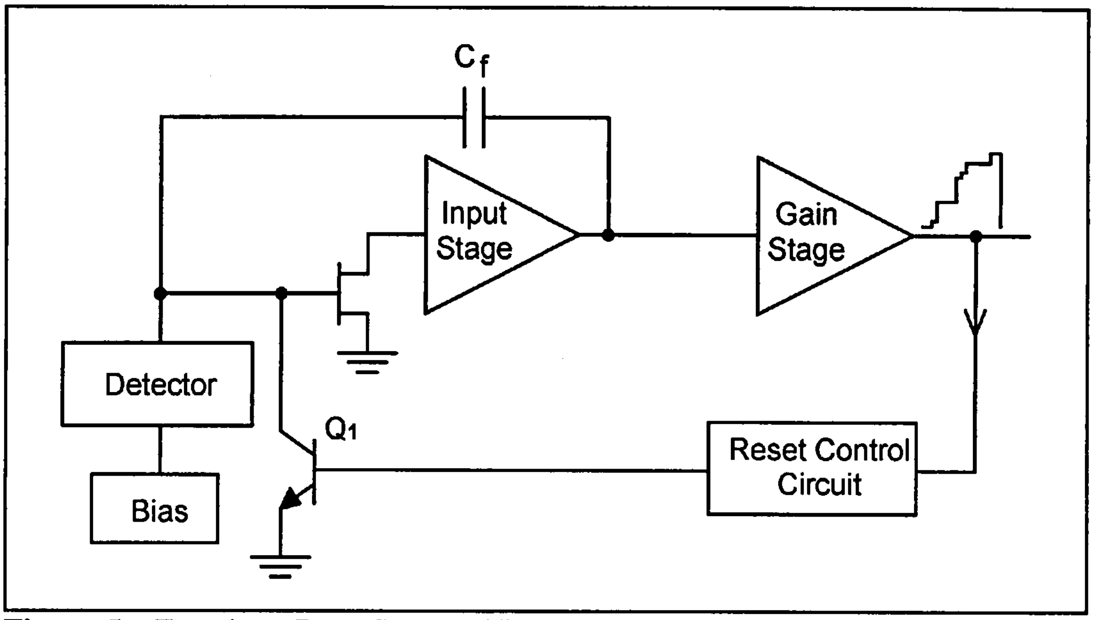

Figure 5. Transistor Reset Preamplifier Block Diagram

transistor (Q1) to discharge the capacitor and return the preamplifier output to its original level. Since each arriving pulse is superimposed on a random DC level, transistor reset preamplifiers must cover a very wide dynamic range and have outstanding differential linearity to achieve optimum performance.

Shaping Amplifier

A typical shaping amplifier is shown in block diagram form in Figure 6. First, the signal passes through a pole-zero network to further reduce the input time constant before amplification. If a TRP is used, the pole-zero network is only a differentiator. This converts the step input from the TRP into an exponential. After the pole-zero network, the signal is further amplified in the gain stage. A DC restorer circuit[2] is usually placed around the gain stage to control the DC level.

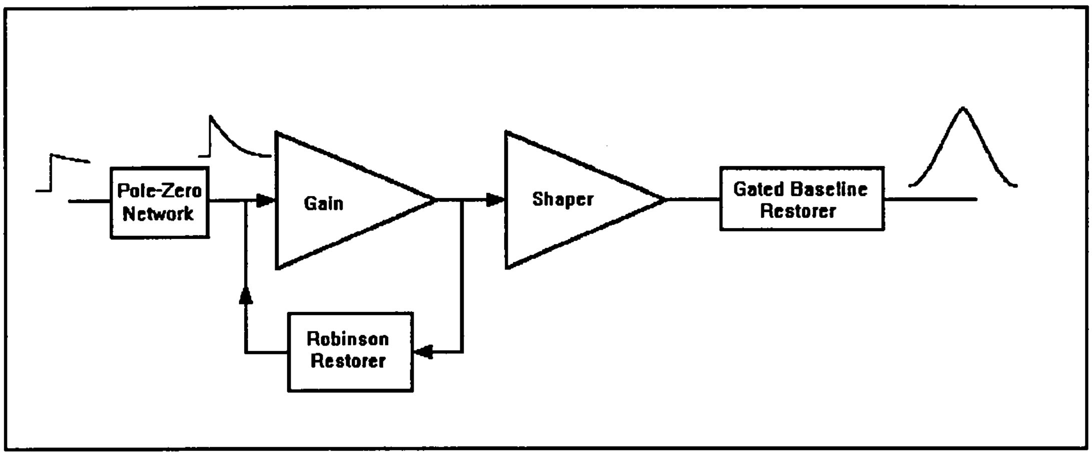

Figure 6. Typical Spectroscopy Amplifier Block Diagram.

The signal is then passed through the shaper. In modern spectroscopy amplifiers, the shaper is a 7-pole Gaussian or triangular shaper. After shaping, the signal passes through a gated baseline restorer (BLR) to remove any low frequency noise from the signal[3][4]. A BLR is an adaptive filter which is a differentiator with a relatively long time constant when no pulses are present and a simple buffer when pulses are present. This removes low frequency components from the output signal without affecting the shape of the output pulse. The shaper network used in the amplifier determines most of the resolution and count rate characteristics of the system.

Spectroscopy Analog-to-Digital Converter

A typical spectroscopy analog-to-digital converter (ADC) is shown in Figure 7. The ADC input passes through a peak detecting and stretching circuit. This circuit captures the maximum amplitude of a pulse and holds it for the analog-to-digital converter to translate into a digital value. Since HPGe detectors have very low noise,

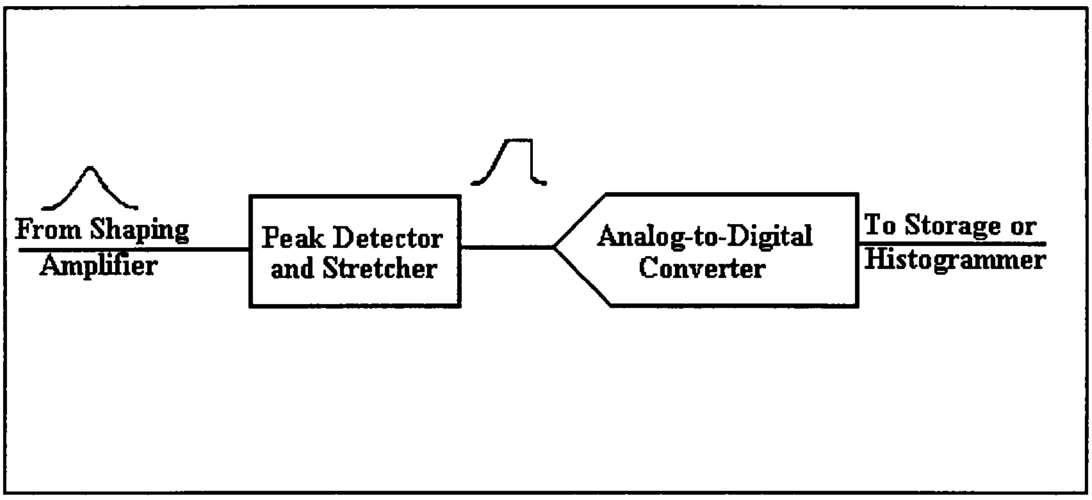

Figure 7. Spectroscopy ADC Block Diagram.

the ADC must have very high resolution (14 bits). The ADC must also be relatively fast (<10 μs) and have excellent differential linearity ($<1\%$). A Gatti Slider[5] is implemented on most ADCs to achieve this differential linearity specification. The digital value from the ADC is available for storage or histogramming.

Resolution

The width of a peak in a HPGe spectrum is usually referred to as the resolution of a peak. Resolution is usually reported as the width at half of the maximum amplitude (FWHM) in units of electron volts (eV) of a Gaussian probability density function which has been fit to the peak after any background has been removed from the peak. Background removal usually entails fitting a straight line between the data at the left and right edge of a peak and subtracting that line from the peak before fitting a Gaussian probability density function to it. The goal of any spectrometer is to generate spectra with the smallest possible resolution for a given input pulse rate. The resolution of a peak of a particular energy level is largely determined by the intrinsic detector resolution, the effect of the electronic noise in the processing electronics, and the effect of ballistic deficit. Each of these effects will be examined in detail in the following sections.

Intrinsic Detector Resolution

When a gamma-ray strikes an HPGe detector, not all of the energy in the gamma-ray is used to create electron/hole pairs which can be collected by the preamplifier. Part of the energy is randomly lost to lattice vibration. The resulting resolution due to this phenomena has been found to be[8]

$$R_{fwhm}=2.35\sqrt{F\cdot E\cdot\epsilon} \tag{4}$$

where R_{fwhm} is the intrinsic detector resolution, E is the energy of the gamma-ray, ϵ is the average energy required to produce a hole/electron pair (2.96 eV for germanium at 77 K) and F is the Fano factor which is usually 0.12. As an example, the intrinsic detector resolution of a peak at 1.3 MeV is 1.6 keV. A well designed spectrometer with a good HPGe detector can usually achieve 1.7 keV. On the other hand, a 5.9 keV peak has an intrinsic detector resolution of 110 eV. A large HPGe detector has a resolution of 600 eV at 5.9 keV while a smaller detector might achieve 130 eV. So depending on the energy of the peak and the size of the detector, the intrinsic detector resolution may or may not dominate the resolution of a peak. The intrinsic detector resolution adds in quadrature with all other noise sources in the spectrometer.

Noise Performance

To analyze the noise performance of an HPGe system, all of the white noise sources in the system are modeled as two noise sources at the input of the preamplifier. One noise source is a voltage source in series with the input of the preamplifier, and the other is a current noise source in parallel with the detector. Figure 8 shows the front-end of such a system with the noise sources included. Both of the noise sources are white, so in the time domain the output of the noise sources consists of small impulses of voltage or current respectively. When an impulse of current is generated by the parallel noise source, the current is integrated by the feedback capacitor in the charge sensitive preamplifier to create a voltage step at the output of the preamplifier. For this reason, the noise due to the parallel generator is often referred to as step noise. On the other hand, noise impulses generated by the series generator are not integrated by the capacitor, so they emerge from the preamplifier as voltage impulses. The noise created by the series noise generator is often called delta noise. Step noise is mainly due to leakage currents in the detector

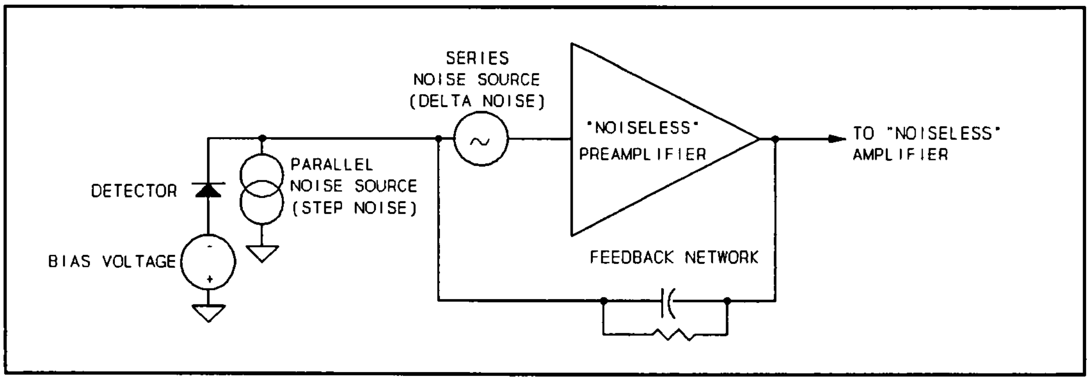

Figure 8. Front-end Electronics with Noise Sources

and the input stage of the preamplifier, while delta noise is due to noise sources in the preamplifier, amplifier and filter.

When analyzing filters for this application, time domain noise analysis is preferred over frequency domain noise analysis because it gives a better indication of the trade-off between performance at high counting rates and signal-to-noise ratio[8]. Time domain noise methods use the residual weighting function of the filter to determine the mean square effect of old noise pulses on a measurement.

For example, assume a time-invariant filter has an output pulse as shown in Figure 9 in response to a step input. If a noise step occurs at the filter input 1s before a measurement is made, the noise pulse would still have a magnitude of 0.5 at the output at the time of the measurement. Likewise if a noise step occurs 0.2s before a measurement is made, the noise step would have a magnitude of 0.1 at the

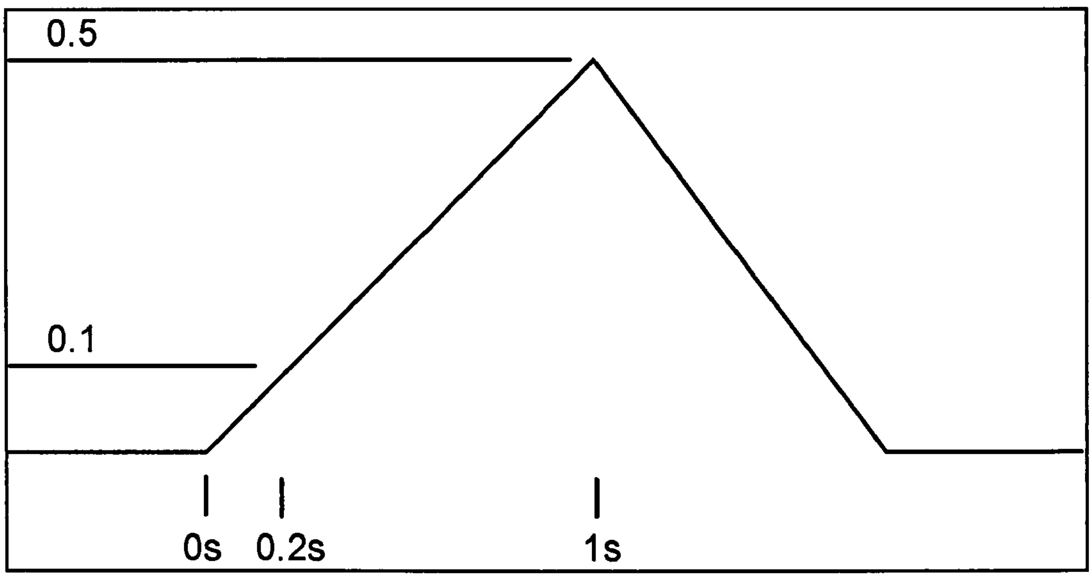

Figure 9. Example Pulse for Noise Index Calculation.

time of the measurement. In order to find the effect of all noise steps which occur before a measurement is made, the residual effect of all of the noise pulses must be summed in quadrature, since white noise is random. This leads to a step noise index which is defined as

$$<N_s^2> = \frac{1}{A^2}\int_0^{\infty}[W(t)]^2 dt \qquad (5)$$

where A is the amplitude of the output pulse in response to a unit impulse of charge at the preamplifier input, and *W(t)* is the weighting function of the filter. For time-invariant filters, the weighting function is simply the time-reversed shape of the output pulse, when an impulse of charge is applied to the input of the preamplifier.

Since delta noise is the mathematical equivalent of the derivative of step noise, the delta noise index is the same as the step noise index with the weighting function replaced by its derivative.

$$<N_\Delta^2> = \frac{1}{A^2}\int_0^{\infty}[W'(t)]^2 dt \qquad (6)$$

These two indices show the relative influence of the step and delta noise for a given filter.

The weighting function which results in the best signal-to-noise ratio is the cusp[6]. The cusp weighting function is

$$W_c(t) = e^{\frac{-|t|}{\tau_c}} \tag{7}$$

where τ_c is the noise corner time constant at the output of the preamplifier. An ideal noise power spectral density graph at the output of a preamplifier is shown in Figure 10. The noise corner time constant is defined as the time constant at which the noise power due to the step noise is equal to the noise power due to the delta noise. By substituting Equation (7) into Equations (5) and (6), the noise indices for the cusp are

$$<N_s^2> = \tau_c \tag{8}$$

and

$$<N_\Delta^2> = \frac{1}{\tau_c} \tag{9}$$

Ballistic Deficit

The optimum signal-to-noise ratio is obtained with the cusp. However the cusp would not give optimum resolution due to ballistic deficit effects. Ballistic deficit occurs because a finite amount of time (usually 400ns or less) is required to collect all of the charge created by an event in the detector due to finite charge mobility. This slow collection time causes the pulse to not reach the final amplitude that it would have attained if all of the charge arrived simultaneously. This only causes a problem because the collection time varies from pulse to pulse, so the amplitude of the pulse changes depending on where in the detector an event occurs.

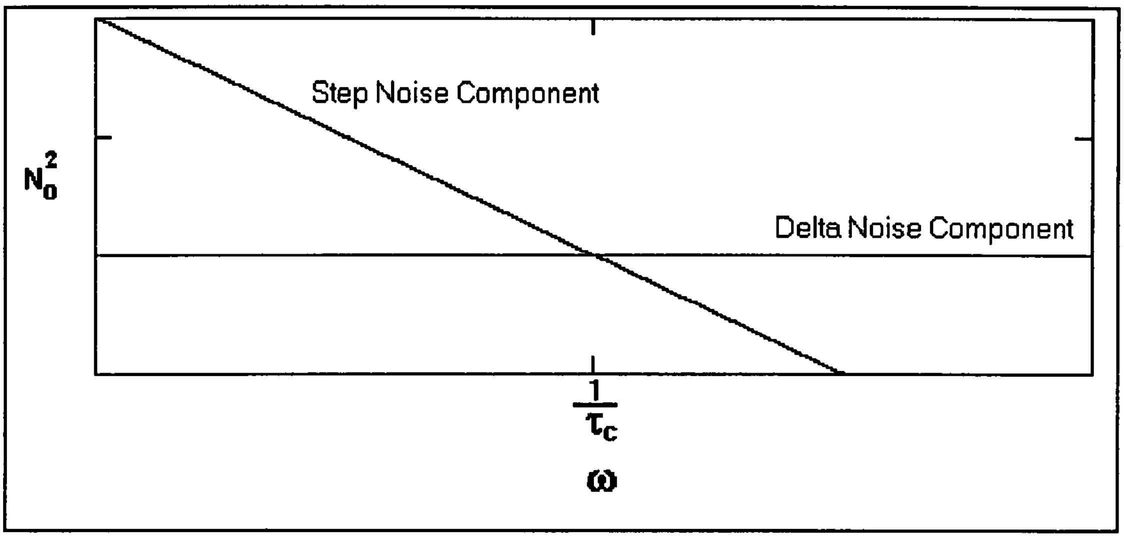

Figure 10. Noise Power Spectral Density Graph

To combat this problem, it is desirable for the filter pulse shape to have a flat top with a duration of at least 400ns. Figure 11 illustrates how the flat top eliminates the effect of ballistic deficit. In this figure, a triangular and a trapezoidal pulse are shown. An event which is composed of two impulses of charge is shown along with the response of the filter to each impulse individually and the superimposed response. As shown in the figure, the triangular shaped pulse does not reach the correct amplitude, but the trapezoid does.

Furthermore, the infinite tails on the cusp would prevent the spectrometer from performing well as the input pulse rate increases. A filter which eliminates some of the problems of the cusp produces a trapezoid. A trapezoidal pulse shape is defined in Figure 12. Applying Equations (5) and (6) to the trapezoid results in the following noise indices:

$$\langle N_s^2 \rangle = \tau_2 + \frac{\tau_1 + \tau_3}{3} \tag{10}$$

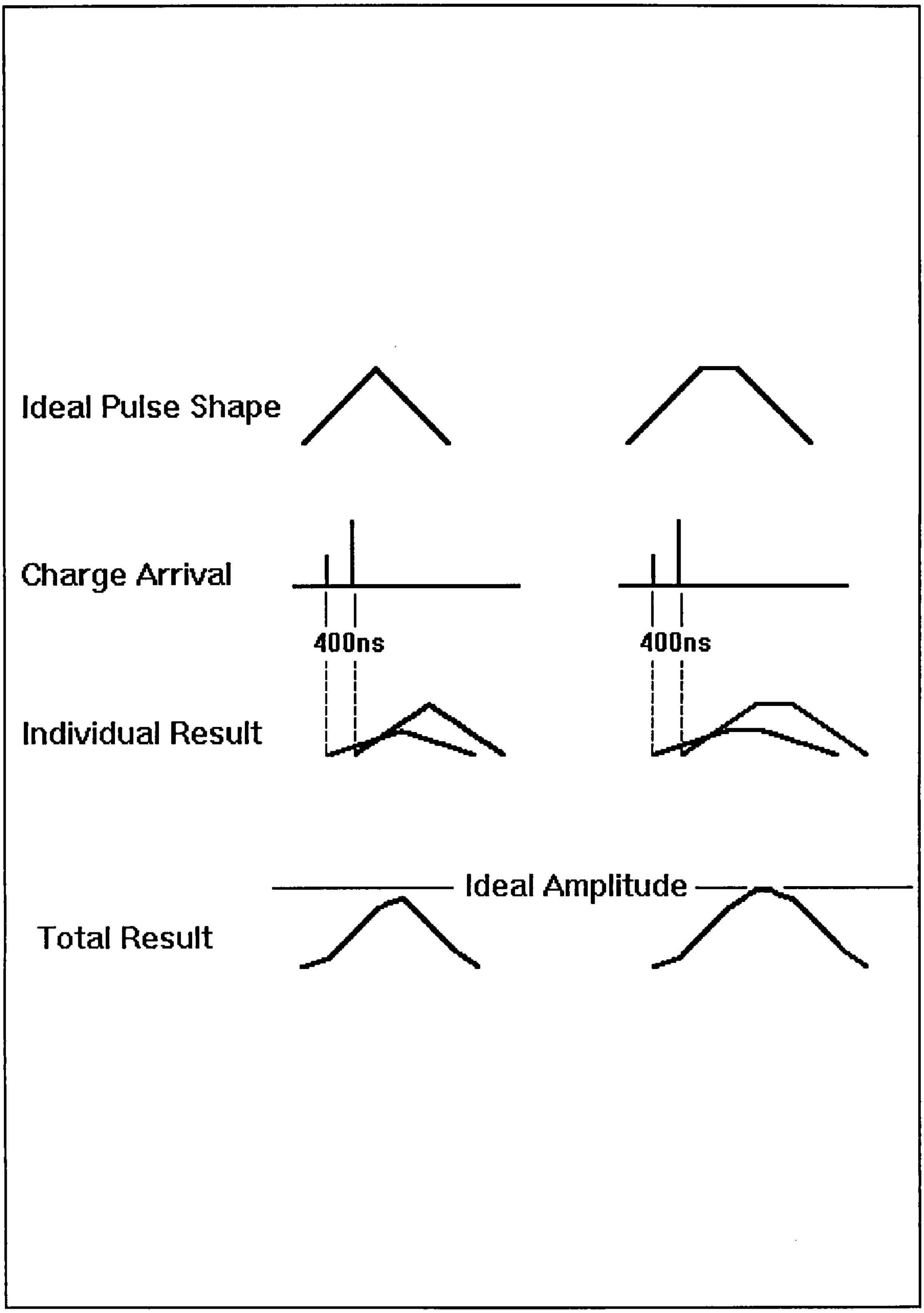

Figure 11. Illustration of Ballistic Deficit

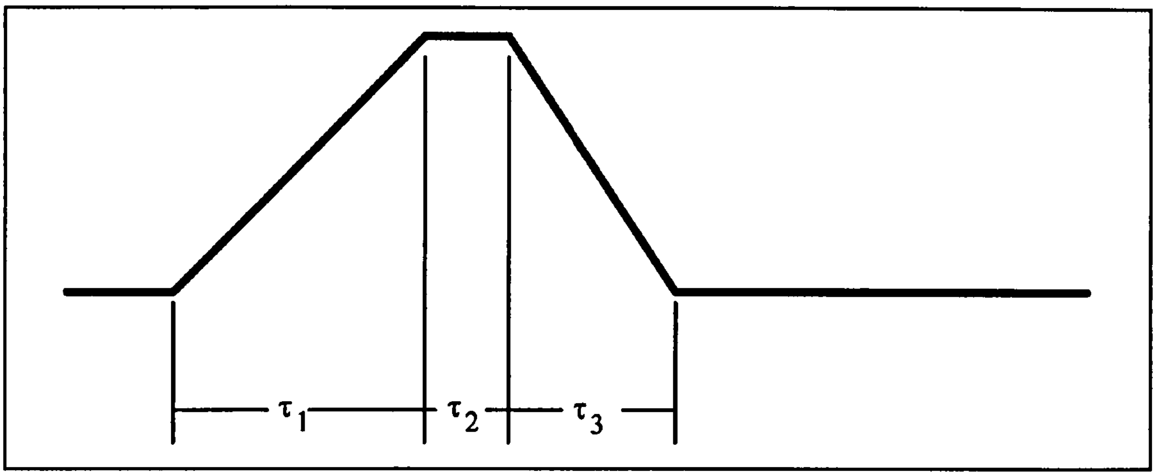

Figure 12. Definition of Trapezoidal Pulse.

and

$$<N_\Delta^2> = \frac{1}{\tau_1} + \frac{1}{\tau_3} \tag{11}$$

where τ_1 is the 0 to 100% rise time of the trapezoid, τ_3 is the 0 to 100% fall time of the trapezoid and τ_2 is the width of the flat top of the trapezoid as shown in Figure 12. If τ_1 is equal to τ_3 and τ_2 is small, the noise indices reduce to

$$<N_s^2> = \frac{2}{3}\tau_1 \tag{12}$$

and

$$<N_\Delta^2> = \frac{2}{\tau_1} \tag{13}$$

If τ_1 is set equal to 1.73 x τ_c, then the step noise index and delta noise indices are each 16% larger than the cusp indices, and the resulting noise is 8% worse than the cusp. See Appendix I for details making a comparison between a particular filter and the ideal cusp signal-to-noise ratio. Figure 13 is a plot of noise relative to the ideal noise of a cusp versus rise time for the symmetrical trapezoid with a short flat top.

Since the total time required to process the trapezoid is twice the rise time plus the flat top width, a tradeoff can be made between noise performance and count rate performance. In fact the trapezoid is the optimum filter[7] in high input pulse rate situations when a narrow pulse width is required. However in low counting rate situations when a wider output pulse is acceptable, a filter more similar in shape to the cusp has a better signal-to-noise ratio than the trapezoid. Goulding[8][9] used these same techniques to describe the noise characteristics and pulse width requirements for a number of common filters and has tabulated the results.

Pile-Up Losses

Obtaining the best possible resolution is only one of the factors in selecting a pulse shape for a spectroscopy amplifier. Equally important is the selection of a pulse shape which fits the pile-up loss criteria of the experiment. Since pulses from an HPGe detector arrive at random time intervals with a Poisson distribution, some pulses will arrive at nearly the same time creating a distorted waveform at the output of the amplifier. These distorted pulses are usually detected and rejected by the spectrometer.

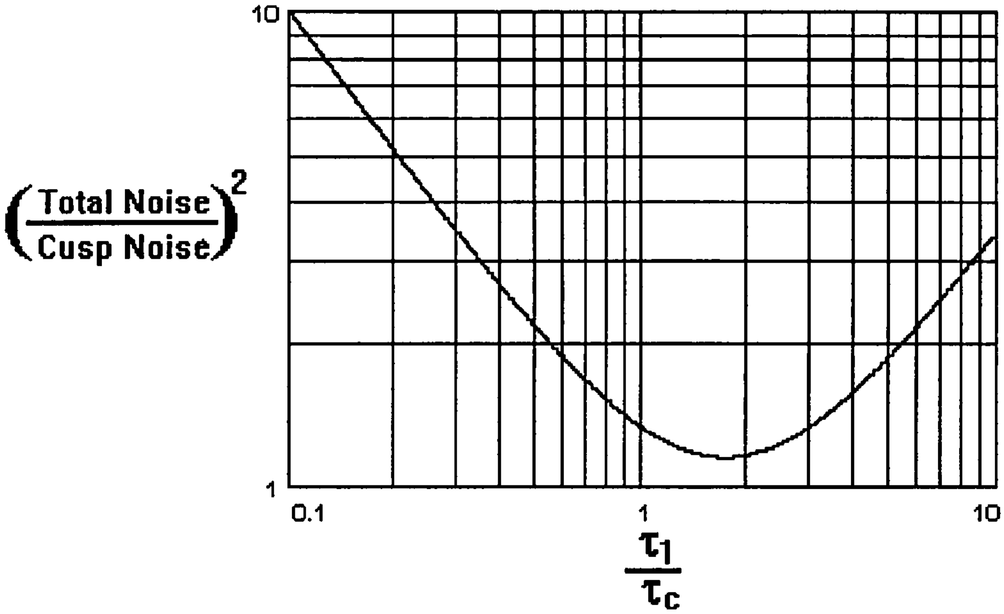

Figure 13. Noise Performance of Trapezoid vs. Risetime

Figure 14 shows the effect of two closely spaced pulses on the output of the amplifier. In this example, the third, fourth and fifth pulses would all be lost due to pile-up.

The effect of a particular pulse shape on the pile-up free output rate of an amplifier can be determined by computing the probability that a pulse will be lost due to pile-up. Figure 15 shows a sample pulse which occurs at time 0. Any pulses which occur during the time interval from $-T_F$ to $+T_R$ distort the peak of the pulse which occurs at time equal 0 making the pulse unacceptable. Furthermore in most spectrometers, the peak stretching circuit requires that the amplifier output return to 0 volts between pulses in order to re-arm the peak stretcher. So, if any pulses arrive from the time $-T_F$-T_R to time T_R, the pulse occurring at time equal 0 will be rejected. Since gamma-rays from nuclear reactions have a Poisson distribution in time, the

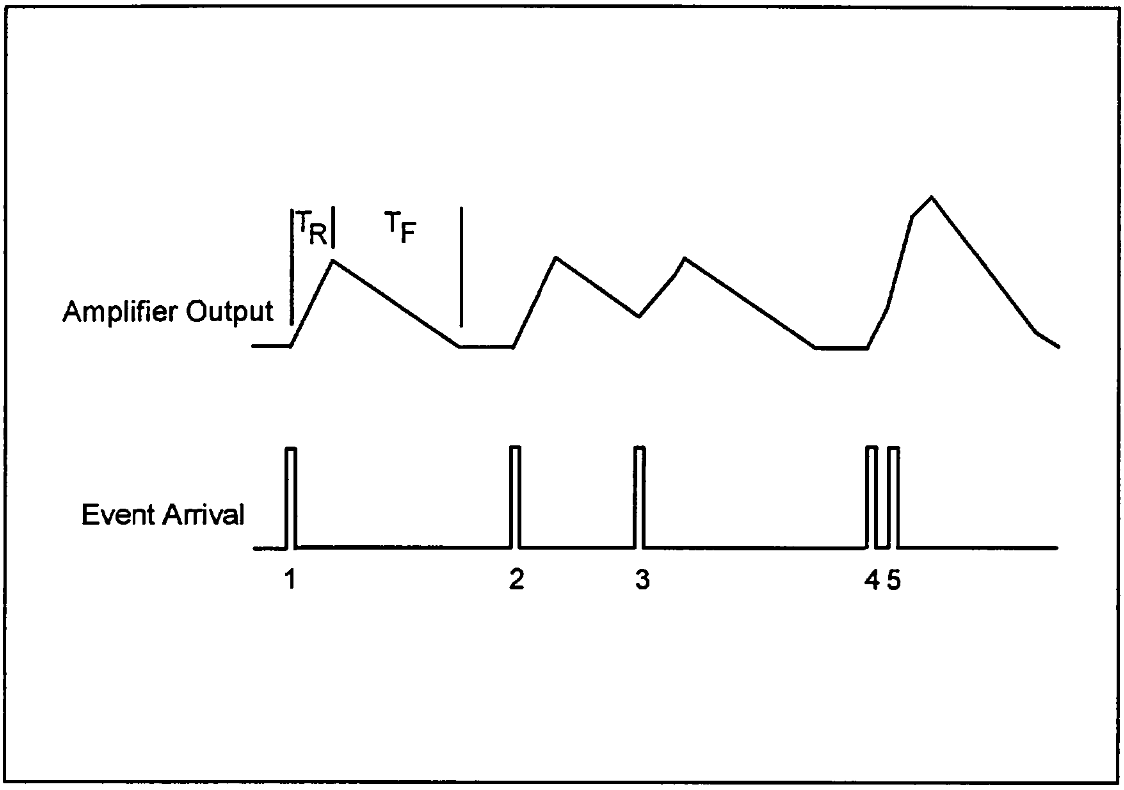

Figure 14. Example of Piled-Up Pulses. Pulses 3,4 and 5 are Lost.

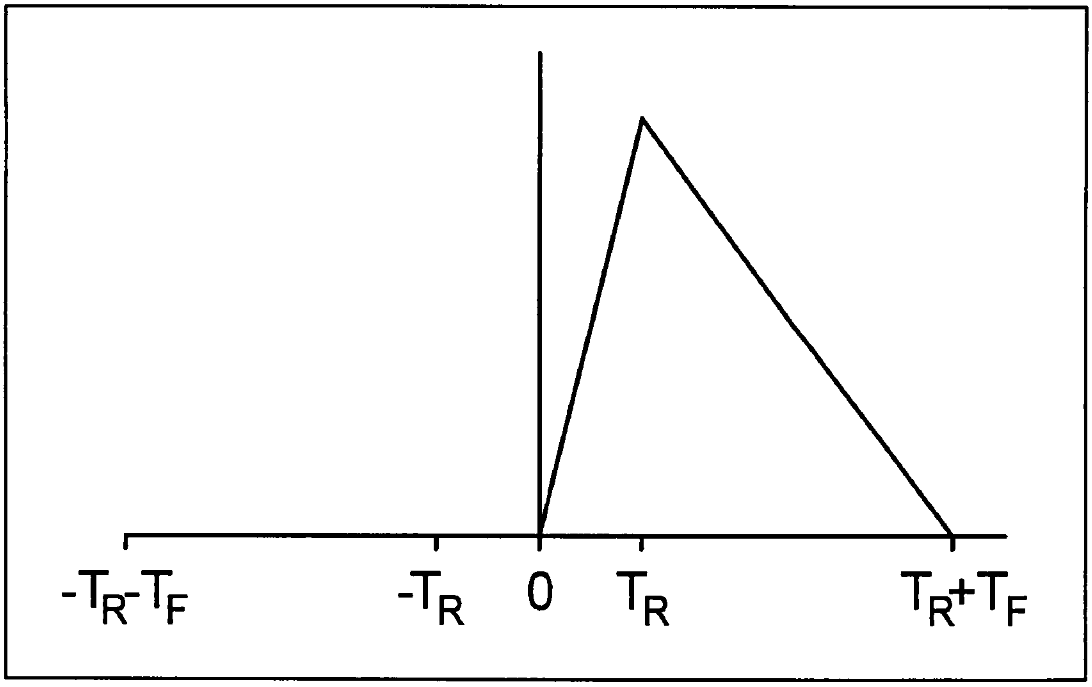

Figure 15. Pulse Piles-Up if any Other Pulse Occurs after $-T_1$-T_2 and Before T_1.

probability that no pulses will occur during a time interval from $-T_F - T_R$ to time T_R is[10]

$$P(0) = e^{-R_i(2T_R + T_F)} \tag{14}$$

where R_i is the input rate of pulses in pulses per second. The pile-up free output rate (R_o) is then determined by multiplying the input rate by the probability that a pulse did not pile up.

$$R_o = R_i e^{-R_i(2T_R + T_F)} \tag{15}$$

Figure 16 shows the effect of pile-up losses on the output rate. Once the throughput curve peaks, further increases in input count rate actually reduce the number of pulses which are processed by the ADC.

The ADC can also degrade the output rate of a spectrometer. If the ADC conversion time is longer than the decay time of a pulse, then the ADC contributes to the spectrometer dead time. The expression for the ADC output rate is[11]

$$R_{adc} = \frac{R_i}{e^{R_i(2T_R + T_F)} + R_i(T_m - T_F)U(T_m - T_F)} \tag{16}$$

where T_m is the measurement time of the ADC, $U(x)$ is the unit step function, and all other variables are defined as before. As can be seen from Equation (16), the ADC

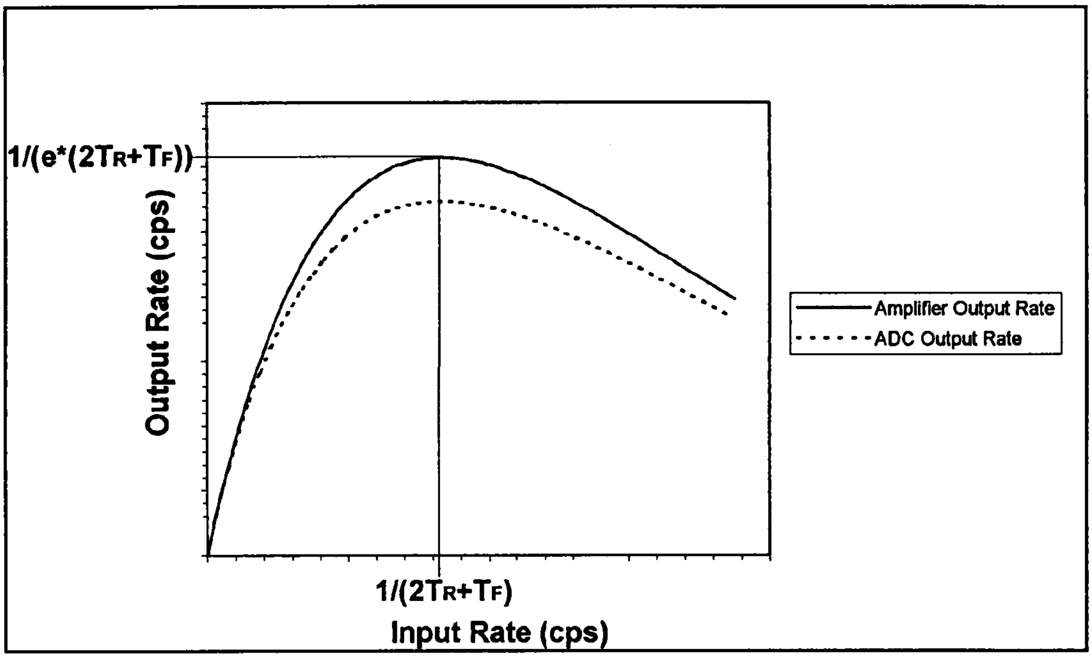

Figure 16. Amplifier Pile-Up Free Output Rate Versus Input Rate. ADC Output Rate for $T_1=T_2=2T_M$ Versus Input Rate.

has no effect if the measurement time of the ADC is less than the fall time of the output pulse. Figure 16 also shows a graph of throughput versus input rate when the amplifier pulse is assumed to be symmetrical and the ADC measurement time is twice the pulse fall time.

Digital Techniques

In the Ballistic Deficit Section, it was pointed out that a trapezoidal pulse shape is advantageous to eliminate ballistic deficit effects. Unfortunately, pulses with flat tops are difficult to implement in analog filters, although some quasi-triangular and trapezoidal filters have been implemented.[12] Lately, much focus has turned to using a digital filter to implement the shaping network in an HPGe detector system.

A block diagram of a spectrometer with a digital shaping filter is shown in Figure 17. In this system, the analog-to-digital converter continuously samples the preamplifier output creating a digital waveform. A digital filter converts the exponentially shaped pulse into the desired pulse shape. A gated baseline restorer follows the digital filter to stabilize the DC level and a digital version of the peak detector finds the peaks of the pulses and sends them to the digital controller.

A number of researchers have reported on digital filters for this application. Koeman[13] described digital filters which implement a triangular weighting function and a piecewise linear approximation to a cusp. It is a simple extension to add the flat top portion to his filter to make it useful for applications which have long charge collection times. (Koeman was working with devices which have a short charge collection time, so the flat top on the pulse was not necessary.) Koeman's implementation requires a large number of arithmetic operations be performed once a pulse arrives. The filter is inactive when pulses are not arriving. In order to implement a gated baseline restorer, the shaping filter must continue to operate even when no pulses are present.

Georgiev and Gast[14] describe a digital filter which implements the trapezoid with a recursive algorithm which minimizes the number of computations required for each data value coming from the digitizer, making the BLR feasible.

Jordonov[15],[16] described recursive algorithms to implement a number of digital filters including the triangle, trapezoid and a cusp-like filter. He also showed circuits to implement the trapezoid and triangle along with a peak

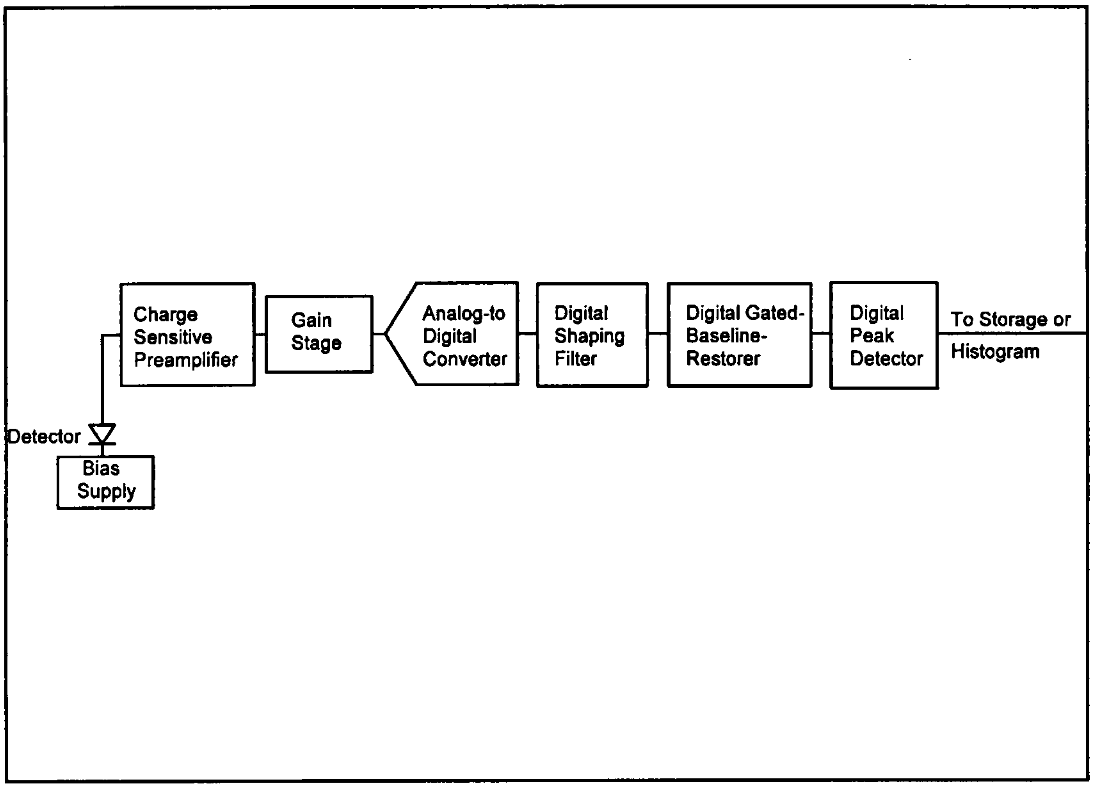

Figure 17. HPGe Spectrometer with Digital Shaping.

detection circuit to select the peak amplitudes of the output pulses. Jordonov's implementations tend to avoid digital signal processors; as a result he avoided multiplications in his algorithms.

Ripamonti et al.[17][18] describe a number of weighting functions implementable with digital circuits based on delay line and double delay line shaping in which a pulse is partially filtered in the analog domain and partially filtered in the digital domain.

Audet et al.[19] describe a digital X-ray analysis system in which the trapezoidal pulse shape adaptively changes width from pulse-to-pulse. The adaptive nature of the system improves the resolution and count rate performance of the system.

Another advantage of digitizing the signal before filtering is to suppress Compton events. A Compton event occurs when only part of the energy of the gamma-ray is absorbed by the detector. The result is a pulse which does not reach its full amplitude. A number of papers[20][21] demonstrate techniques for rejecting the Compton events by analyzing the shape of the input pulse.

When two gamma-rays strike the detector at nearly the same time, the resulting output is some combination of the two energies. These undesirable events are called piled-up events. Several researchers[22][23] have improved the pile-up rejection circuit by digitizing the signal from the preamplifier and either accepting or rejecting events based on the shape of the preamplifier signal.

The remainder of this dissertation describes a spectrometer with an HPGe detector in which a digital filter with a quasi-cusp pulse shape was used to minimize the resolution of the spectrometer. By adjusting a single parameter in the filter, the noise to signal ratio can be improved at long pulse settings while maintaining the optimum trapezoidal shape at short pulse width settings. Furthermore, the inclusion of a flat top on the output pulse eliminates ballistic deficit errors without resorting to a time-variant filter. Chapter II describe the theory of operation of the filter and contains an analysis of the quantization effects. Chapter III describes the circuit that was used to implement the filter. Chapter IV contains results obtained with the spectrometer and the final chapter concludes the dissertion with a summary of the work.

Chapter II

Theory

This chapter describes the digital quasi-cusp shaping filter, the digital prefilter, the digital gated baseline restorer and the peak detector. This chapter also contains analyses of the count rate and noise performance characteristics of the filter.

Quasi-Cusp Digital Shaping Filter

Figure 18 shows the shape of the quasi-cusp filter pulse. The leading and trailing edges are mirror images of each other and are composed of two line segments which join at the midpoint of the rise or fall period. The slope of the second line segment is always one while the slope of the first line segment may be adjusted with a single filter coefficient, α. Since the slopes of the line segments can by adjusted with the addition of gain, α is actually the ratio of the slopes of the two line segments. The mathematical definition of the pulse shape is

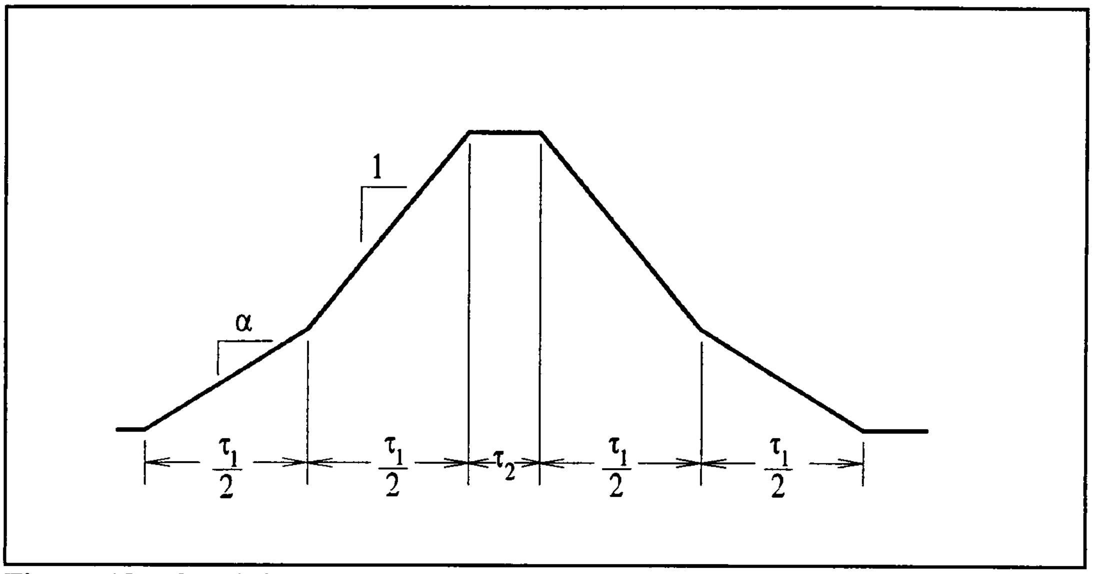

Figure 18. Quasi-Cusp Pulse Shape

$$V(t)=\begin{cases} \alpha t & , \quad \frac{\tau_1}{2}>t\geq 0 \\ \alpha\frac{\tau_1}{2}+t-\frac{\tau_1}{2} & , \quad \tau_1>t\geq\frac{\tau_1}{2} \\ (1+\alpha)\frac{\tau_1}{2} & , \quad \tau_2+\tau_1>t\geq\tau_1 \\ (1+\alpha)\frac{\tau_1}{2}-(t-\tau_1-\tau_2) & , \quad \tau_2+\frac{3}{2}\tau_1>t\geq\tau_1+\tau_2 \\ \alpha(2\tau_1+\tau_2-t) & , \quad 2\tau_1+\tau_2>t\geq\tau_2+\frac{3}{2}\tau_1 \end{cases} \tag{17}$$

where τ_1 is the 0% to 100% rise and fall time, τ_2 is the width of the flat top, and α is a filter coefficient which determines the shape of the rise and fall time. Figure 19 shows a plot of some of the possible pulse shapes as a function of α. Since the filter is time-invariant, the mathematical definition of the pulse shape is equivalent to the time-reversed residual weighting function. Therefore, substituting *V(t)* from Equation (17) into Equations (5) and (6) as *W(t)* results in the following noise indices for the Quasi-Cusp filter:

$$<N_s^2> = \frac{4\alpha^2+3\alpha+1}{(\alpha+1)^2}\frac{\tau_1}{3}+\tau_2 \tag{18}$$

and

$$<N_\Delta^2> = 4\frac{\alpha^2+1}{\alpha^2+2\alpha+1}\frac{1}{\tau_1} \tag{19}$$

If α is set equal to 1, the noise indices reduce to the noise indices of the symmetric trapezoid as expected, so if high counting rates are in use, α can be set equal to 1 and the rise and fall times can be set short to achieve optimum resolution for a particular throughput. For slower counting rates, α can be set smaller to achieve better resolution.

Figure 20 is a plot of the Quasi-Cusp noise relative to the optimum cusp noise as a function of rise time for various values of α. The α equal to 0.4 curve (see Appendix III) has the minimum noise for this filter with a noise contribution only 3.4% worse than the optimum cusp noise. If high count rate performance is required

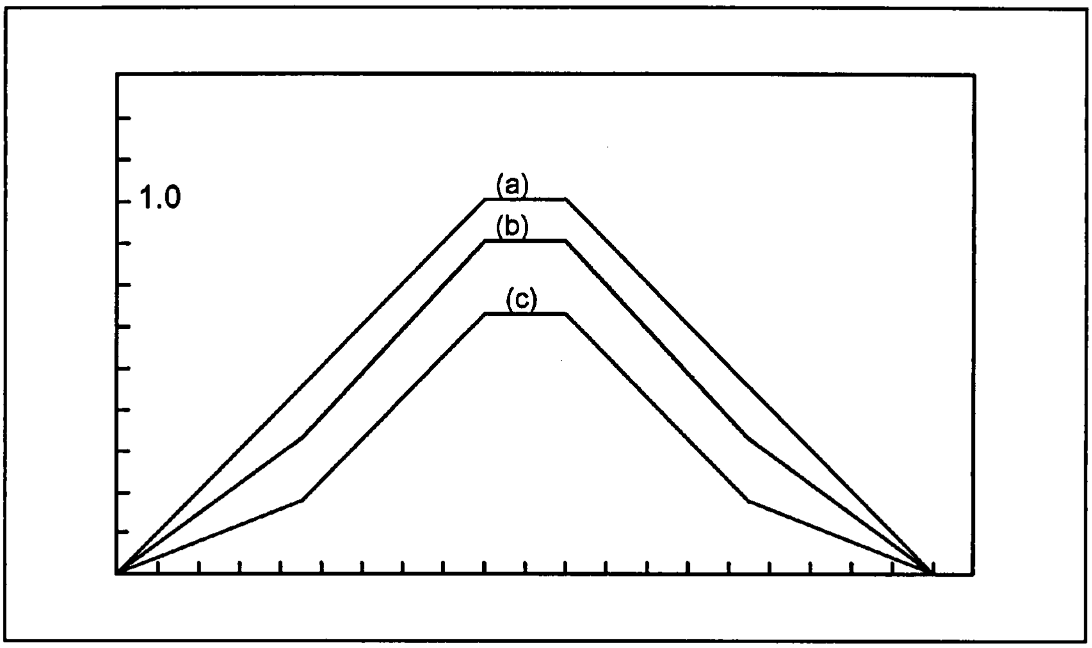

Figure 19. Possible Weighting Functions. (a) $\alpha=1$ (b) $\alpha=0.75$ (c) $\alpha=0.4$

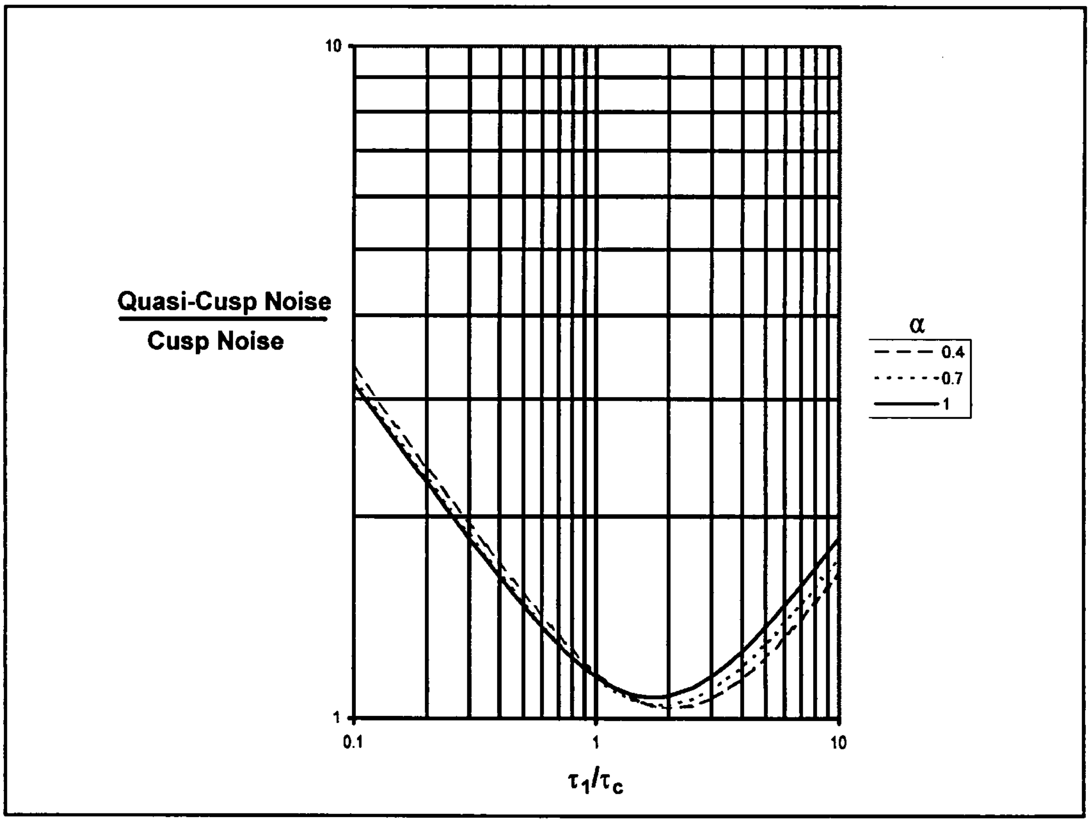

Figure 20. Noise Plot for Various Values of α. ($\tau_1=\tau_3$, $\tau_2=0$)

(i.e., τ_1 is small), α can be set to 1 and the noise curve lies on the trapezoid noise curve. Therefore, this filter has optimum noise for short pulses and noise characteristics better than the trapezoid at long shaping times.

The transfer function of the filter can be determined by sampling *V(t)* (Equation (17)), transforming the result to the Z-domain, and dividing the transformed pulse by the Z-transform of the exponential input pulse. Appendix IV carries out this process in detail with the following result:

$$H(Z)=\left(1-Z^{-\frac{T_1}{2}}\right)\left(\alpha-\alpha Z^{-\frac{3}{2}T_1-T_2}+Z^{-\frac{T_1}{2}}-Z^{-T_1-T_2}\right)\frac{1-e^{-\frac{\tau_s}{\tau_p}}Z^{-1}}{\left(1-Z^{-1}\right)^2} \tag{20}$$

where τ_s is the period of the sample clock for the digital filter, T_1 is τ_1/τ_s,T_2 is τ_2/τ_s, and τ_p is the time constant of the preamplifier. If the preamplifier output is passed through a pole-zero network, τ_p would be replaced by the resulting time constant. Figure 21 shows a block diagram implementation of the filter. The filter requires seven summations and two multiply operations for each data value from the digitizer.

Gated Baseline Restorer

In order to eliminate DC shifts and low frequency noise, a digital gated baseline restorer must be applied to the signal as it leaves the shaping filter. A gated baseline restorer is only active when pulses are not being processed by the shaping filter. When no pulses are present, the BLR differentiates the signal from the shaping filter with a long time constant (typically 90 μs) thereby eliminating errors due to DC shifts and low-frequency noise.

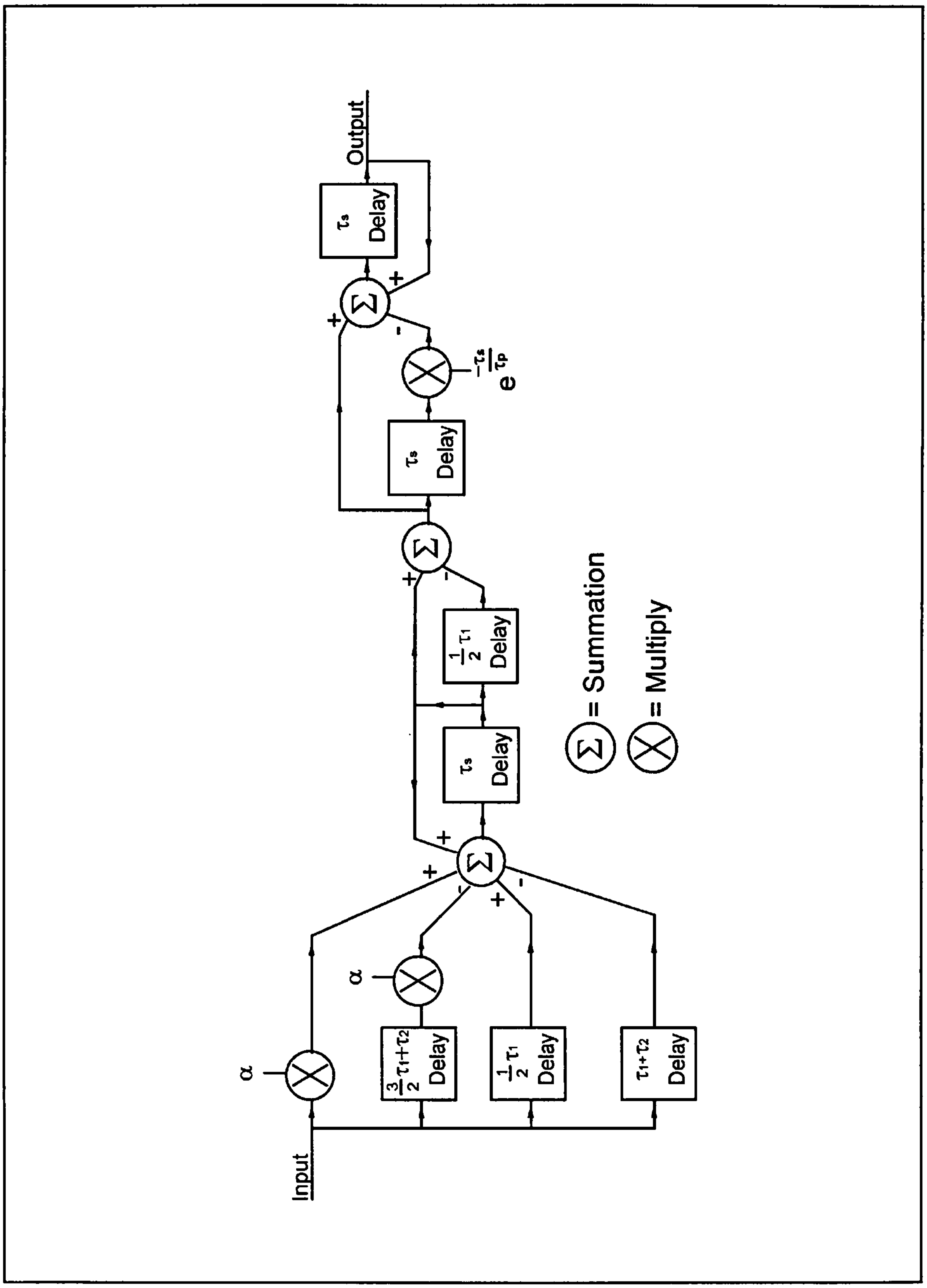

Figure 21. Block Diagram of Digital Filter

In this design, the gated baseline restorer is included in the final stage of the shaping filter by removing the final delay and summation and including the filter shown in Figure 22. The feedback path in the final stage of the shaping filter has been replaced with a multiply operation. The constant changes from 1 when a pulse is present to

$$e^{-\frac{\tau_s}{\tau_{blr}}} \tag{21}$$

when no pulses are present. This filter is easy to implement in a digital signal processor, because a multiply and accumulate operation takes the same number of cycles as an accumulate operation. Therefore, the BLR takes no extra processing

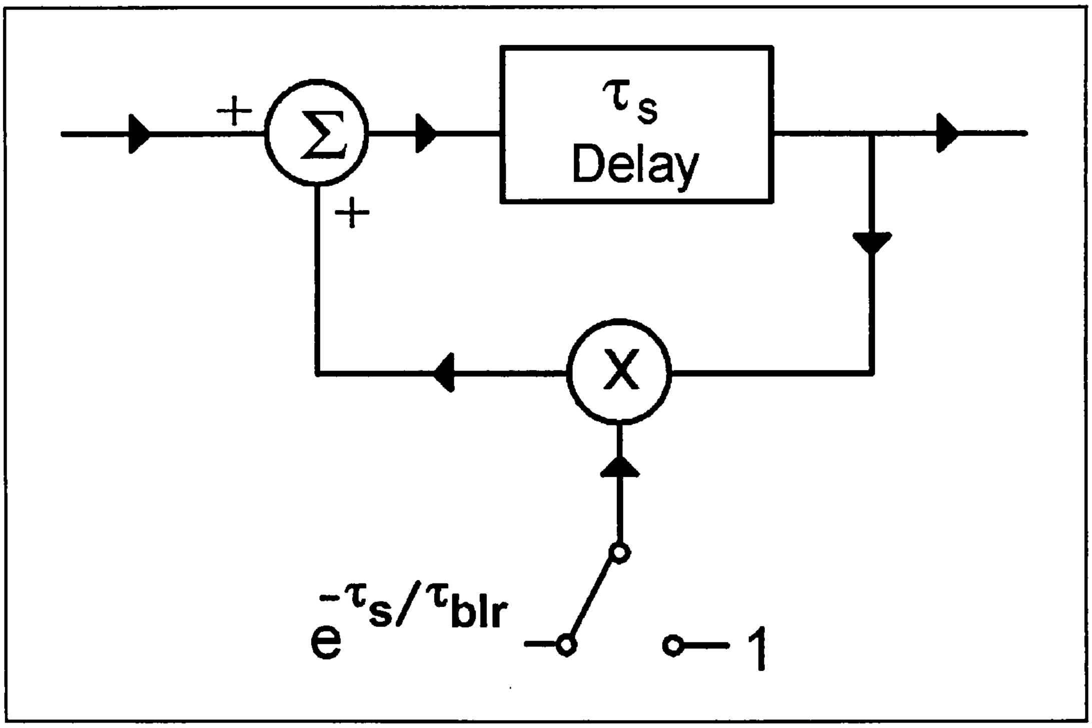

Figure 22. Block Diagram of Digital Gated-Baseline Restorer.

power or memory beyond determining which constant to use in the multiplication operation.

Quantization Errors

A source of noise in the digital filter which is not present in the analog domain is the noise introduced due to errors made while quantizing the analog signal. Assuming that the quantization noise is uniformly distributed over a single quantile,the RMS noise introduced by the quantizer is[24]

$$\sigma_v = \frac{q}{\sqrt{12}} \tag{22}$$

where q is defined as the size of one quantile or

$$q = \frac{V_{\max}}{2^b} \tag{23}$$

where V_{max} is the range of the quantizer and b is the number of bits in the quantizer. To minimize the effect of the quantization noise, the quantile should be as small as possible relative to the input signal. Since the number of bits in a quantizer is fixed, the only way to decrease the size of the quantile is to decrease the range of the converter. Unfortunately, decreasing the range of the converter will increase the likelihood that the quantizer input will saturate as the counting rate increases and thereby distort the digital waveform. This leads to a tradeoff between quantization noise and the number of pulses lost due to saturation of the quantizer. These two errors are analyzed independently below.

Quantization Noise

One way to evaluate the effect of the quantization noise is to refer the noise to the output of the digital filter and convert the noise from voltage units to energy units. The effect of the digital filter may be found by assuming that the quantization error can be modeled as an impulse of noise with no correlation from sample to sample. If the impulse response of the digital filter is *h(n)*, then the noise gain (NG) of the quantization noise from the quantizer input to the output of the filter is

$$NG=\sqrt{\sum_{n=-\infty}^{\infty} h(n)^2} \tag{24}$$

By taking the inverse Z-transform of Equation (20), the discrete impulse response of the quasi-cusp filter is found to be

$$h(n)=\begin{cases} \alpha n\rho+\alpha & , \frac{T_1}{2}>n\geq 0 \\ \alpha\frac{T_1}{2}\rho+(n-\frac{T_1}{2})\rho+1 & , T_1>n\geq\frac{T_1}{2} \\ (1+\alpha)\rho\frac{T_1}{2} & , T_2+T_1>n\geq T_1 \\ (1+\alpha)\rho\frac{T_1}{2}-(n-T_1-T_2)\rho-1 & , T_2+\frac{3}{2}T_1>n\geq T_1+T_2 \\ \alpha(2T_1+T_2-n)\rho-\alpha & , 2T_1+T_2>n\geq T_2+\frac{3}{2}T_1 \\ 0 & , \textit{Otherwise} \end{cases} \tag{25}$$

where

$$\rho = 1 - e^{-\frac{\tau_s}{\tau_p}} \tag{26}$$

The noise gain is then

$$NG = \sqrt{\left(\frac{\alpha^2}{3} + \frac{\alpha}{4} + \frac{1}{12}\right)\rho^2 T_1^3 + \frac{T_2 \rho^2 (1+\alpha)^2 T_1^2}{4} + \left(\frac{\rho^2}{6} + 1 - \rho\right)(1+\alpha^2) T_1} \tag{27}$$

In order to evaluate the effect of the noise gain of the filter, it is also necessary to evaluate the signal gain of the filter as a function of α and T_1. The signal gain (SG) of the filter is found by determining the magnitude of the output pulse during the flat top interval as a function of α and T_1. Inspection of Equation (17) reveals the magnitude to be

$$SG = (1+\alpha)\frac{T_1}{2} \tag{28}$$

Now that the signal and noise gains are known, the noise can be converted to energy units at the spectrometer output. Assume the maximum energy pulse to be processed by the spectrometer (E_{max}) has an input pulse amplitude at the quantizer input of V_{max}/K volts, where K is a constant which is greater than 1. Since the output of the spectrometer is E_{max} and the signal gain is known, the conversion factor from volts to energy is

$$E_{\max}=SG\cdot\frac{V_{\max}}{K}\cdot C_{eV} \tag{29}$$

where C_{eV} is the conversion factor to convert volts at the input of the quantizer to electron volts at the output of the spectrometer. Now the noise at the output of the spectrometer (σ_o) may be expressed as:

$$\sigma_o=\sigma_v\cdot C_{eV}\cdot NG \tag{30}$$

Substituting for C_{eV}, the noise equation becomes

$$\sigma_o=\sigma_v\frac{K\cdot E_{\max}}{V_{\max}}\frac{NG}{SG} \tag{31}$$

At this point it is useful to analyze the noise equation to determine which parameters may be adjusted to decrease the noise at the output of the spectrometer. σ_v and V_{max} are both fixed once a specific part is selected to perform the conversion from analog to digital. E_{max} is a parameter which is selected by the user for the energy range of a particular experiment. K may be adjusted by adjusting the analog gain before the quantizer, so K should be minimized to minimize the quantization noise. SG depends only on T_1 and α which are parameters which must be completely flexible to permit all desired pulse shape settings, so there are no optimizations to be made by their adjustment. NG depends on T_1, T_2, α and ρ. The first three cannot be adjusted to decrease the effect of the quantization noise because they determine the pulse shape, but ρ may be adjusted to reduce the noise gain substantially. To reduce the value of ρ, the τ_s/τ_p ratio must be small. Since the sample time of the quantizer is set by the commercial ADCs which are available, τ_s cannot be shorter than the specified value. However τ_p may be modified by adding an analog pole-zero network before the quantizer. In summary, τ_p should be as long as possible and the maximum pulse amplitude should cover as much of the ADC range as possible to minimize the effect of the quantization noise.

Unfortunately, the criteria used to minimize the effect of the quantization noise adversely affect the throughput of the quantizer. Figure 23(a) shows an input pulse in which the quantization noise has been minimized. The quantizer range is very close to the peak amplitude of the signal and the input has a long exponential decay time. Figure 23(b) demonstrates the disadvantage of such an arrangement. When two closely spaced pulses arrive at the quantizer input, the quantizer saturates and the second pulse and possibly the first would be lost by the spectrometer. Figure 23(c) shows how a shorter exponential time constant would eliminate the overrange error. A graph of the noise gain to signal gain ratio as a function of τ_p demonstrates how shorter values of τ_p affect the performance of the system. Figure 24 shows such a graph for various values of T_1, with T_2 equal to 12, α equal to 1 and τ_s equal to 100ns. With the figure, an appropriate τ_p can be selected based on the amount of quantization noise that can be tolerated for a given pulse shape.

For example, assume that the desired energy range is 3 MeV, K is 2, V_{max} is 2.5 V, and $\sigma_v = 100\ \mu$V rms. Substituting these values into Equation (31) yields

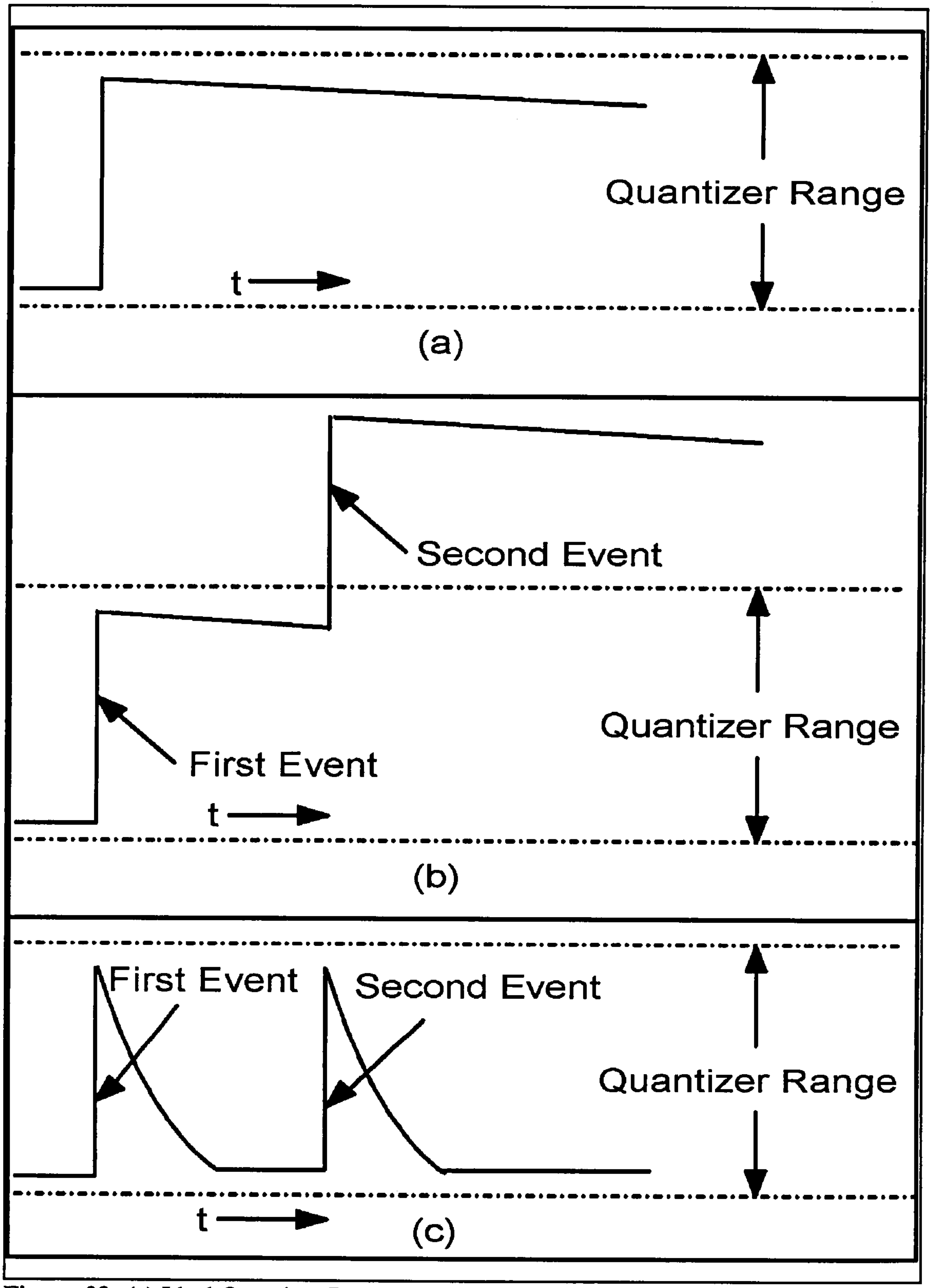

Figure 23. (a) Ideal Quantizer Range and Pulse Shape for Minimum Noise. (b) Adverse Effect of Optimum Range and Pulse Shape. (c) Pulse Shape after Pole-Zero Network.

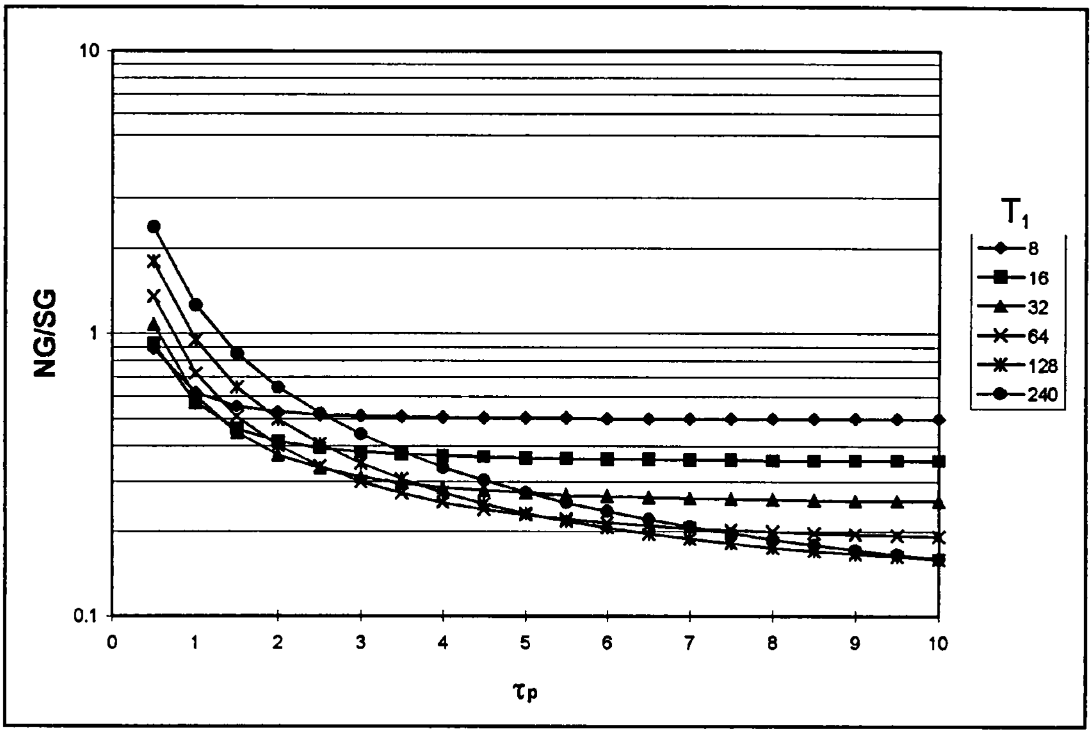

Figure 24. Quantization Noise/Signal Gain Versus τ_p. T_2=12, τ_s=100ns, α=1.

$$\sigma_o = 240\frac{NG}{SG}\ eV\ rms \tag{32}$$

From Figure 24, if T_1 is 128 and τ_p is 10 μs, then the NG/SG ratio is 0.15, so the noise at the output of the spectrometer is 240 x 0.15 = 36 eV rms or 2.35 x 36 = 84.6 eV FWHM. Reducing τ_p to 4.5 μs, increases the NG/SG term to 0.249, so the noise at the output of the spectrometer would be 140 eV FWHM. A further reduction in τ_p to 1.5 μs would increase the noise to 367 eV FWHM.

Quantizer Overrange Losses

As outlined above, τ_p and the quantizer input range can greatly affect the output pulse rate of the digital spectrometer, so it is useful to determine the percentage of pulses lost due to saturation of the quantizer. A precise result depends on the particular distribution of pulse amplitudes, but a pessimistic result can be found by assuming that all of the pulses have a uniform amplitude equal to the maximum energy to be analyzed by the spectrometer. A mathematical definition of the signal which is to be quantized is

$$V_q(t) = \frac{V_{\max}}{K} \sum_{i=0}^{\infty} e^{-\frac{t-T_i}{\tau_p}} U(t-T_i) \tag{33}$$

where T_i is a set of Poisson points and $U()$ is the unit step function. In order to determine the percentage of the time that the quantizer spends in a saturated condition, it is necessary to find the probability density function (pdf) for the waveform at the quantizer input. Papoulis outlines a technique to determine the density function for such a process[25], but the technique requires that the response of the system to a single Poisson point be finite. This is not the case for this system, because the exponential has an infinite response. The exponential response does approach zero amplitude after several time constants, so one way to attack the problem is to truncate the exponential after the response gets within an acceptable error limit. Taking this approach results in a signal with the following mathematical definition:

$$V_q(t) = \frac{V_{\max}}{K} \sum_{i} e^{-\frac{t-T_i}{\tau_p}} \left(U(t-T_i) - U(t-T_i-N\tau_p)\right) \tag{34}$$

where N is an integer which determines how many time constant periods to wait before truncating the exponential. If $N=5$, then the exponential has decayed to 0.0067, so the truncation would only introduce a slight error in the pdf. With this simplification to the signal definition, only pulses which occur after $t\text{-}N\tau_p$ can affect the signal at time t.

Let n_N be a random variable indicating the number of Poisson points occurring from time $t\text{-}N\tau_p$ to time t. Now the pdf ($f_i(x)$) of the input signal may be written as the sum of the conditional pdfs for each possible n_N.

$$f_i(x)=\sum_{k=0}^{\infty} f_i(x|n_N=k)P\{n_N=k\} \tag{35}$$

Since this is a Poisson process,

$$P\{n_N=k\} = \frac{e^{-R_iN\tau_p}(R_iN\tau_p)^k}{k!} \tag{36}$$

where R_i is the average input rate. Now the problem is to compute the conditional probability functions for a given number of points in an interval. If $n_N=0$, no events occurred in the interval and the conditional pdf is the delta function

$$f_i(x|n_N=0)=\delta(x) \tag{37}$$

If $n_N=1$, only one event occurred in the interval and since the point is equally likely to appear anywhere in the interval, the pdf can be found by applying an exponential transformation to a uniformly distributed random variable as shown in Appendix II. The resulting pdf is

$$f_i(x|n_N=1) = \frac{1}{Nx}(U(x-\frac{V_{\max}}{K}e^{-N}) - U(x-\frac{V_{\max}}{K})) \tag{38}$$

For n_N greater than 1, the process is more complex. One of the properties of a Poisson process is that if it is known that k events arrived during an interval, the events are completely independent random variables each with uniform distributions over the interval. Each of the k independent random variables has the pdf given in Equation (38), and the sum of the k events would be the convolution of Equation (38) with itself k-1 times or

$$f_i(x|n_N=k) = f_i(x|n_N=k-1) * f_i(x|n_N=1) \tag{39}$$

Unfortunately, this calculation is difficult to carry out for the given pdf in closed form. However, the problem is solvable numerically by taking the fast Fourier transform (FFT) of the n_N=1 pdf, multiplying it by itself the appropriate number of times and taking the inverse FFT to produce the final result. Figure 25 shows a graph of the conditional pdf for n_N equal 0 to n_N equal 10. The complete pdf may now be found by selecting a particular input rate and decay time and applying Equation (35) to the curves in Figure 25.

Finding the total probability function is only part of the problem. What is actually required is to determine the percentage of pulses lost due to saturation for a given quantizer range, input rate and exponential time constant. A pulse which occurs at time t will be lost if the quantizer input signal is within V_{max}/K Volts of the quantizer maximum (V_{max}) at time t. This probability may be written as

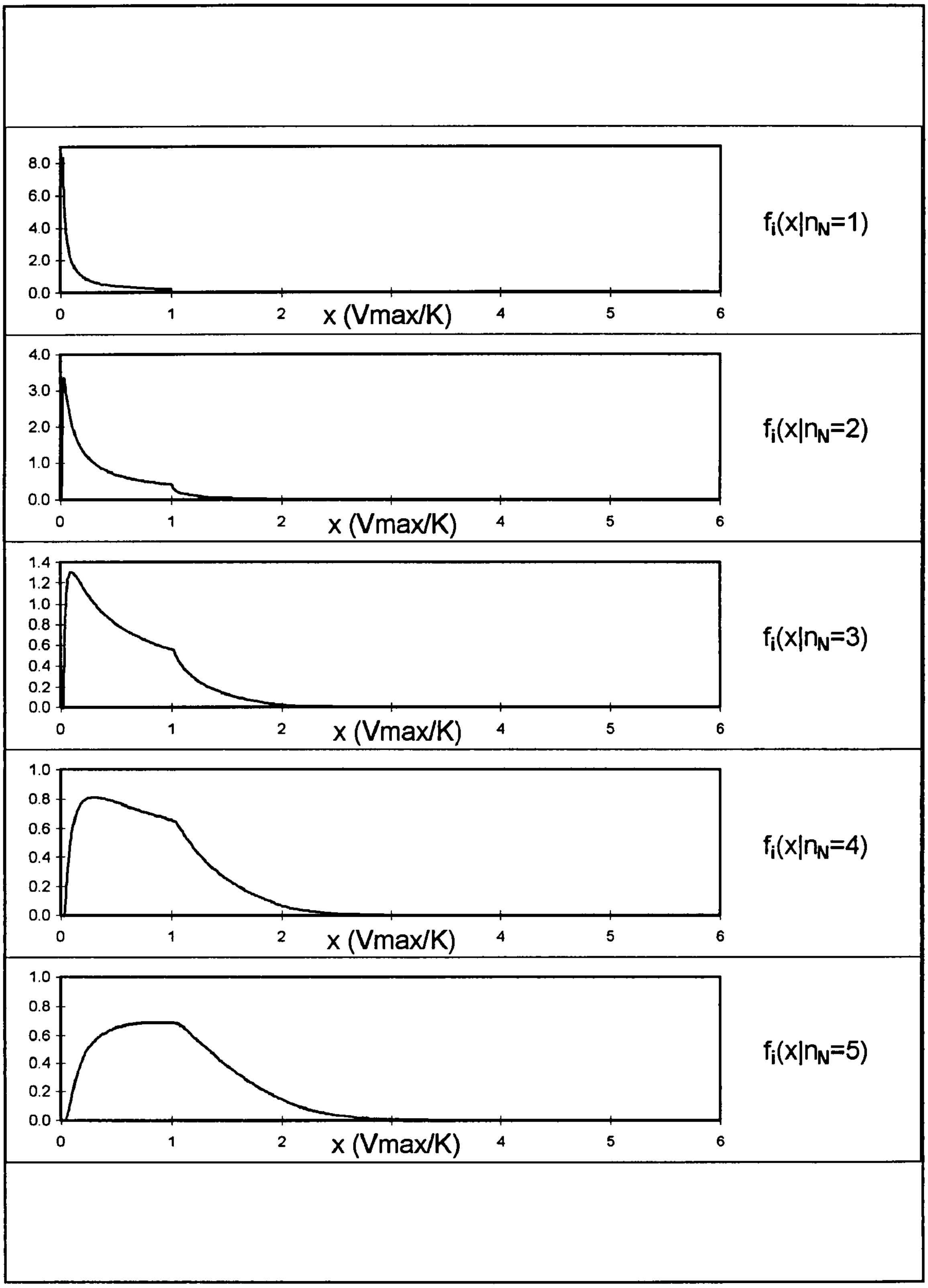

Figure 25. Conditional Probability Density Functions for n_N=1 to n_N=10.

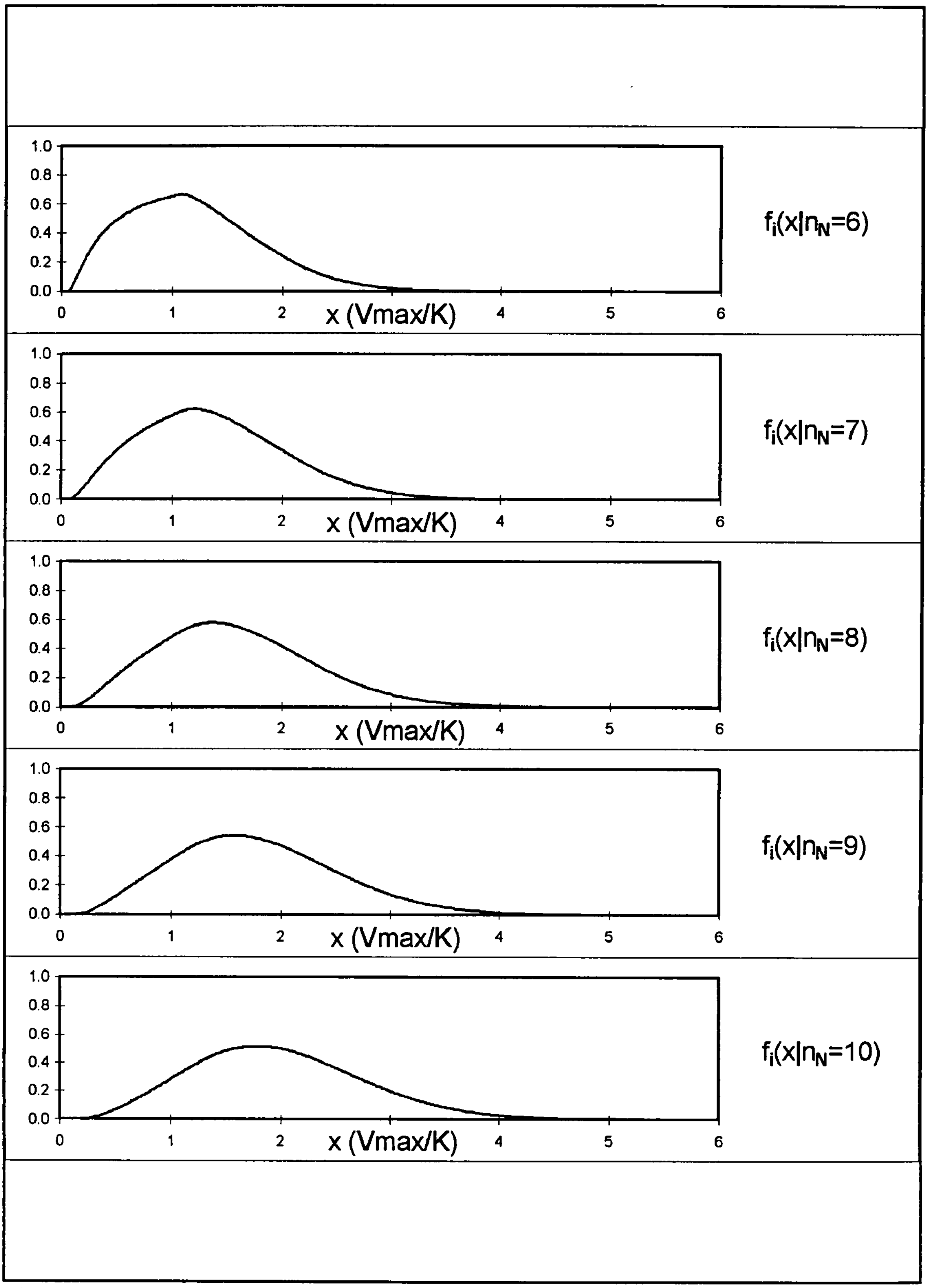

Figure 25 (continued). Conditional Probability Density Functions for $n_N=1$ to $n_N=10$.

$$P_{overload}\{Vmax\} = \int_{V_{max}-\frac{V_{max}}{K}}^{\infty} f_i(x)dx \tag{40}$$

By substituting Equation (35) into Equation (40) and rearranging, the expression becomes

$$P_{overload}\{Vmax\} = \sum_{k=0}^{\infty} P\{n_N=k\} \int_{V_{max}-\frac{V_{max}}{K}}^{\infty} f_i(x|n_N=k)dx \tag{41}$$

The integral in the equation is the integral of the curves in Figure 25. By approximating the integral as a summation of the curves in Figure 25, a new family of curves may be generated which show the probability of losing a pulse given that n_N equals a particular value. Figure 26 shows these conditional probability curves for various values of n_N.

Finally, by selecting specific values of input rate and input time constant, curves can be created which indicate the percentage of pulses lost for a given quantizer input range. As seen in Equation (36), the product of input rate and time constant determines the statistics of the input signal, so let

$$\nu = R_i \tau_p \tag{42}$$

Figure 27 shows a graph of percentage of pulses lost versus quantizer range for various value of ν. Perhaps a more useful graph is a contour plot which indicates a certain percentage of losses as a function of ν and quantizer range. Figure 28 is such a graph. Using the contour graph, if a certain percentage of losses is acceptable

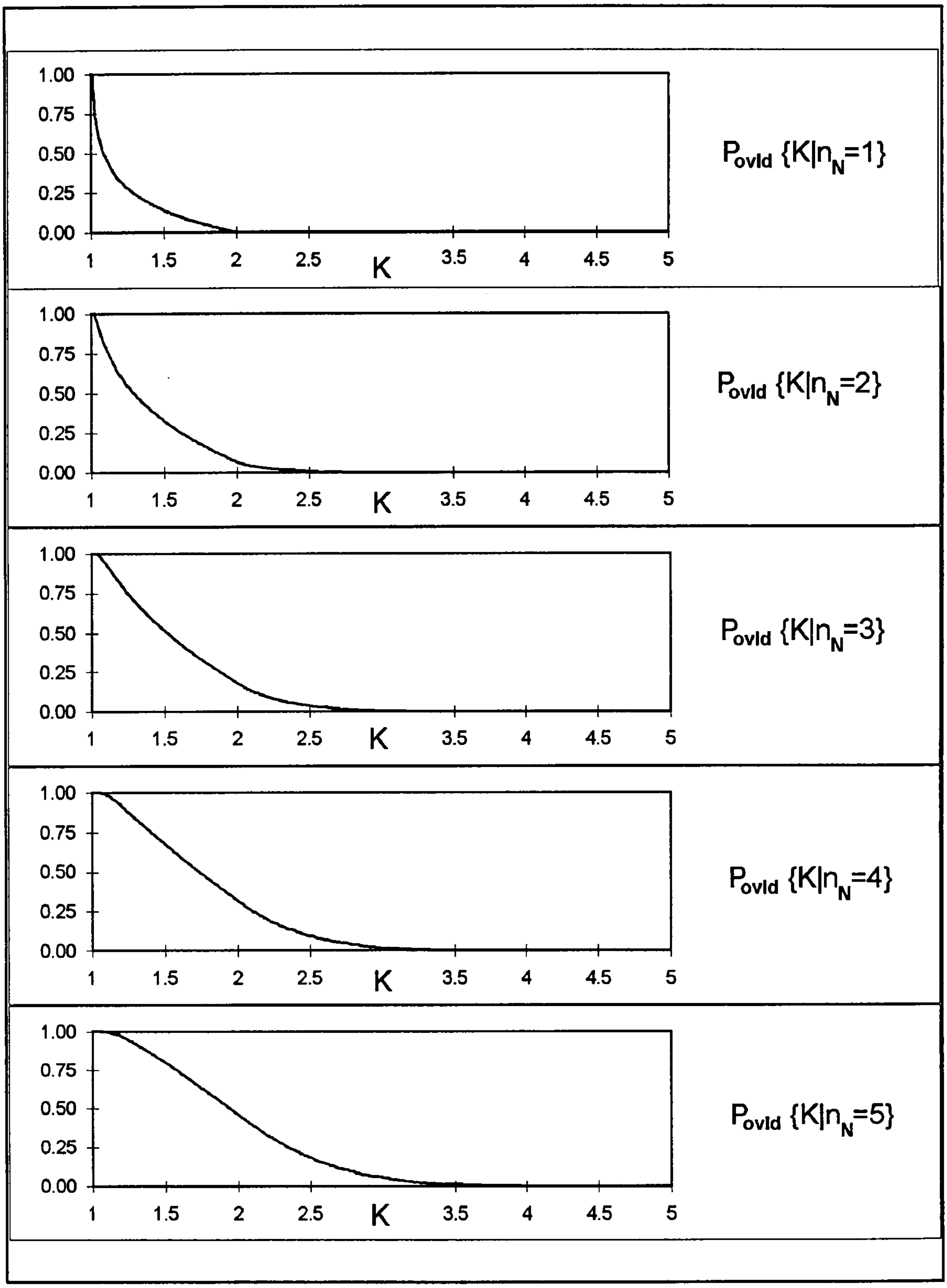

Figure 26. Conditional Probability of Quantizer Saturation as a Function of Quantizer Range and n_N.

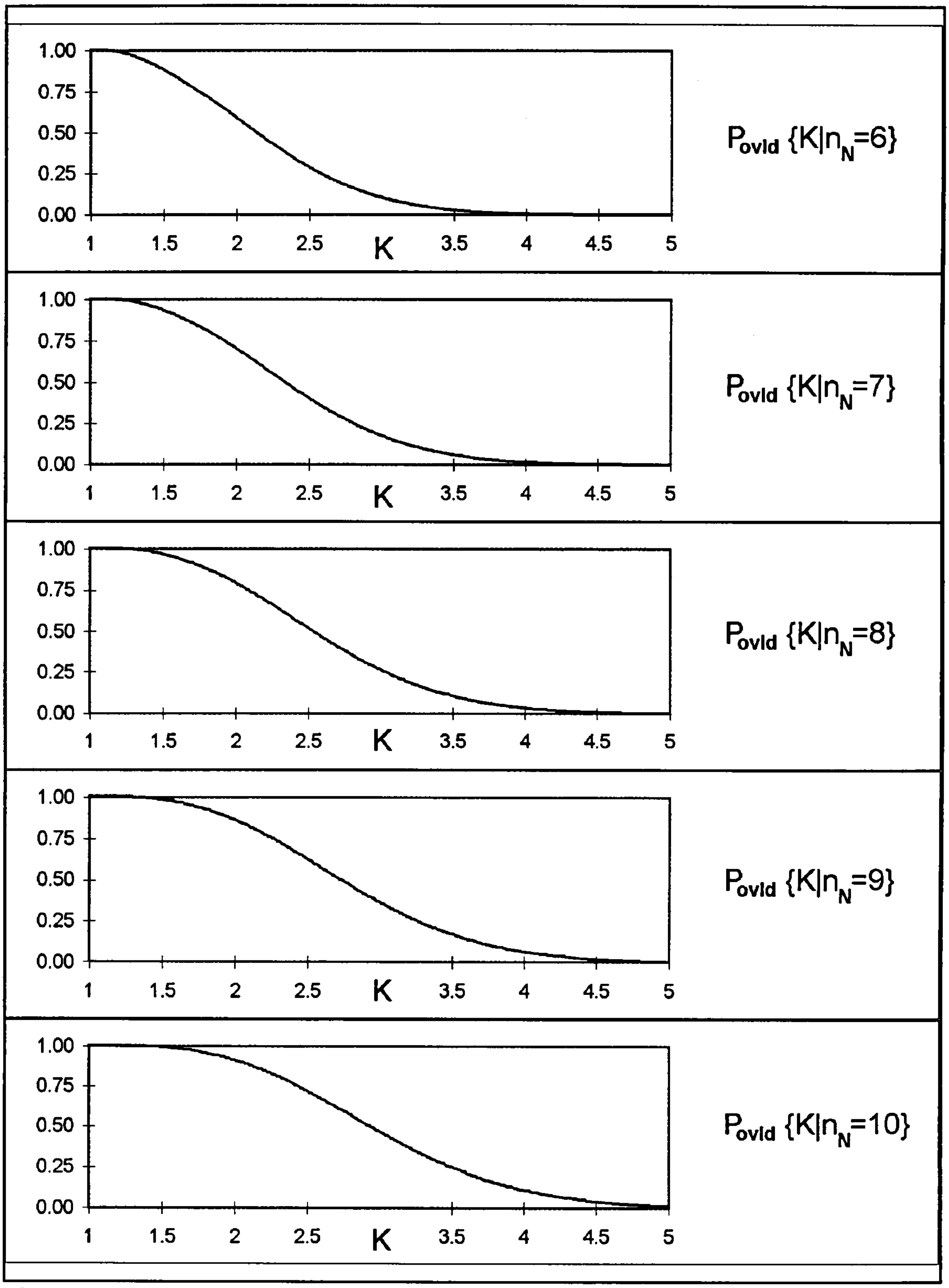

Figure 26 (continued). Conditional Probability of Quantizer Saturation as a Function of Quantizer Range and n_N.

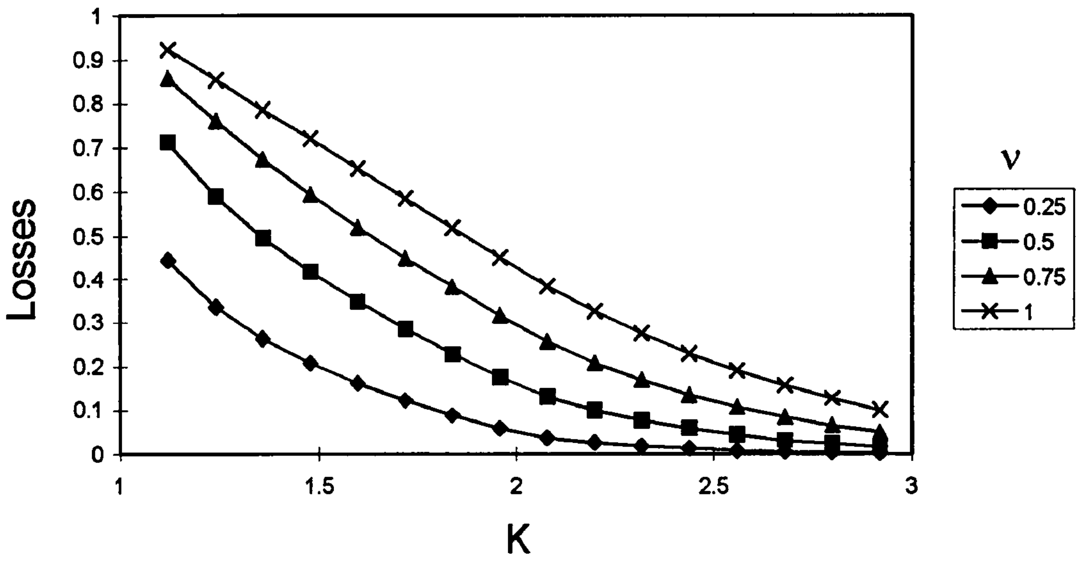

Figure 27. Fraction of Pulses Lost due to Quantizer Saturation as a Function of ν and K.

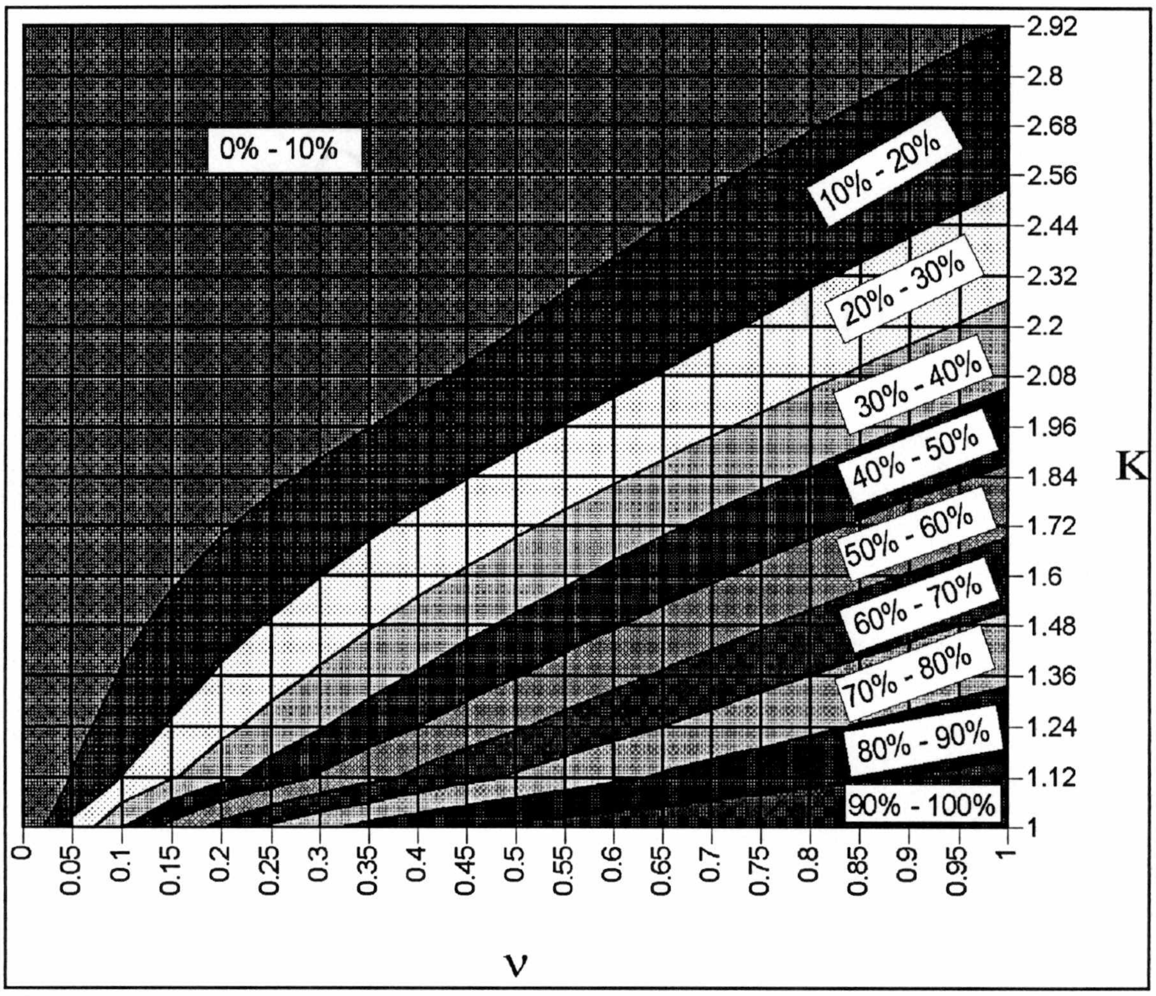

Figure 28. Percentage of Pulses Lost due to Quantizer Saturation as a Function of ν and K.

(10% for example) at a certain maximum input rate (100,000 pulses per second for example), τ_p and K can be traded against each other to achieve an acceptable setting. For example, if τ_p is set to 4.5 μs, then υ is 0.45 at 100,000 pulses per second. From the contour graph, K must be greater than 2.1 to lose less than 10% of the pulses. However if τ_p is 1.5 μs, then υ is 0.15 and K must be greater than 1.6 for 10% losses.

Dither Theory

In the quantizer noise computation, the assumption was made that the error introduced by the quantizer was uniformly spaced over a quantile and that all quantizations are uncorrelated. However, at low counting rates, the input to the quantizer is nearly a DC level with an occasional exponential pulse superimposed on it. This constant DC level will cause the quantizer to use nearly the same code for every conversion as demonstrated in Figure 29. This introduces a large error in the computation of the location of the baseline at the output of the digital filter because all of the quantization errors are in the same direction and are determined by a single quantizer code. This error leads to an unacceptable peak shift at the output of the spectrometer when the input DC level shifts due to a temperature change or an increase in counting rate. The error can be eliminated by including a dither signal with the signal to be quantized to spread the baseline calculation over a number of quantizer codes.

An ideal dither signal eliminates the peak shifting errors without substantially disturbing the resolution of the spectrometer. To achieve this goal, a dither should be added which has frequency components which are filtered out by the digital filter which follows the quantizer. The quasi-cusp filter transfer function (Equation (20)) does not have a large frequency range with very low response, but it does have a number of null points in which a dither signal could be placed. One set of null points results from the first term of the Quasi-Cusp transfer function (Equation (20)),

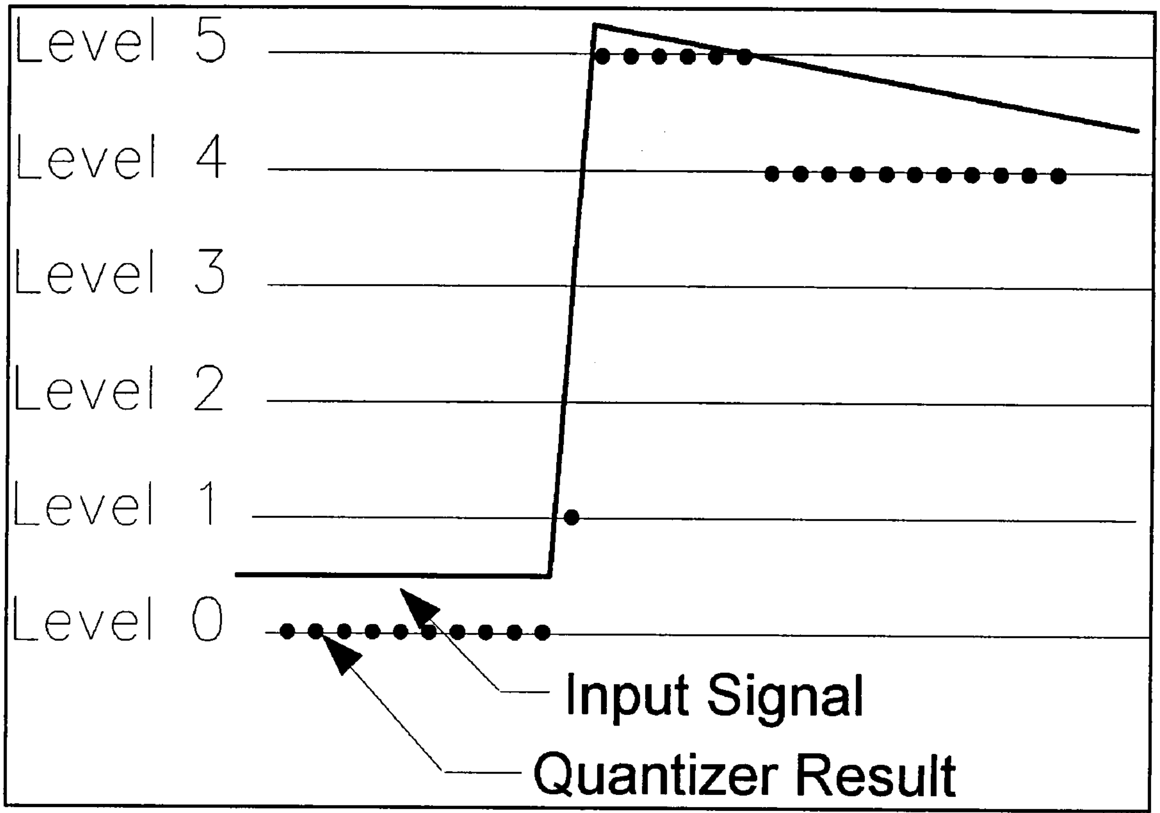

Figure 29. Quantization of Noiseless Input Signal.

$$(1 - Z^{-\frac{T_1}{2}}) \tag{43}$$

An acceptable dither signal only has frequency components which cause

$$Z^{-\frac{T_1}{2}} = 1 \tag{44}$$

Substituting for the Z operator to return to the frequency domain, the criteria becomes

$$e^{-2\pi j \tau_s f \frac{T_1}{2}} = 1 \tag{45}$$

Taking the natural log of both sides of the equation in the most general complex form reduces the criteria to

$$f=\frac{1}{\tau_s}\frac{2}{T_1}n \tag{46}$$

where n is any integer. T_1 will always be an even integer greater than 2 for the filter to be implementable because a 0.5 T_1 delay element is present in the filter. If T_1 is further limited to

$$T_1=4j \tag{47}$$

where j is a non-zero integer, then a dither with frequency components defined by

$$f=\frac{n}{j}\frac{1}{2\tau_s} \tag{48}$$

is acceptable.

One dither signal which meets this criteria is a sine wave which has a frequency that is half of the sample frequency of the quantizer ($n=j$). Unfortunately such a signal does a poor job of spreading the input signal over a large number of quantizer codes because it is only sampled at two points in the waveform. A much better dither is one which is not synchronized to the quantizer so that the sine wave is sampled at many different points. Figure 30 demonstrates how a sine wave with a frequency slightly lower than half the sample clock covers many more quantizer codes. The digital filter does not have absolute zero response for the unsynchronized dither, but the response is quite low because it is very close to the null in the frequency response, so the resolution of the spectrometer is not substantially degraded by the dither.

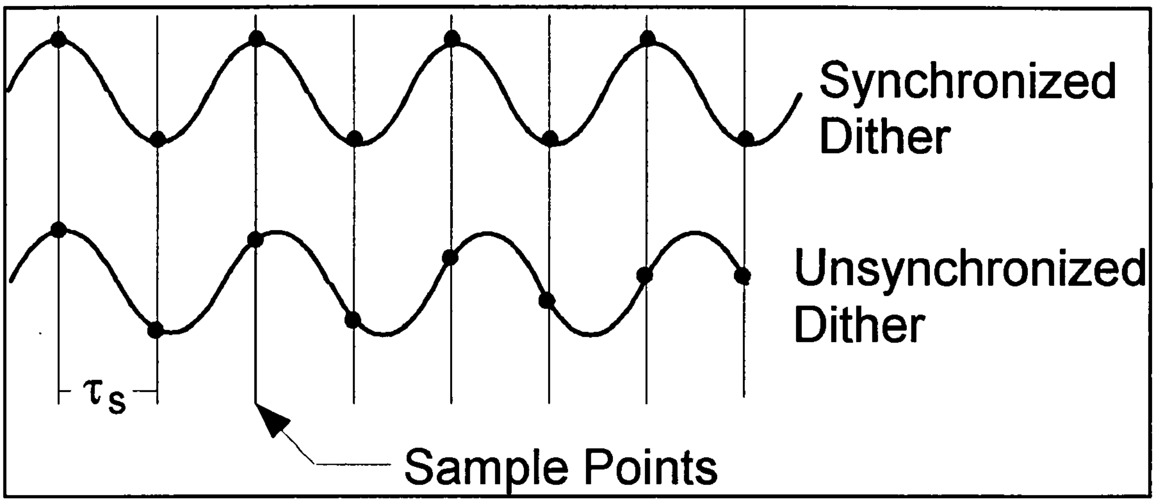

Figure 30. Sample Points on Synchronized and Unsynchronized Dither.

The dither signal which was actually implemented in the spectrometer was a nearly triangular signal with a frequency which was close to half the sampling frequency. Since a triangular waveform is composed of harmonics of its fundamental frequency, Equation (48) was satisfied.

Chapter III

Implementation

Figure 31 is a simplified block diagram of the circuitry which makes up the spectroscopy system. The Sampler Circuit accepts a preamplifier input and converts the analog waveform into a suitable digital one. Following the Sampler Circuit is a Digital Filter which implements the Quasi-Cusp filter. Finally the result of the digital filter is passed to a Digital Controller Circuit which forms a histogram of the data and provides an interface to the computer. This chapter gives a detailed description of each of the circuits.

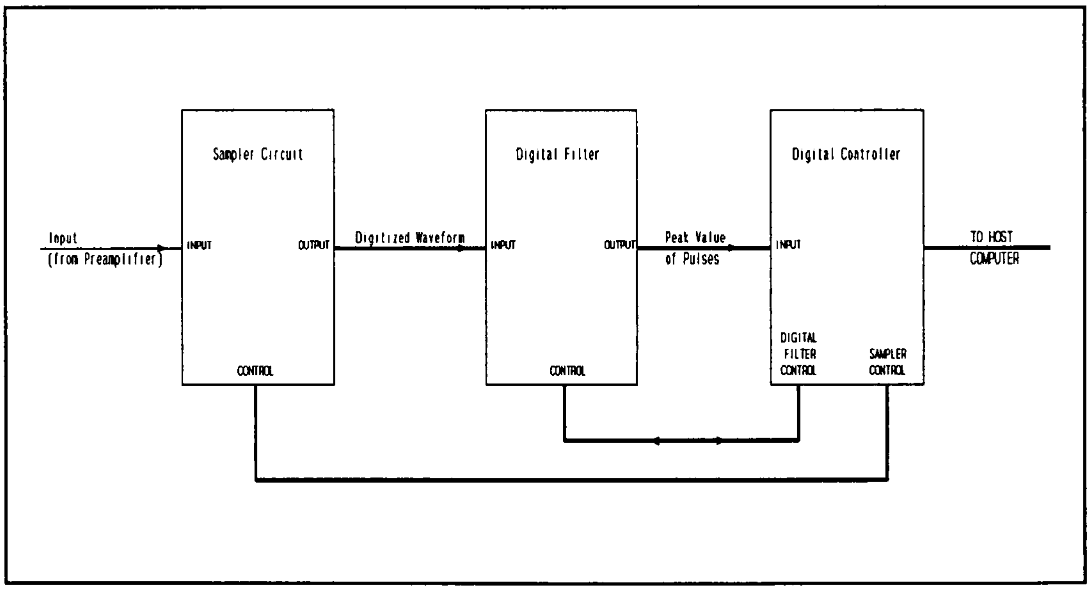

Figure 31. Block Diagram of the Digital Spectroscopy System

Sampler Circuit

The Sampler Circuit converts the preamplifier output signal into a digital waveform. The Sampler Circuit is composed of an input circuit, a gain and conversion circuit, a fast channel discriminator circuit and a dither circuit.

Input Circuit

The Input Circuit accepts the output of a standard Resistor Feedback or Transistor Reset Preamplifier and converts the signal to the proper polarity for further processing. Figure 32 is a block diagram of the input circuitry used in the system. Since different detectors have different polarity output signals, the input stage has a switch (S1) which can be used to make the stage non-inverting or inverting. In order to minimize the effect of noise in the later stages of circuit, this stage is normally configured to have a gain of two. However, in some high-energy applications, the gain must be lower than two, so the switch S2 permits the gain to be set to one or

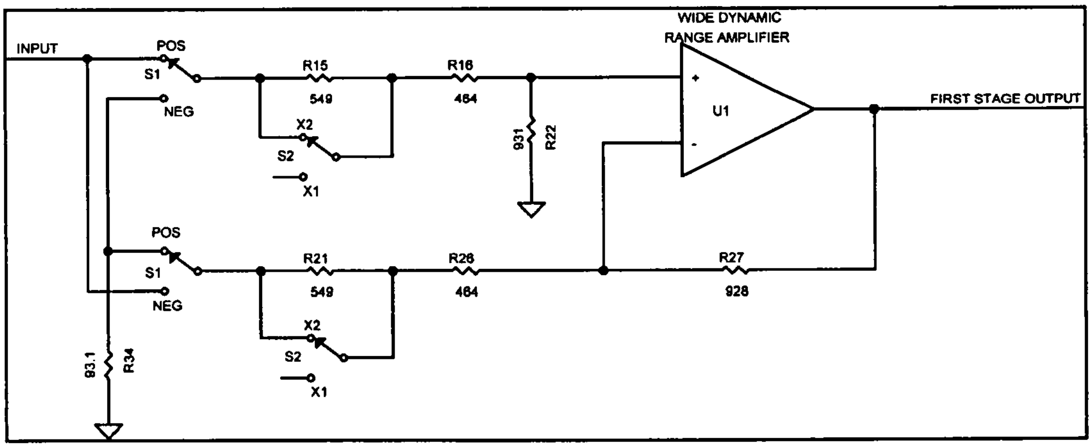

Figure 32. Input Circuit

two. The input stage must have a wide dynamic range due to the large voltage range of most preamplifiers, so the circuit was implemented with discrete transistors to maximize the linearity and the dynamic range of the stage.

Gain and Conversion Circuit

The Gain and Conversion Circuit accepts the signal from the Input Circuit and performs the following three functions:

- Applies pole-zero cancellation.
- Applies the appropriate gain.
- Converts the analog signal to a digital waveform.

Figure 33 shows a simplified schematic of the Gain and Conversion Circuit. As indicated in Figure 28, in order to achieve high data rates the input exponential time constant of the preamplifier must be reduced to reduce the number of pulses which saturate the quantizer. However, as indicated in Figure 24, if the time constant is too short, then the quantization noise becomes a major contributor to the noise of the spectrometer as the pulse widths increase. For these reasons, two different time constants were implemented in this design. One is used at long pulse widths to minimize the quantization noise, and the other is used at short pulse widths to minimize the number of pulses lost due to overrange errors.

Exponential pulses from a resistor feedback preamplifer have the following Laplace transform:

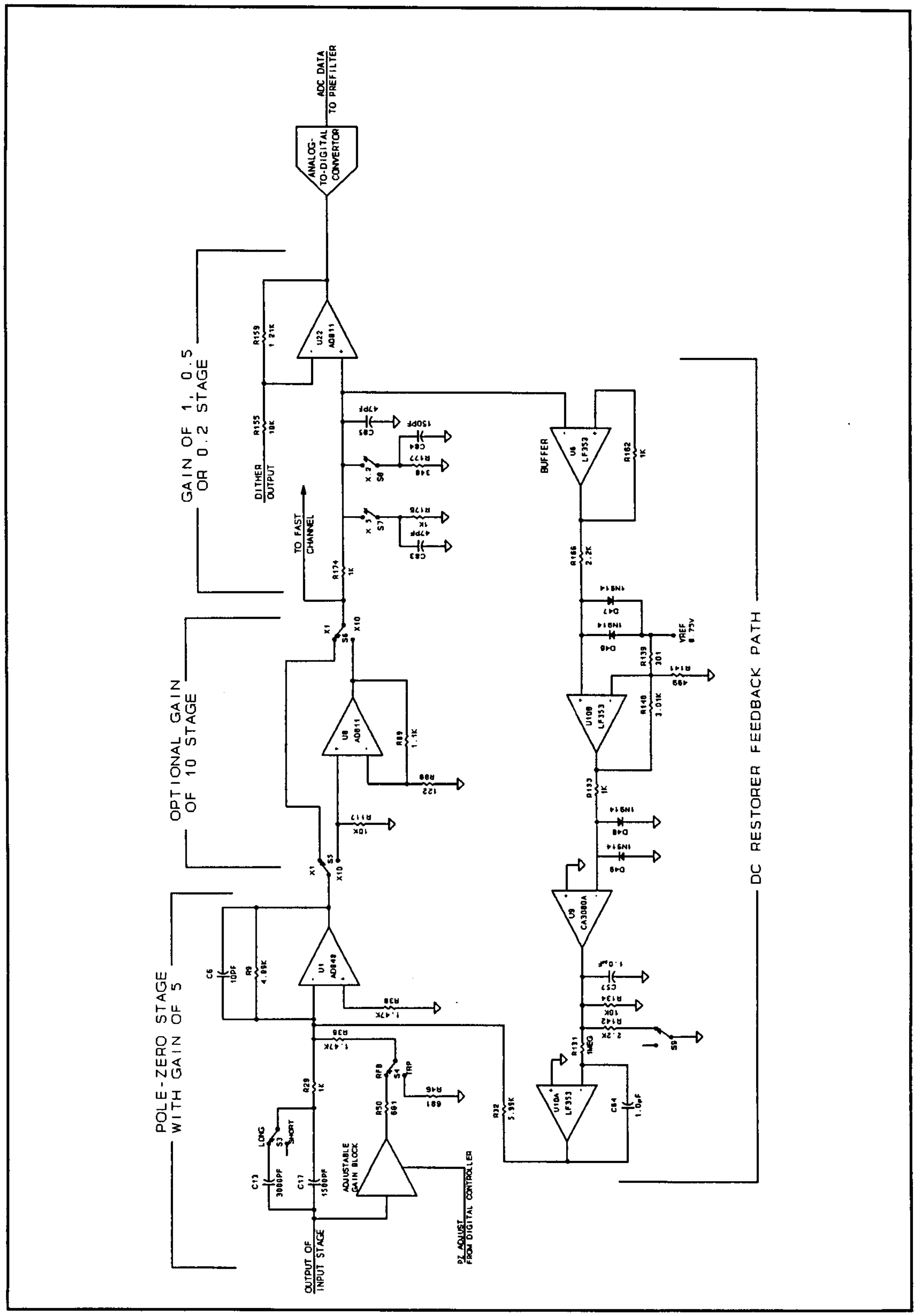

Figure 33. Gain and Conversion Circuit

$$Y(s)=\frac{1}{s+\frac{1}{\tau}} \tag{49}$$

where τ is the time constant of the exponential pulse. To convert the pulse into an exponential with a shorter time constant, a filter with the following frequency response must be employed:

$$H(s)=\frac{s+\frac{1}{\tau}}{s+\frac{1}{\tau_n}} \tag{50}$$

where τ_n is the new exponential time constant. In Figure 33, R29, C17, C13 and the adjustable gain amplifier perform this function. Switch S3 allows τ_n to be set to either 4.5 μs or 1.5 μs. The adjustable gain amplifier is used to match the filter to the exact time constant of the preamplifier pulse.

TRP preamplifier pulses, on the other hand, have a pulse shape which is a step. The Laplace transform of a step is

$$Y(s)=\frac{1}{s} \tag{51}$$

The appropriate filter for converting this signal into an exponential has a frequency response of

$$H(s)=\frac{s}{s+\frac{1}{\tau_n}} \tag{52}$$

This filter is implemented by placing switch S4 in the TRP position.

Once the input pulse is converted into an exponential with the desired time constant (τ_n), U1 amplifies the signal by a factor of five. If desired, an additional gain of ten can be inserted by placing switches S5 and S6 in the X10 position. The signal can then be attenuated by one-half by closing switch S7, or by one-fifth by closing both switches S7 and S8. Therefore, the signal may be amplified by 1, 2, 5, 10, 20, 50 or 100 before being digitized by the analog-to-digital converter. In order to reduce aliasing effects, most of the gain stages have been bandwidth limited to 5MHz or less. Capacitors C85, C84 and C83 perform this function in the attenuation stage.

Amplifier U22 buffers the attenuated signal and adds the dither before the signal is passed to the analog-to-digital converter. The analog signal is converted to a digital waveform with a 14-bit analog-to-digital converter (ADC) at a sampling rate of 10MHz. In order to maximize the use of the -1.25 volt to 1.25 volt input range of the ADC, a DC offset of 0.75 volts is added to the signal in the DC restorer feedback path.

In the DC restorer feedback path, U6 buffers the input signal and feeds it into a diode clamp (D46 and D47) which clamps at 0.6 Volts above and below 0.75 Volts. U10B then amplifies the signal by a factor of 10 and subtracts the equivalent of 0.75 Volts from the clamped signal. The output of U10B is then clamped at one diode drop above or below 0 Volts. This signal drives the transimpendence amplifier U9. The amplifier charges C57 while R134 and R142 continuously discharge C57. R142 is only switched in when the gain is greater than 10. The integrator stage composed of U10A, C64 and R131 integrates the voltage on C57 and feeds the result around to the input of the gain of five stage. The total effect of this circuit is to attempt to keep the DC level at the input of the ADC at 0.75 Volts. It is accomplished by clamping the unipolar pulses to a small amplitude and integrating the remaining DC level. Since the clamps do not clamp at exactly 0.75 Volts, as the pulse rate increases, the DC level at the ADC input shifts. This shift will be taken into account in the digital filter and removed by the digital baseline restorer.

Dither Circuit

The dither generation circuit is shown in Figure 34. The dither is derived from a 9.83MHz oscillator which is not synchronized to the system clock. The frequency is reduced to 4.915MHz with a divide by two circuit. This signal also has a duty cycle which is very close to 50 percent. This is important because any even harmonics in the dither signal get aliased at low frequencies which can be in the passband of the digital filter. For example the second harmonic gets aliased into 170 kHz which is in the passband of the digital filter at most pulse width settings. The 4.915MHz square wave is converted into an ECL waveform and passed to the analog board. On the analog board the signal is passed through a single pole low-pass filter to remove the high frequency components and summed into the main signal by amplifier U22.

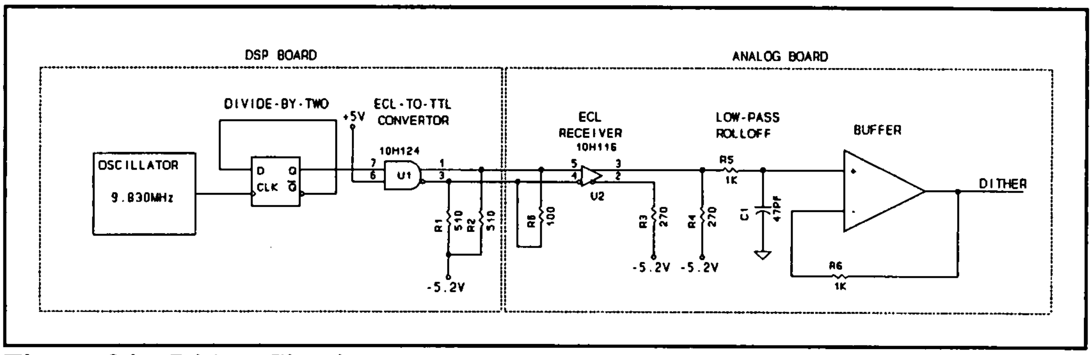

Figure 34. Dither Circuit

Fast Channel Circuit

The Fast Channel is an analog circuit which is used to generate a fast discriminator signal (FD) which indicates that a pulse is arriving at the ADC input. The fast channel is a standard circuit used in many commercial analog spectroscopy systems. A simplified schematic is show in Figure 35. Buffer U13 isolates the fast channel circuit from the gain circuitry. The fast channel filter converts the exponential signal from the gain stage into a narrow pulse. Figure 36 illustrates the effect of the fast channel filter by showing the voltage across R73 in response to an exponential pulse with a 4.5 μs time constant. Switch S3 allows the fast channel circuit to operate with either a 4.5 μs or a 1.5 μs exponentially shaped input pulse. The fast channel amplifier (U14) has a gated baseline restorer around it that stabilizes the DC level at the amplifier output at zero volts. A comparator (U5) triggers when the fast discriminator pulse exceeds the fast threshold. An automatic thresholding circuit, which assumes that the noise on the signal is symmetrical around zero volts, determines the fast threshold by setting the threshold to a fixed fraction above the average peak height of the negative noise pulses on the signal. When the reset occurs

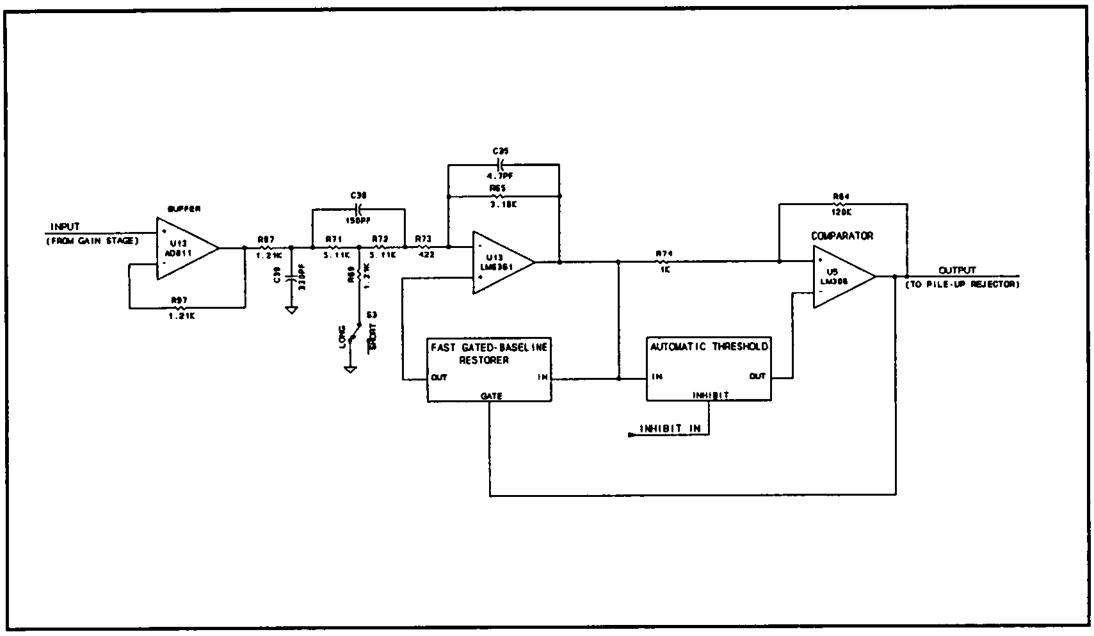

Figure 35. Fast Discriminator Circuit

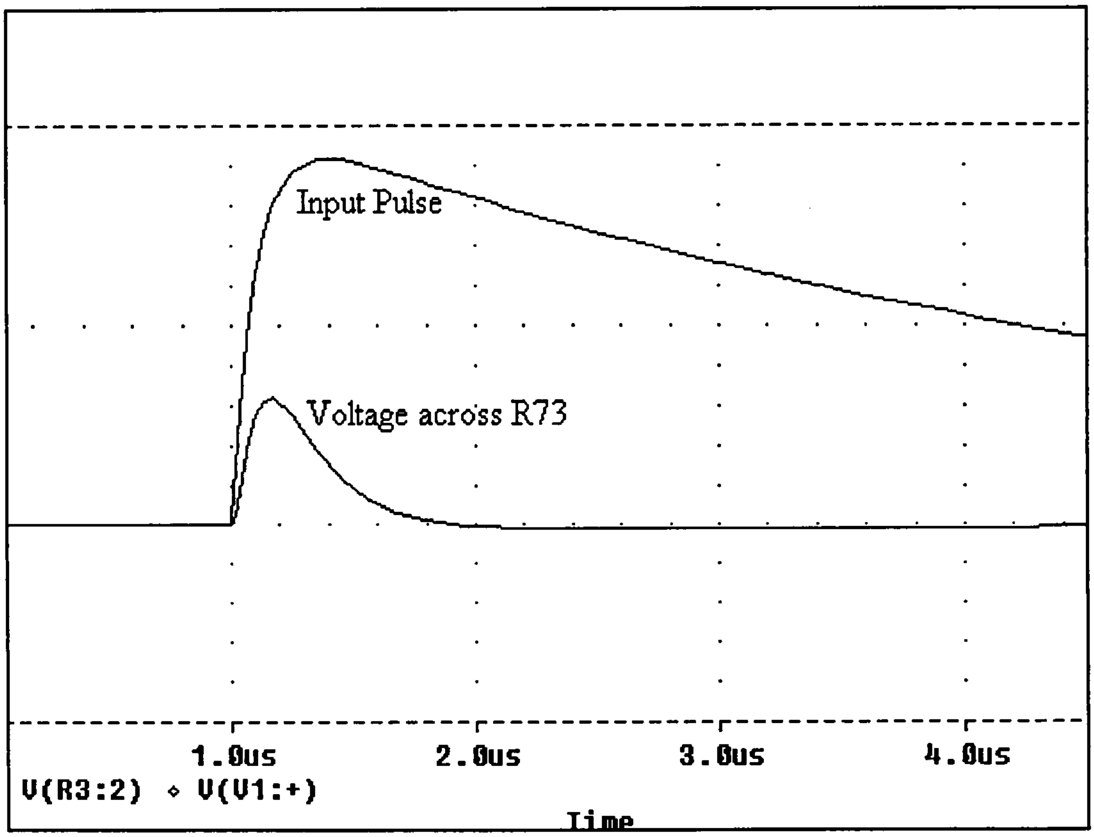

Figure 36. Fast Discriminator Input and Output Pulses

on a transistor reset preamplifier, the fast channel input has a large negative pulse. Normally this would cause an error in the automatic threshold circuit; however, the inhibit input turns off the automatic threshold when the reset occurs to avoid the problem. The fast discriminator output signal is used by the pile-up rejection circuitry to determine when pulses are too close together to be properly analyzed.

Digital Filter

A simplified schematic diagram of the digital filter implementation is shown in Figure 37. The digital filter consists of a prefilter implemented in a field programmable gate array (FPGA), four digital signal processors (DSP) which implement the main filter, a clock generator circuit, a peak detection circuit and a thresholding circuit.

Clock Generator

The clock generator keeps all of the various parts of the digital filter synchronized. All of the clock signals are derived from a single 40MHz oscillator which directly drives each of the four DSP chips. The 40MHz clock is divided by four to generate a 10MHz clock used by the prefilter and the ADC. Finally, the 40MHz clock is divided by 16 to create the SYNC signal with a pulse width of 100ns and a period of 400ns. The SYNC signal guarantees synchronization between the DSPs.

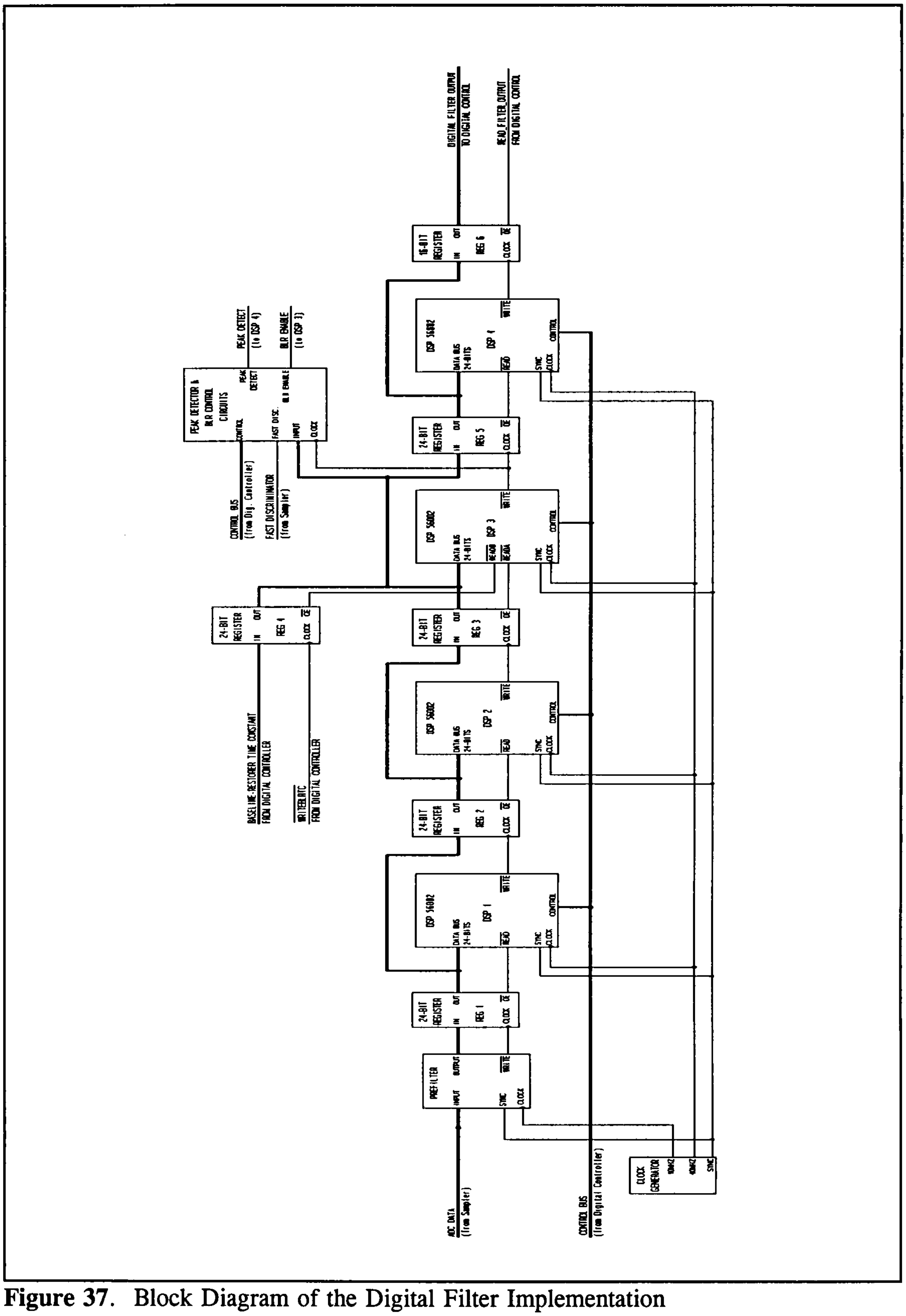

Figure 37. Block Diagram of the Digital Filter Implementation

Prefilter

The prefilter accepts 14-bit data from the ADC at a rate of 10MHz, filters the data and outputs an 18-bit data word at 2.5MHz. Decimation of the data is necessary because the DSP chips have a cycle time of 50ns. Without the prefilter, the DSPs have only two cycles for each incoming digital value. After decimation, eight cycles are available in each DSP chip for each incoming data point. An unfortunate consequence of the decimation process is that the minimum rise time (τ_1) can be no shorter than 0.8 μs and is adjustable in units of only 0.8 μs. Also the flattop width (τ_2) can be no shorter than 0.8 μs and is adjustable in units of only 0.4 μs. If the main filter could keep up with the ADC, much shorter pulse shapes would be possible. The prefilter implements a second-order Sinc decimator as described by Candy and Temes[26]. The decimated signal is placed in the 24-bit register for use by the first DSP.

Quasi-Cusp Filter

The remaining portion of the digital filter was implemented with four Motorola DSP56002 DSP chips operating at 40MHz. The DSP56002 is a 24-bit fixed-point DSP which is capable of performing a multiply and accumulate operation along with two memory moves in two clock cycles. Since each DSP chip has only 16 cycles (40MHz/2.5MHz) to operate on each data word exiting the prefilter, the processing chain has been optimized to maximize the number of cycles available for actual filtering operations. As a result, the DSPs are synchronized, and are programmed to expect data to arrive at their input at precisely the correct time. This approach eliminates the time consuming operation of checking to see if data is at the input before acting on it. The consequence of this design approach is that the interface circuit between the processors is very simply, just a 24-bit register. DSP 1 writes data to the register (REG 1) just before DSP 2 is expecting new data. DSP 2 then reads the data just before DSP 1 writes the next value in the register. The synchronization signal from the clock register starts all of the DSP programs together, from that point the programs naturally stay synchronized due to the fixed number of cycles in each program.

DSPs 1 and 2 implement the Quasi-Cusp filter. DSP 3 implements the digital baseline restorer. Register REG 4 is used to pass the baseline restorer time constant to DSP 3. This register is loaded by the microprocessor controller. The BLR time constant can change during an acquisition, so a separate data path is required to get the value into the DSP without disturbing the synchronization of the DSP programs. DSP 3 also has two output paths. The first path is to DSP 4 which selects the peak of the pulse, applies the fine gain and outputs the value to the microprocessor. The second path is to the peak detector and baseline thresholding circuitry. Comparing two values and acting on the result consumes several cycles in most DSP chips. For example, in the Motorola DSP56002, comparing two values requires two cycles and acting on the compare with a jump instruction requires four cycles. However, compare operations are quite simple with field-programmable gate arrays. Since the BLR control and peak detection functions have a number of compare operations they were implemented in a field-programmable gate array. DSP 4 uses the Peak Detect signal to select peaks in the digital waveform and DSP 3 uses the BLR enable signal to determine when the baseline restorer should be turned off and on.

Two 256 x 24-bit data memories and one 512 x 24-bit program memory are built into the Motorola DSP56002, so no external memory is required. The digital controller downloads the correct program into each DSP program memory via the Host Port on the DSP560002. While the filter is operating, the internal data memory is used to implement the delay operations in the filter and for general storage.

Peak Detector

In the spectrometer, the amplitude of the output pulses is the information which is of interest, so the peak amplitude of each pulse must be located accurately. The peak detector should be sensitive enough to catch all of the legitimate pulses, but not so sensitive that it continuously triggers on small noise pulses causing time to be wasted on invalid pulses. A pattern matching algorithm which operates on the polarity of the first difference of the output waveform was employed to locate the peaks of the output pulses in this design. The pattern which is matched is defined with three programmable parameters which are defined as:

PP = Number of positive points to find.

PS = Number of points to skip.

PN = Number of negative points to find.

A peak is detected when the slope of the output waveform is positive for PP points in a row followed by PS points in a row in which the slope can be either polarity followed by PN points in a row in which the slope is negative. Figure 38 shows a block diagram of the circuit which determines the polarity of the slope of the filtered waveform. Register REG1 delays the waveform by one clock cycle. Comparator CMP2 compares the current amplitude to the amplitude of the delayed point to generate a SLOPE signal which is active when the waveform increases in value. Figure 39 shows a block diagram of the circuitry which performs the pattern matching function. CNT1 is a down counter which is loaded with PP whenever the SLOPE signal is low. When CNT1 reaches 0, the POSOK signal goes active and disables further counting by the counter. The POSOK signal will only return inactive when the SLOPE signal returns inactive. POSOK indicates that at least PP points in a row have a positive slope. CNT2 operates like CNT1 except SLOPE is inverted, so

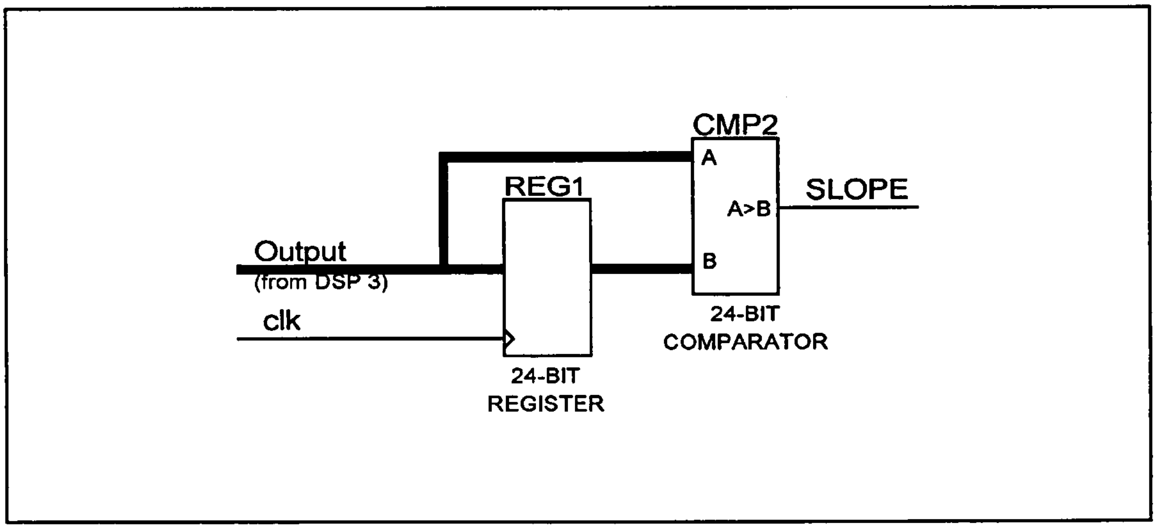

Figure 38. Circuit to Generate SLOPE Signal for Peak Detector.

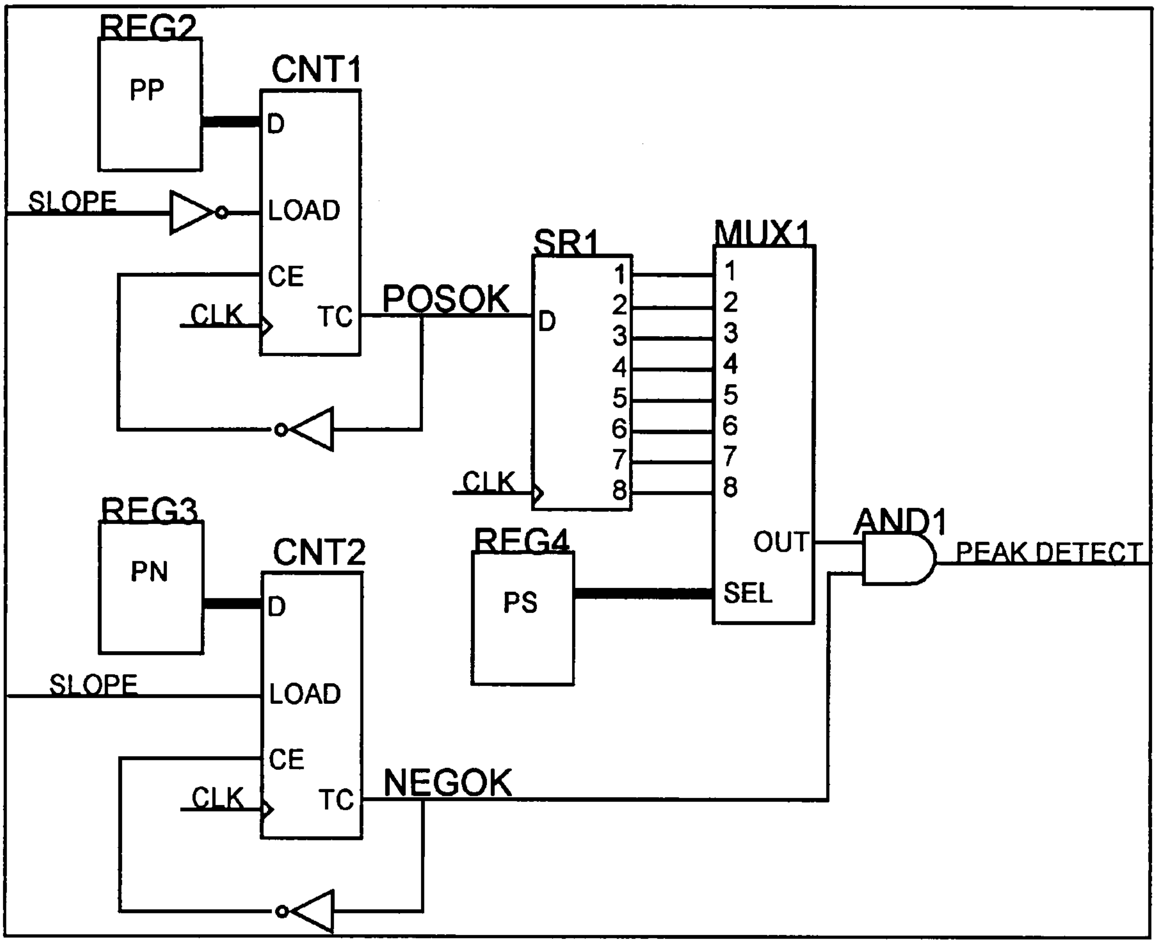

Figure 39. Peak Detection Circuit.

NEGOK indicates that at least PN negative points have occurred in a row. Shift Register SR1 and Multiplexer MUX1 effectively delay the POSOK signal by PS points. The gate AND1 combines the delayed POSOK signal and NEGOK signal to generate a peak detect signal. Since the peak detect signal does not occur for PN points after the peak of the pulse, the output waveform must be delayed for PN points to align the peak detect signal with the output waveform. Registers REG2, REG3 and REG4 are loaded by the digital controller at the beginning of an acquisition.

Digital Controller

The Digital Controller function is performed by a custom designed microprocessor board which uses an INTEL i386 processor running DOS. A DOS based controller board simplified the programming task as a standard C compiler could be used to write the control program and standard drivers could be used to implement the Ethernet interface which was used to communicate with the host computer. The microprocessor oversees the setup and operation of the entire system by performing the following tasks:

- Sets the gain and shaping of the preamp signal before the signal is digitized.
- Loads the control programs into the DSPs and the FPGAs.
- Loads the digital shaping parameters into the DSPs.
- Forms a histogram of the peak values which exit the digital filter forming a spectrum of the number of pulses received versus the amplitude of the pulse.
- Assists in determining and setting the baseline restorer time constant in real time.
- Assists in setting the positive and negative thresholds in real time.
- Keeps track of the real and live times in real time.
- Handles all communication with the host computer.

Chapter IV

Results

This Chapter contains the experimental results obtained with the spectrometer which implemented the digital filter. Detector resolution measurements show that including the cusp in the digital filter does indeed improve the resolution at longer shaping times. They also show substantial improvement in resolution due to the elimination of the ballistic deficit errors at short pulse widths. The improvement in peak shift due to the addition of the dither is shown along with data which shows that the gated baseline restorer keeps the peak position stable with changing conditions.

Detector Resolution

As outlined in Chapter I, the resolution of a particular peak in a spectrum is mainly a function of the intrinsic detector resolution, the step noise contribution, delta noise contribution and the contribution due to ballistic deficit effects. A particular filter has no effect on the intrinsic detector resolution, but the other three are affected by the shape of the filtered pulse.

Effect of the Cusp Factor on Detector Noise

Figure 13 demonstrated the ideal effect on the delta and step noise combination as a function of peaking time and the cusp factor. To measure this effect with the spectrometer, it is necessary to remove the intrinsic detector resolution and the ballistic deficit contribution from the measurement. This is most easily accomplished by randomly selecting points from the output of the digital filter while no source of radiation is in front of the detector and forming a histogram. The resulting histogram is composed of a peak at Channel zero and a small number of counts at higher channels due to background radiation entering the detector. The resolution of the peak at Channel 0 is a measure of the noise contribution from the delta and step noise sources. Figure 40 shows the result of such a measurement. The data were collected with a flat top setting of 1.2 μs with a small HPGe detector suitable for low energy applications. As shown in the Figure, the $\alpha=0.5$ curve has the smallest noise at longer peaking times and the $\alpha=1$ curve has the smallest noise at shorter peaking times as expected.

Comparing the results in Figure 40 with the ideal noise curve in Figure 20 requires curve fitting to determine relative contributions of the step, delta and *1/f* noise sources. To this point the *1/f* noise source has been largely ignored because the shape of the filtered pulse has little effect on the total output noise due to *1/f* sources. However, to fit the measured noise to an ideal noise model, the *1/f* noise source must be considered.

A graphical construction of the three main noise types was performed on the $\alpha=0.5$ data from Figure 40 and is reproduced in Figure 41. Referring to the figure, the *1/f* noise component is constant with changing τ_1, the step noise component is proportional to τ_1 and the delta noise component is proportional to $1/\tau_1$. The portion

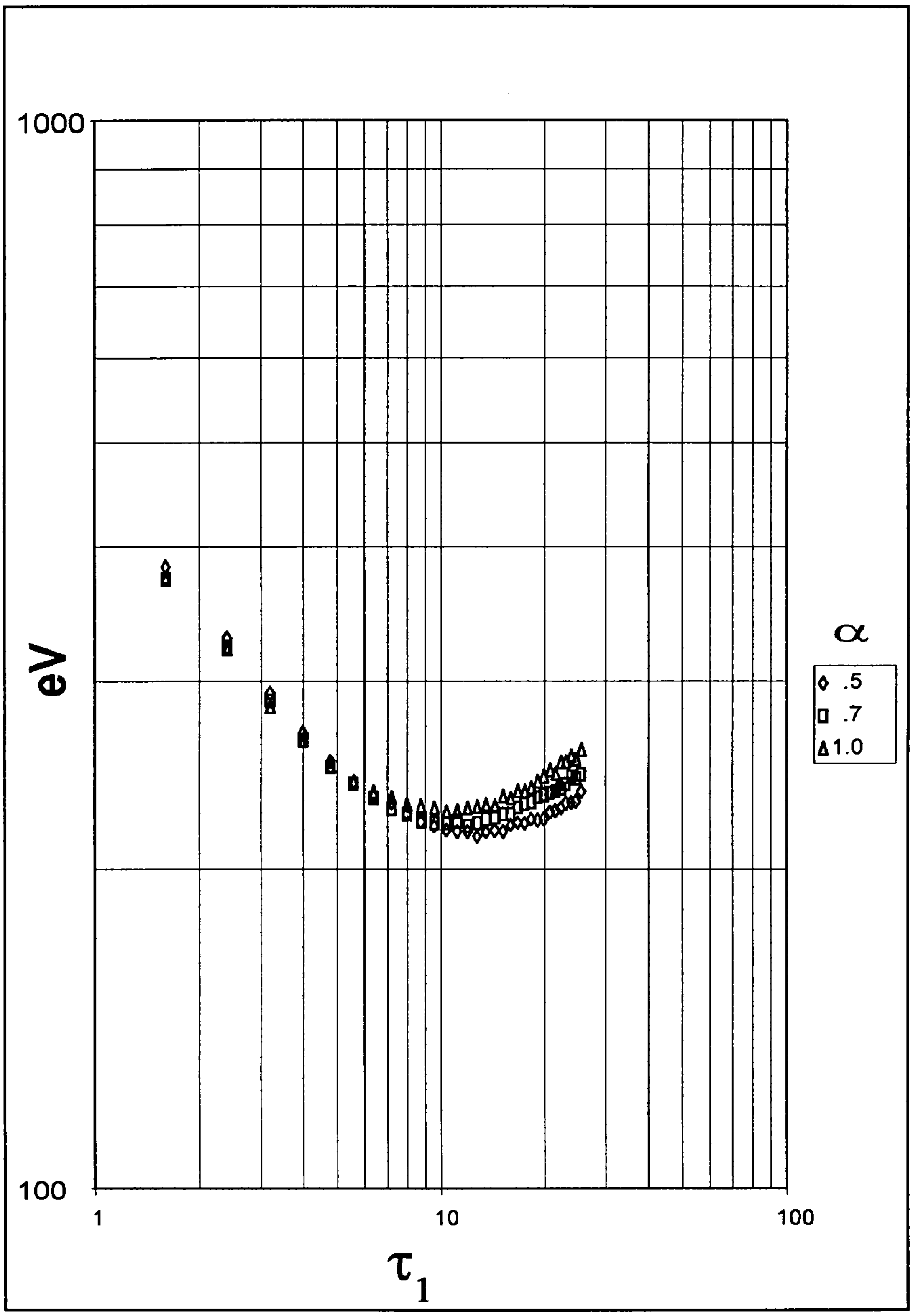

Figure 40. Measured Noise as a Function of Peaking Time and Cusp Factor.

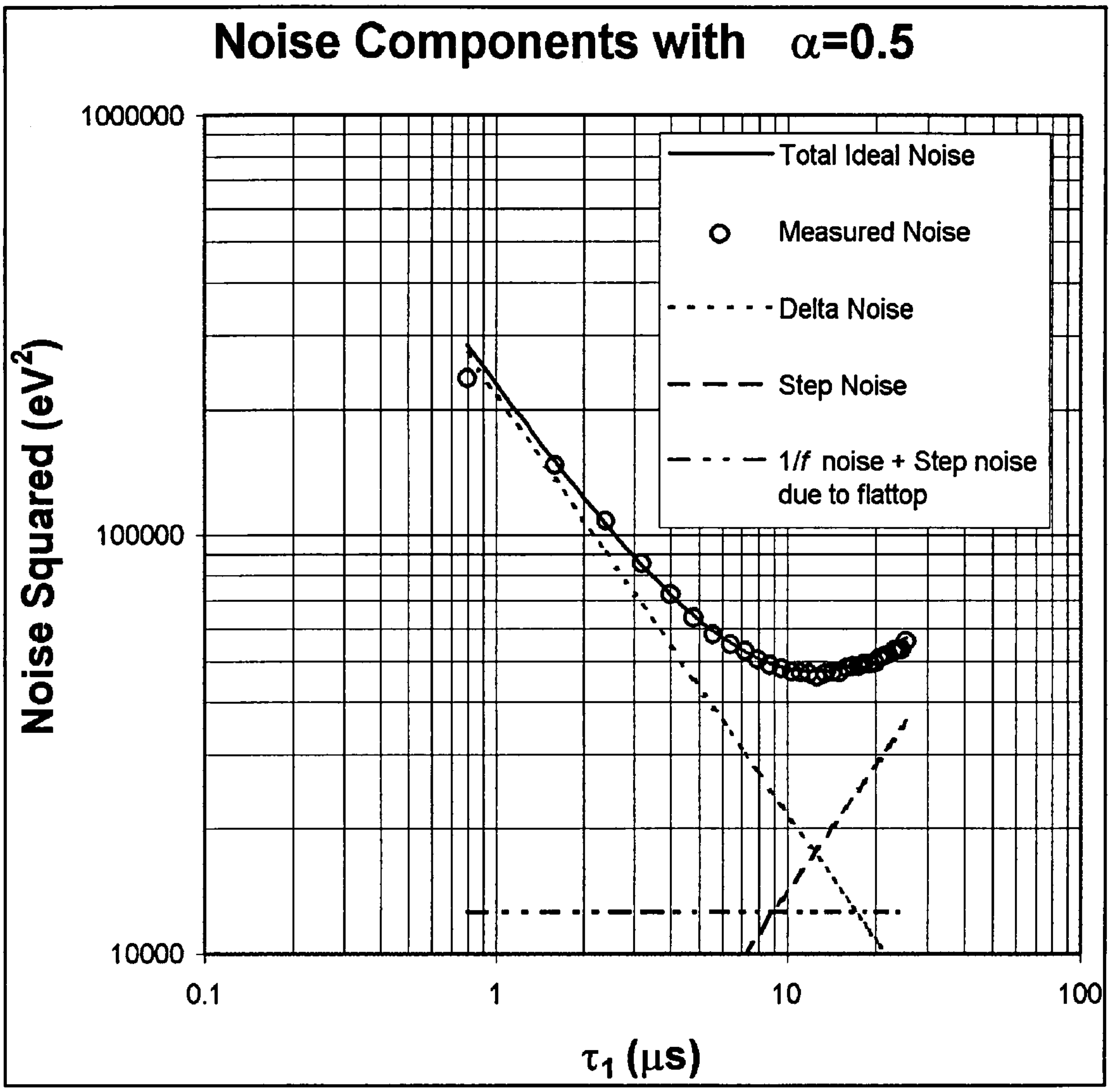

Figure 41. Resolution with $\alpha=0.5$ with Ideal Noise Components.

of the step noise index which is proportional to the flattop width (τ_2) is independent of τ_1, so it was included with the *1/f* contribution. The resulting ideal noise curve matches closely with the measured data except at the shortest rise time.

A possible explanation for the poor matching at the shortest pulse width is that the prefilter, which is used to decimate the data from the ADC before the quasi-cusp filter, is effectively increasing the length of τ_1 by a small amount. So the data point at $\tau_1=0.8$ μs should be at 1 μs. At the shortest shaping time, errors in τ_1 have the greatest impact, so it is possible that all of the τ_1 values should be larger. There is further evidence indicating this is the case in that the ideal throughput at $\tau_1=0.8$ μs should be 76,000 counts per second (using Equation (15)), but only 70,000 counts per second was achieved. A pulse with a rise time of 1 μs and a 1.2 μs flattop would have an ideal throughput of 70,000 counts per second.

Using the step, delta and *1/f* noise contributions experimentally found in Figure 41, the step and delta noise contributions were calculated for $\alpha=1$ using the step and delta noise indices. (See Equations (18) and (19).) This ideal noise curve was plotted along with the measured $\alpha=1$ data in Figure 42. Once again there is good agreement except at the shortest rise time.

Ballistic Deficit Improvement

The flat top portion of the quasi-cusp filter removes most of the errors made due to ballistic deficit. In order to evaluate the improvements, it is useful to compare the resolution measured with the digital filter to measurements made with a standard analog system in which the shaping filter does not have a flat top. Since the width of the shaped pulse has a drastic effect on the resolution and the total pulse throughput of the system, a good way of comparing pulse shapes is to determine the resolution obtained with filters which have similar maximum throughput values.

The maximum throughput is determined by placing a source of radiation in front of the detector, collecting pulses for a fixed period of time, and counting the total number of pulses processed by the spectrometer. Moving the source closer to

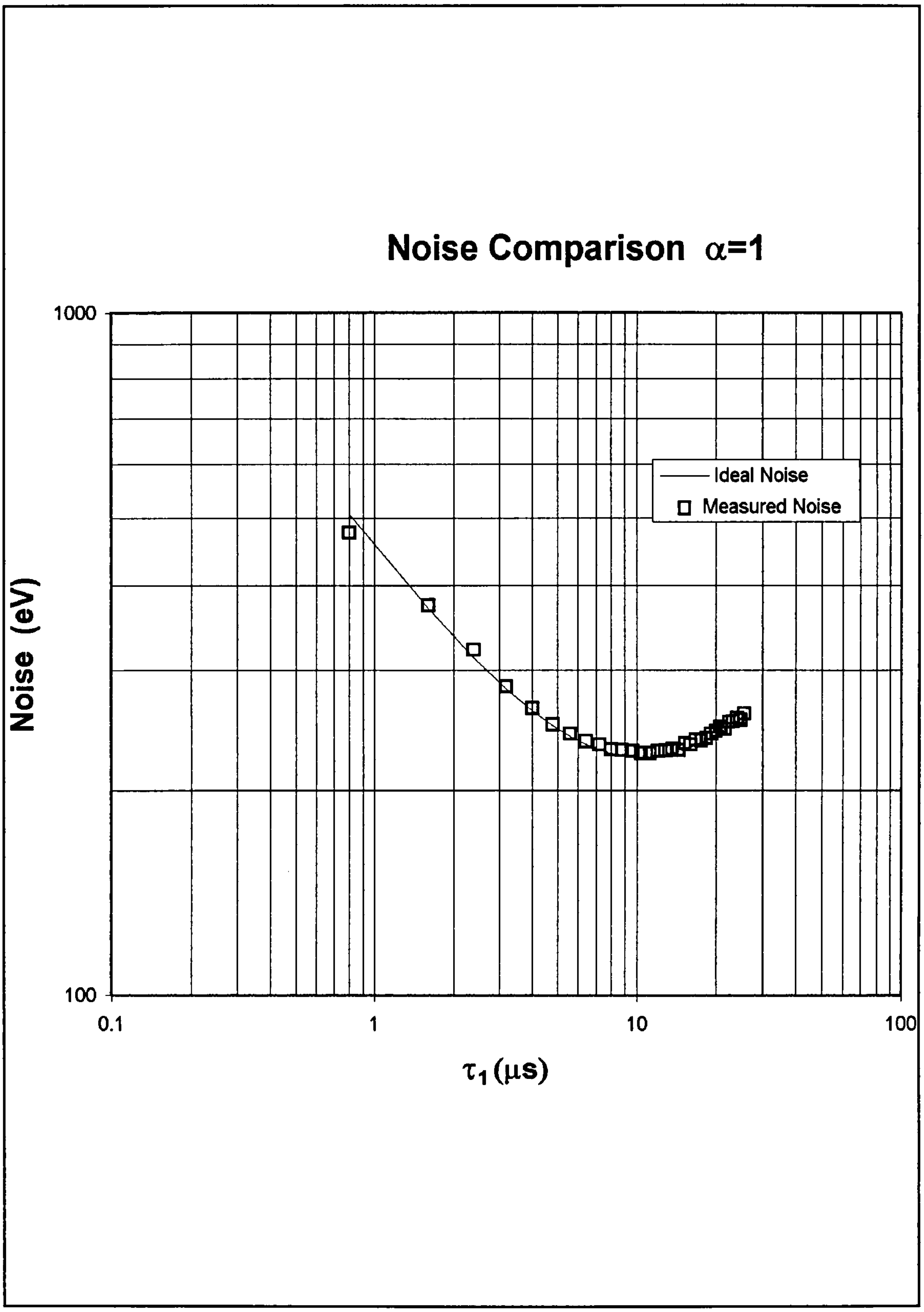

Figure 42. Measured and Ideal Noise with $\alpha=1$.

the detector causes the number of pulses to increase up to a maximum before pile-up effects cause the number to decrease (See Figure 16). The maximum throughput is the maximum number of pulses obtained divided by the collection time. In order to automate this type of measurement, the measurement system shown in Figure 43 was designed. In the system, the computer which is used to control the digital spectrometer also moves a radioactive source allowing automatic changes in counting rate. To move the source, the computer drives a stepper motor which turns a long screw. A trolley is mounted on the screw such that it moves up or down the screw depending on which way the screw is turning. The EG&G ORTEC 974 counter/timer counts the number of pulses which occur for one second and reports that number to the computer. With this arrangement, spectra can be collected at multiple counting rates and pulse settings without operator intervention.

Using the measurement system, the maximum throughput along with the resolution at 1.3 MeV for each setting of τ_1 was determined and is shown in Table I. During the measurement, τ_2 was set to 1.2 μs. A very large (140% efficient, P type) detector was used to make the measurements because large detectors have longer collection times and as a result are more susceptible to ballistic deficit errors. A similar measurement was made with an analog system composed of an EG&G ORTEC 672 amplifier and an EG&G ORTEC 921 spectroscopy ADC (see Figure 44) with the results shown in the bottom of Table I. The 921 has an effective conversion time of 1.5 μs, so the ADC has very little impact on the performance of the system.

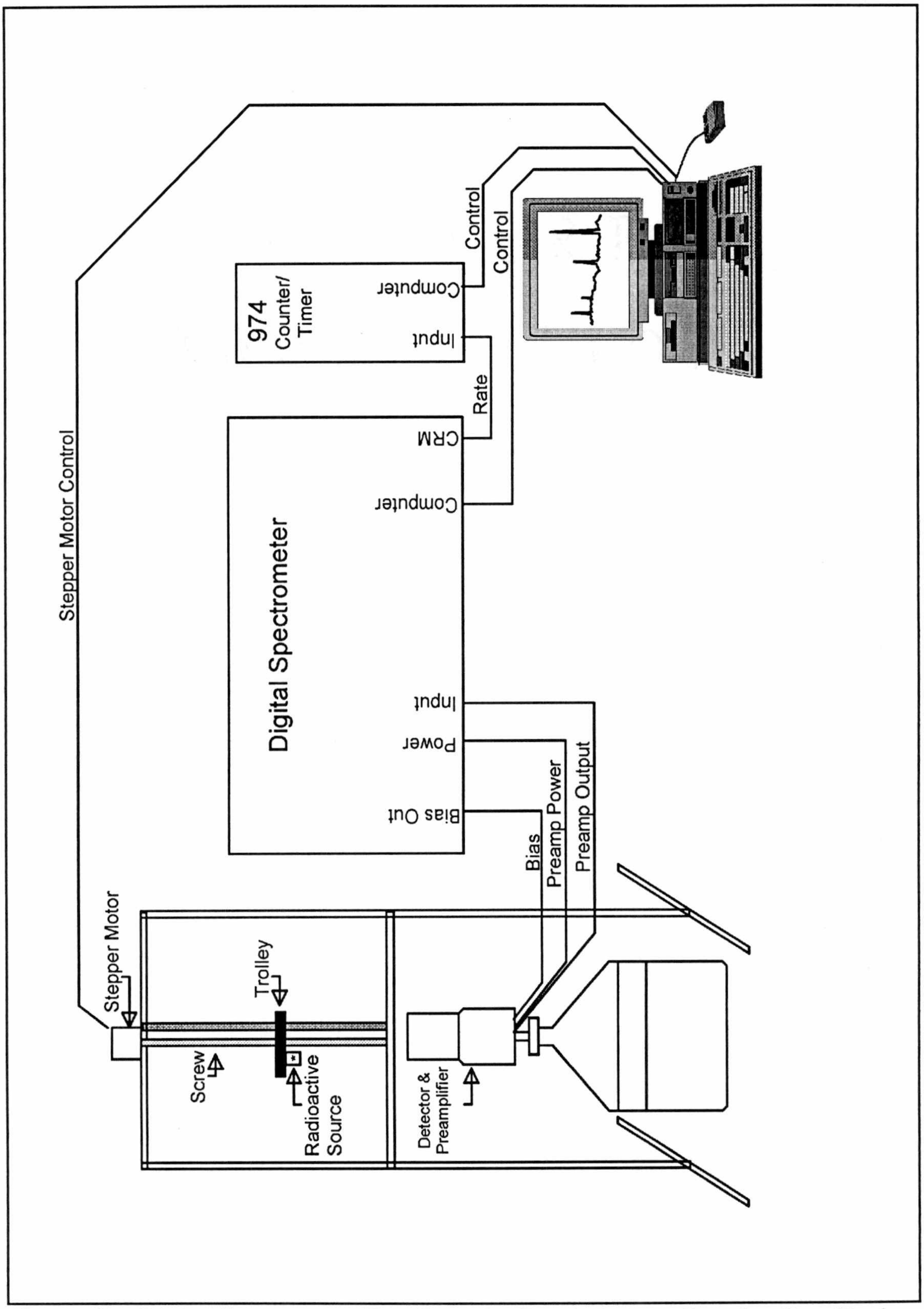

Figure 43. Digital Spectrometer Test Setup for Resolution vs. Counting Rate Testing.

Table I. Maximum Throughput versus τ_1. Measured with 140% Efficient P-type Detector with Resistor Feedback Preamplifier using Co-60.

Digital Filter					
Rise Time τ_1 (μs)	Maximum Throughput (cps)	Resolution 1.33MeV (keV)	Rise Time τ_1 (μs)	Maximum Throughput (cps)	Resolution 1.33MeV (keV)
0.8	69700	3.67	13.6	8500	1.79
1.6	48200	2.78	14.4	8300	1.82
2.4	36600	2.22	15.2	7800	1.84
3.2	29600	2.06	16.0	7500	1.79
4.0	24700	2.04	16.8	7100	1.79
4.8	21600	1.96	17.6	6800	1.83
5.6	18600	1.92	18.4	6500	1.85
6.4	17000	1.87	19.2	6300	1.86
7.2	15400	1.84	20.0	6000	1.82
8.0	14100	1.86	20.8	5800	1.83
8.8	12900	1.78	21.6	5600	1.84
9.6	11900	1.81	22.4	5400	1.82
10.4	11300	1.81	23.2	5200	1.85
11.2	10500	1.79	24.0	5000	1.84
12.0	9800	1.82	24.8	4900	1.85
12.8	9100	1.83	25.6	4800	1.87
Analog Filter System					
Shaping Time (μs)	Maximum Throughput (cps)	Resolution 1.3MeV (keV)	Shaping Time (μs)	Maximum Throughput (cps)	Resolution 1.3MeV (keV)
0.5	70000	38.71	3	14000	2.35
1	41000	15.46	6	7100	1.82
2	21000	4.04	10	4200	1.95

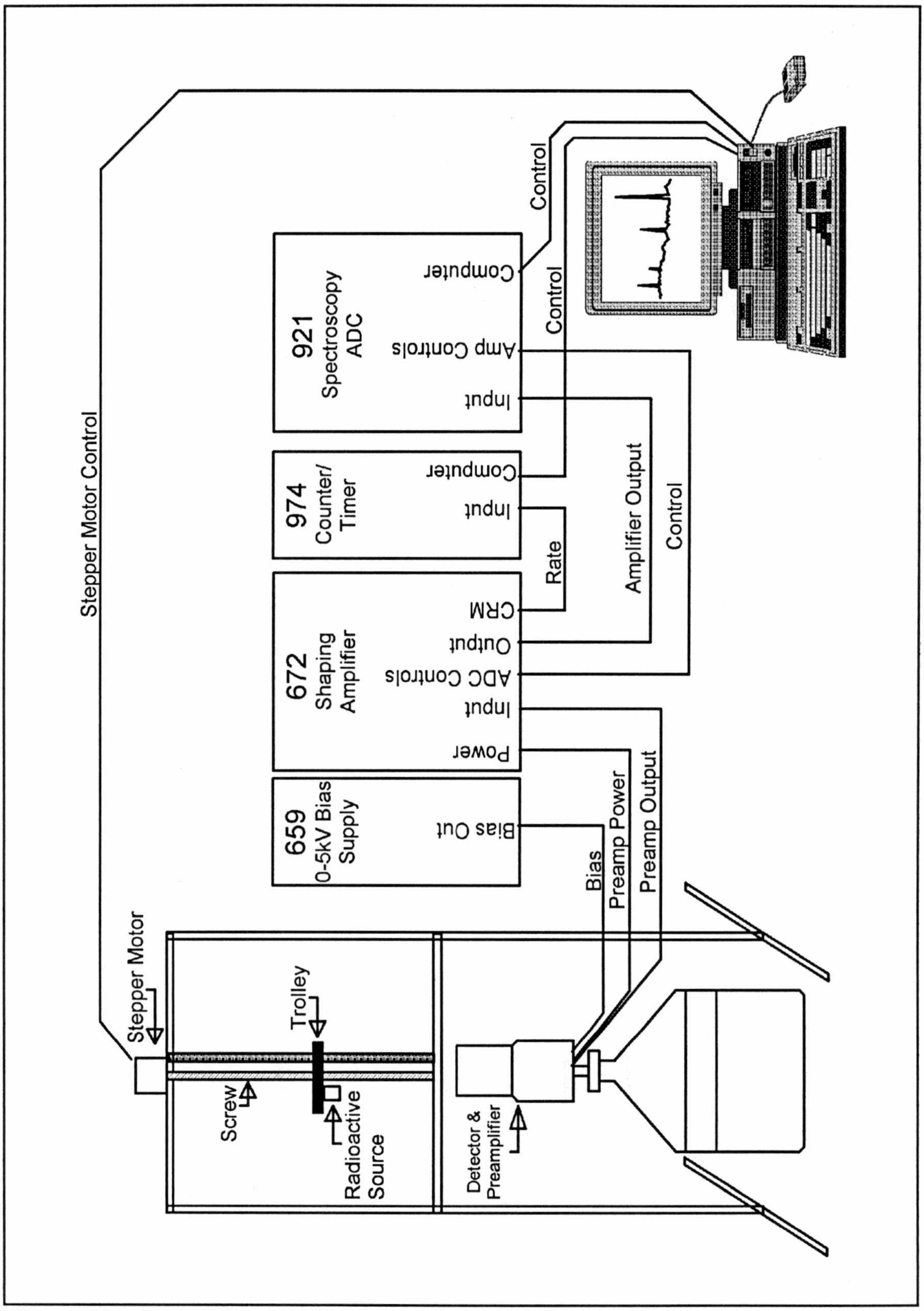

Figure 44. Analog Spectrometer Test System.

The amplifier is capable of generating a number of pulse widths referred to as shaping times on the 672.

To make the comparison between the analog and digital system, compare the resolution obtained with the two systems at filter widths that give equal maximum throughputs. For example, the digital filter has a maximum throughput of nearly 70,000 cps at τ_1=0.8 μs and the analog system has a maximum throughput of 70,000 cps at 0.5 μs shaping, so these two pulse widths are comparable. From the table, the resolution of the digital system at τ_1=0.8 μs was 3.67 keV while the measured resolution of the analog system was an order of magnitude worse at 38.71 keV.

Quantizer Overrange Losses

The results of the overrange losses calculation in Chapter II can be verified experimentally on the spectrometer with a pulse generator which can generate randomly (Poisson) distributed constant amplitude pulses. For this measurement a Berkeley Nucleonics Corp. DB-2 Random pulser was used as the input to the spectrometer and the losses due to saturation of the quantizer were determined at a number of quantizer range and input rate settings. Figure 45 shows the results of the measurements with the ideal curves repeated on the same graph. The measured losses are slightly higher than the calculated losses at all settings. Slight errors are not surprising due to the truncation of the exponential in the theoretical calculation.

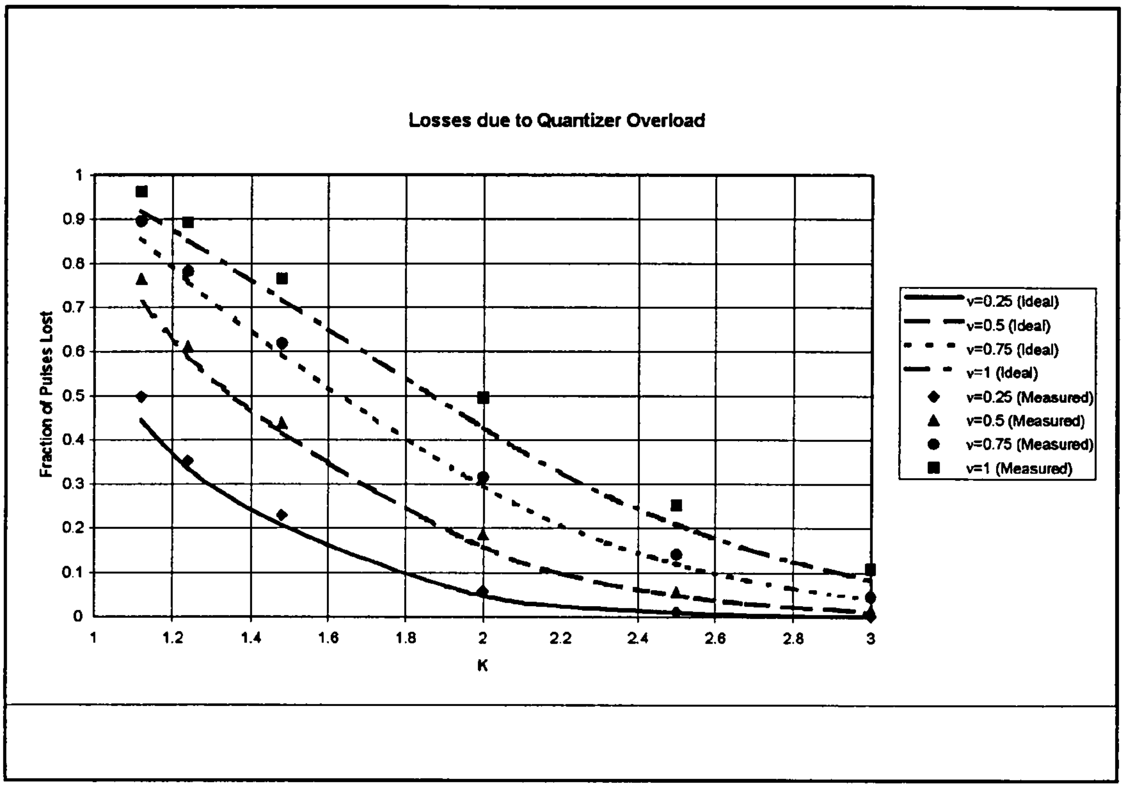

Figure 45. Measured and Theoretical Losses due to Quantizer Saturation.

Furthermore, only the first 10 terms of Equation (41) where used to compute the theoretical losses. Omission of the higher order terms would tend to give optimistic results.

Quantization Noise

As outlined in Chapter II, the output noise due to quantization is a function of the exponential time constant (τ_p) of the input pulse and the rise time of the output pulse (τ_1). In order to verify the theory, the effect of the quantization noise was measured by measuring the noise at the output of the digital filter at different τ_p and τ_1 settings with the spectrometer input shorted to ground. The noise was measured by randomly sampling the output of the digital filter and forming a histogram of the sampled values. The Full-Width at Half the Maximum (FWHM) of the resulting peak is a measure of the noise of the system. In order to have a peak which covers more than just a few channels in the spectrum, the gain of the digital filter was increased by a factor of three over the normal gain.

Figure 46 shows the measured results versus the theoretical results. In this figure, the theoretical curves were found by assuming that the measured noise at the data point in which τ_p=0.5 and τ_1=12.0 μs was exactly correct. All other curves were referenced to this single point. The measured results closely match the calculated noise.

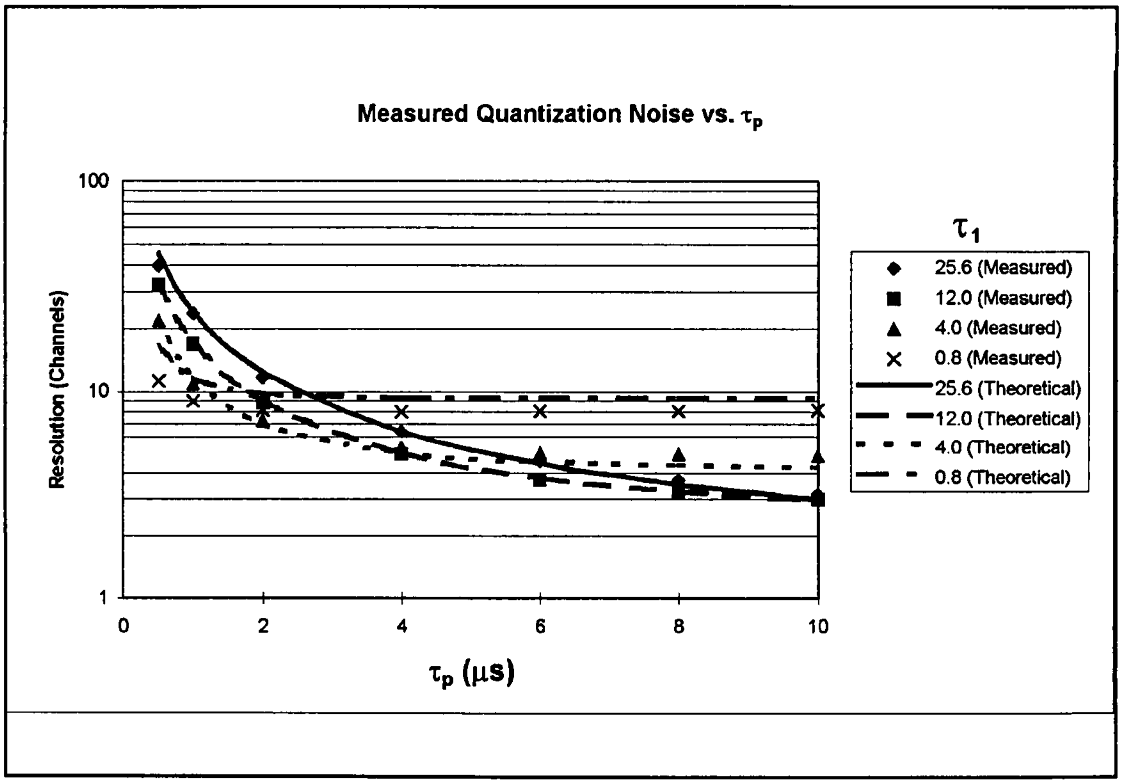

Figure 46. Quantization Noise Versus τ_1 and τ_p.

Effect of the Dither

The dither signal was included in the spectrometer to eliminate the undesirable peak shift which occurs when the offset voltage of the signal to be quantized shifts due to temperature or count rate changes. In order to demonstrate the improvement in performance that the dither provides, a low-noise pulser signal was connected to the input of the spectrometer and a small adjustable offset voltage was added to the signal at the ADC input. Peak shift as a function of the offset voltage was recorded with the dither signal enabled and disabled. As seen in Figure 47, the peak shift is an order of magnitude smaller when the dither signal is enabled. The inclusion of the dither signal did have a measurable effect on the measured resolution of the pulser

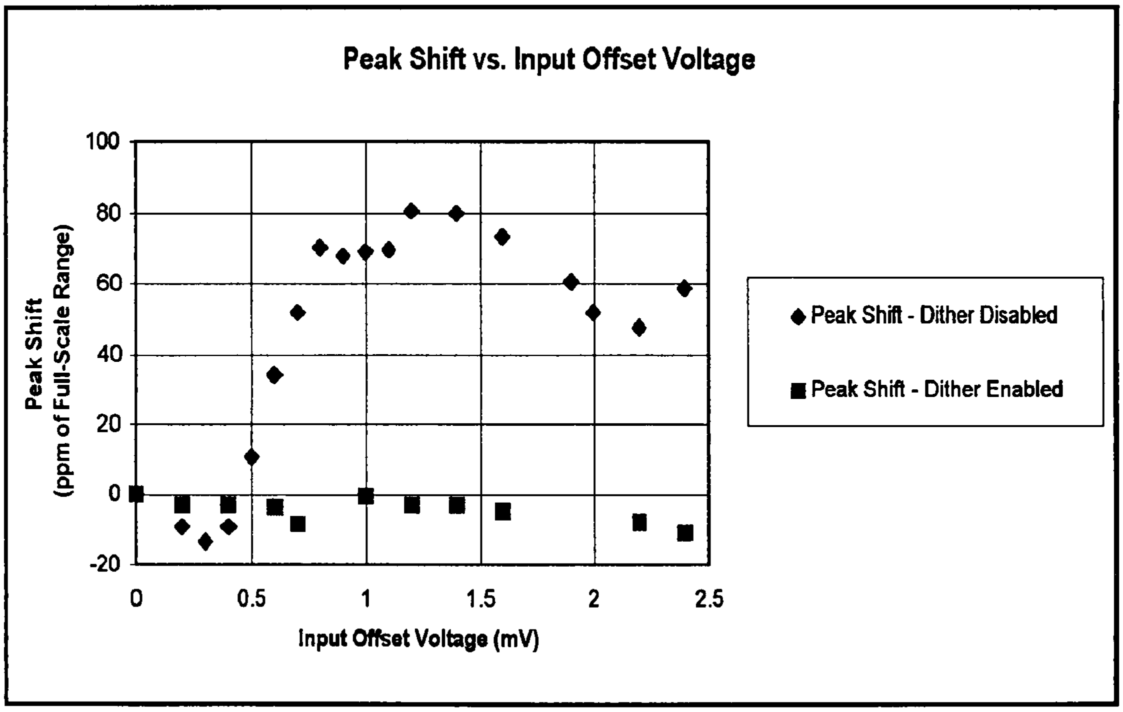

Figure 47. Peak Shift as a Function of Input Offset Voltage with Dither Enabled and Disabled.

peak. With a full-scale range of 16384 channels and the coarse gain set to minimum, the FWHM of the pulser peak was 1.52 channels with the dither signal disabled and 1.62 channels with the dither signal enabled.

Effectiveness of the Gated Baseline Restorer

The best way to measure the effectiveness of a gated baseline restorer is to measure the position of a peak in the spectrum as a function of input counting rate. To test the effectiveness of the digital gated baseline restorer which was implemented in the spectrometer, spectra were collected with a CO-60 source placed at varying distances from the detector to give many different input counting rates using the measurement system shown in Figure 43. The location of the centroid of the 1.3 MeV peak was recorded for each input counting rate. Peak shift was calculated using the 1000 count per second input rate as the reference peak and determining the shift from the 1000 cps spectrum. Table II shows the tabulated data for a number of pulse rise times. Table III shows a similar table for a standard spectrometer (Figure 44) with an analog filter. These measurements were made with a 10% n-type detector with a transistor reset preamplifier installed on it. Comparing the data in the two tables it is useful to refer back to Table I to determine which τ_1 setting in the digital system most closely matches the shaping time setting in the analog system. For example, since the τ_1=4.8 μs setting has a maximum throughput of 21600 counts per second, it should be compared with the 2 μs setting on the analog system which has a maximum throughput of 21000 counts per second. Making that comparison in Tables

Table II. Peak Shift Versus Counting Rate with Digital Filter.

Peak Shift in keV (Digital System)								
Rise Time τ_1 (μs)	Input Rate							
	5k	10k	20k	50k	75k	100k	125k	150k
0.8	0.03	0.03	0.04	0.04	0.03	0.05	0.08	0.10
1.6	0.01	0.01	0.01	0.01	0.00	0.07	0.09	0.10
2.4	0.01	0.00	0.00	-0.02	0.03	0.07	0.07	0.07
3.2	-0.02	-0.01	-0.01	-0.01	0.02	0.03	0.04	0.05
4.0	0.00	0.00	0.00	0.02	0.03	0.04	0.04	0.02
4.8	-0.01	-0.01	-0.01	0.02	0.03	0.03	0.01	-0.02
6.4	-0.01	0.00	-0.01	0.03	0.04	0.03	0.00	-0.07
8.0	-0.01	-0.01	-0.01	0.02	0.01	-0.05	-0.20	-0.44
10.4	0.00	0.00	0.00	0.03	0.01			
12.0	0.01	0.00	0.01	0.03	-0.01			
12.8	0.01	0.01	0.02	0.02	-0.02			
16.0	-0.01	-0.02	0.00	-0.01	-0.11			
20.0	0.00	0.00	0.01	-0.06	-0.24			
24.8	0.00	0.01	0.01	-0.10	-0.39			

Table III. Peak Shift Versus Input Counting Rate for Analog System.

Peak Shift in keV (analog system)								
Shaping Time (μs)	Input Rate							
	5k	10k	20k	50k	75k	100k	125k	150k
0.5	-0.12	-0.17	-0.24	-0.31	-0.3	-0.33	-0.27	-0.11
1	-0.08	-0.09	-0.09	-0.08	-0.05	-0.04	-0.03	0.03
2	-0.04	-0.02	-0.05	-0.06	-0.07	-0.08	-0.10	-0.29
3	-0.04	-0.04	-0.06	-0.08	-0.09			
6	-0.02	-0.03	-0.06	-0.16	-0.63			

II and III, at 150,000 counts per second, the digital system has a shift of -0.02 keV while the analog system had a shift of -0.29 keV.

Chapter V

Summary

In a high-purity germanium detector spectrometer, the preferred filter is a function of the size of the detector, the strength of the radioactive source and the desired resolution. The programmable nature of a digital filter in a spectrometer provides for many filter shapes in a single instrument thereby making a single instrument useful in a broad class of applications.

In this dissertation a new quasi-cusp pulse shape was introduced which permits all of the variability in pulse shape that most users require when using an HPGe detector. The digital implementation has 32 different rise time settings to appropriately handle a wide range of input counting rates. In addition, 4 different flattop width settings are available to allow output pulses to be tuned to eliminate charge collection errors (ballistic deficit) which occur at short pulse widths. The cusp adjustment in the filter, which is unique to this work, permits the shape of the leading and trailing edges of the pulse to be modified to best match the noise characteristics of a particular detector. Inclusion of the cusp adjustment results in optimum output noise at short pulse widths, and output noise which is theoretically within 3.4% of the noise attainable with the optimum cusp filter at long pulse width settings.

In order to process input pulses at high rates, a pole-zero network is used to shape the spectrometer input signal before quantization. This shaping network increases the throughput capability of the spectrometer at the expense of quantization noise. This work introduces a technique for evaluating this tradeoff.

For an HPGe spectrometer to be useful for a wide variety of counting rates, the location of the peaks in the spectrum must be stable with changing counting rates. To achieve this goal, a digital version of the classical analog gated baseline restorer was included in the spectrometer. The restorer, introduced in this design, required very few resources and was superior to the equivalent analog system as indicated by the peak shift versus counting rate data which was shown in Table II and Table III. The time constant of the restorer can also be easily changed by changing a single constant in a register, making possible a real-time automatic adjustment of the time constant to best match the current input signal characteristics.

This work represents one of the first fully implemented and commercially available HPGe spectrometers which employs a digital filter for pulse shaping. By moving the spectrometer filter from the analog to the digital realm, spectrometer designers can take advantage of all of the new developments occuring with high-speed sampling ADCs, digital signal processors, and programmable logic. Furthermore, users can expect spectrometers which result in better resolution, higher throughput, and better stability.

References

References

1. D. A. Landis et al., IEEE Trans. on Nucl. Sci., NS-29, No. 1, February 1982, 619.

2. L. B. Robinson, *Rev. Sci. Instrum.*, Vol. 32, (1961), p. 1057.

3. M. Bertolaccini and C. Bussolati, Nucl. Inst. and Meth. 100 (1972) 349.

4. N. Karlovac and T. V. Blalock, IEEE Trans. on Nucl. Sci. NS-22, February 1975.

5. Cottini, C., E. Gatti, and S. Svelto, "A New Method for Analog to Digital Conversion", Nucl. Instr. and Meth, vol. 24, pp. 241-242, 1963.

6. C. H. Nowlin, "Pulse Shaping for Nuclear Pulse Amplifiers", *IEEE Trans. Nucl. Sci.*, NS-17, No. 1, (1970), pp. 226-241.

7. V. Radeka, "Trapezoidal filtering of signals from large germanium detectors at high rates", *IEEE Trans. Nucl Sci.*, NS-19, Feb. 1972, pp 412-421.

8. F. S. Goulding, "Pulse-Shaping in Low-Noise Amplifiers: A Physical Approach to Noise Analysis", *Nucl. Instr. and Meth.*, Vol. 123, 1972,pp 493-504.

9. F. S. Goulding and D. A. Landis, "Signal Processing for Semiconductor Detectors", *IEEE Trans. on Nuc. Sci.*, NS-29, No. 3, 1982, pp. 1125-1141.

10. B. Sklar, *Digital Communications Fundamentals and Applications,* Prentice Hall, New Jersey, 1988. p. 499.

11. R. Jenkins, R.W. Gould and D. Gedcke, *Quantitative x-ray spectrometry* (New York: Marcel Dekker, Inc., 1995).

12. F. S. Goulding, D. A. Landis and N. Madden, "GAMMASPHERE - Elimination of Ballistic Deficit by Using A Quasi-Trapezoidal Pulse Shaper", IEEE Nuclear Science Symposium, 1993.

13. H. Koeman, "Principle of Operation and Properties of a Transversal Digital Filter", *Nuc. Inst. and Meth.*, Vol. 123, 1975, pp. 169-180.

14. A. Georgiev and W. Gast, "Digital Pulse Processing in High Resolution, High Throughput Gamma-Ray Spectroscopy", *IEEE Trans on Nucl. Sci*, Vol 40, No. 4, August 1993, pp. 770-779.

15. V. T. Jordanov, G. F. Knoll, *Nucl. Instr. and Meth. in Phys. Res. A*, 345 (1994) pp. 337-345.

16. V. T. Jordonov, Dissertation: "Some Digital Techniques for Real Time Processing of Pulses from Radiation Detectors", University of Michigan 1994.

17. G. Ripamonti, A. Castoldi, E. Gatti. *Nucl. Inst. and Meth. in Phys. Res. A*, 340 (1994) pp. 584-593.

18. G. Ripamonti, D. Santo and C. Samori, "Digital $(DL)^N$ Shaping with Reduced Quantization Error Penalty", Preprint from IEEE Nucl. Sci. Symposium 1994.

19. S. Audet, "High Resolution Energy Dispersive Spectroscopy with High Purity Germanium Detectors and Digital Pulse Processing", Preprint from IEEE Nucl. Sci. Symp. 1994.

20. B. Aspacher, A. C. Rester, *Nucl. Instr. and Meth. in Phys. Res. A*, 338 (1994) pp. 516-521.

21. H. Takahashi et. al., "A Multi-parametric Waveform Analysis of GE Detector Signal Based on Fast ADC Digitizing Technique", Conference Record for IEEE Nuclear Science Symposium, 1993.

22. R. Aleksan et al., Nucl. Instr. and Meth. A273 (1988) 303-309.

23. E. Cosulich and F. Gatti, Nucl. Instr. and Meth. A321 (1992) 211-215.

24. B. Sklar, *Digital Communications Fundamentals and Applications,* Prentice Hall, New Jersey, 1988.

25. A. Papoulis, *Probability, Random Variables, and Stochastic Processes* (New York: McGraw-Hill Book Company, 1984) pp. 379-381.

26. J. C. Candy and G. C. Temes, "Oversampling Methods for A/D and D/A Conversion," *Oversampling Delta-Sigma Data Converters* (New York: IEEE, Inc., 1992), pp. 1-29.

27. P. Peebles, jr., *Probability, Random Variables, and Random Signal Principles,* McGraw-Hill Inc., New York, 1980. pp. 68-70.

28. C. D. Hodgman, *C.R.C. Standard Mathematical Tables 12 ed.* (Cleveland: The Chemical Rubber Publishing Company, 1959).

29. A. Oppenheim and R. Schafer, *Digital Signal Processing* (New Jersey: Prentice-Hall, Inc., 1975). p. 67.

Appendices

Appendix I. - Comparing Noise Indices

A common figure of merit is the signal-to-noise ratio of a particular filter relative to the signal-to-noise ratio of the ideal cusp. This Appendix describes how to form this ratio.

As indicated in Chapter I, the output noise due to step and delta noise sources can be written as

$$\sigma_o^2 = <N_s^2> \sigma_s^2 + <N_\Delta^2> \sigma_d^2 \tag{53}$$

where $<N_s^2>$ is the step noise index, $<N_\Delta^2>$ is the delta noise index, and σ_s and σ_d are constants for a given detector. In Chapter I, the noise indices for the ideal cusp were found to be

$$<N_s^2> = \tau_c \tag{54}$$

and

$$<N_\Delta^2> = \frac{1}{\tau_c} \tag{55}$$

Substituting these indices into Equation (53) yields

$$(\sigma_o^2)_{cusp} = \tau_c \sigma_s^2 + \frac{\sigma_d^2}{\tau_c} \tag{56}$$

To find the minimum signal-to-noise ratio, the derivative of this equation should be taken with respect to τ_c, the result should be set equal to 0 and the equation should be solved for τ_c. Performing these steps yields

$$\tau_c = \frac{\sigma_d}{\sigma_s} \tag{57}$$

Solving this equation for σ_d results in

$$\sigma_d = \sigma_s \tau_c \tag{58}$$

Substituting back into Equation (56) yields

$$(\sigma_o^2)_{cusp\ \min} = 2\tau_c \sigma_s^2 \tag{59}$$

Now assume that a particular filter is to be compared to the ideal cusp. To make the comparison, the noise of the filter should be divided by the ideal cusp noise. Performing this function results in

$$\frac{\sigma_o^2}{(\sigma_o^2)_{cusp\ \min}} = \frac{<N_s^2>\sigma_s^2 + <N_\Delta^2>\sigma_d^2}{2\tau_c \sigma_s^2} \tag{60}$$

Substituting Equation (58) into this expression yields

$$\frac{\sigma_o^2}{(\sigma_o^2)_{cusp\ \min}} = \frac{<N_s^2>}{2\tau_c} + \frac{<N_\Delta^2>\tau_c}{2} \tag{61}$$

This equation was used to generate the relative noise as a function of input rise time shown in Figure 13.

Appendix II. - Exponential Applied to Uniformly Distributed PDF

During the computation of the percentage of pulses lost due to quantizer saturation, it was necessary to apply an exponential transformation to a uniformly distributed random variable. This Appendix shows this process in detail following the technique shown by Peebles[27].

Assume that x is a uniformally distributed random variable with a probability density function defined as follows:

$$f_x(x)=\frac{1}{T_i}(U(x+T_i)-U(x)) \tag{62}$$

where $U(x)$ is the unit step function. Also assume that any particular value of x is operated on by the transfer function T to form a new random variable y.

$$y_0=T(x_0) \tag{63}$$

In this application, $T(x)$ is defined to be

$$T(x)=Ce^{\frac{x}{\tau}} \tag{64}$$

According to Peebles, if $T(x)$ is monotonically increasing or decreasing as x increases then

$$f_y(y)=f_x[T^{-1}(y)]\frac{dT^{-1}(y)}{dy} \tag{65}$$

Taking the inverse of Equation (64) results in the following:

$$T^{-1}(y)=\tau\cdot\ln\left(\frac{y}{C}\right) \tag{66}$$

Taking the derivative of both sides of the Equation results in:

$$\frac{dT^{-1}(y)}{dy}=\frac{\tau}{y} \tag{67}$$

Substituting into Equation (65) gives

$$f_y(y)=f_x\left[\tau\cdot\ln\left(\frac{y}{C}\right)\right]\frac{\tau}{y} \tag{68}$$

Substituting for f_x results in

$$f_y(y)=\frac{\tau}{y}\frac{1}{T_i}\left[U\left(\tau\cdot\ln\left(\frac{y}{C}\right)+T_i\right)-U\left(\tau\cdot\ln\left(\frac{y}{C}\right)\right)\right] \tag{69}$$

The argument of the second unit step function may be simplified by observing that the argument is always negative if y is less than C and always positive if y is greater than C. The argument of the first unit step function can be simplified in a similar manner, resulting in the desired function,

$$f_y(y)=\frac{\tau}{y}\frac{1}{T_i}\left[U\left(y-Ce^{-\frac{T_1}{\tau}}\right)-U(y-C)\right] \tag{70}$$

Appendix III. - Optimum α

This Appendix shows the calculations for determining the α setting which results in the minimum signal-to-noise ratio. The step and delta noise indices can be used to refer the step and delta noise to the output of the filter as follows:

$$\sigma_o^2 = \langle N_s^2 \rangle \cdot \sigma_s^2 + \langle N_\Delta^2 \rangle \cdot \sigma_d^2 \qquad (71)$$

where σ_0 is the noise at the output of the filter, σ_s is a constant which is proportional to the step noise and σ_d is a constant which is proportional to the delta noise.

Substituting the noise indices of the Quasi-Cusp filter (Equations (18) and (19)) into Equation (71) results in

$$\sigma_o^2 = \left[\frac{4\alpha^2+3\alpha+1}{(\alpha+1)^2}\frac{\tau_1}{3}+\tau_2\right]\sigma_s^2 + \left[4\frac{\alpha^2+1}{(\alpha+1)^2}\frac{1}{\tau_1}\right]\sigma_d^2 \qquad (72)$$

For each setting of α, an optimum value of τ_1 exists for minimum output noise. This value is found by taking the partial derivative of Equation (72) with respect to τ_1, setting the result equal to 0 and solving for τ_1. The resulting expression is

$$(\tau_1)_{min} = \frac{\sigma_d}{\sigma_s}\sqrt{\frac{12\alpha^2+12}{4\alpha^2+3\alpha+1}} \qquad (73)$$

Likewise for each setting of τ_1, there exists a setting of α which results in minimum output noise. In order to find this value of α, first take the partial derivative of Equation (72) with respect to α,

$$\frac{\partial\sigma_o^2}{\partial\alpha}=\frac{\tau_1}{3}\sigma_s^2\left(\frac{(8\alpha+3)(\alpha+1)^2-2(\alpha-1)(4\alpha^2+3\alpha+1)}{(\alpha+1)^4}\right)+\frac{4}{\tau_1}\sigma_d^2\left(\frac{2\alpha(\alpha+1)^2-2(\alpha+1)(\alpha^2+1)}{(\alpha+1)^4}\right) \tag{74}$$

After setting this equation equal to 0 and simplifying the equation becomes,

$$\frac{\tau_1^2}{24}\frac{\sigma_s^2}{\sigma_d^2}(5\alpha_{min}+1)+\alpha_{min}-1 \tag{75}$$

where α_{min} represents the value of α which results in minimum output noise for a given τ_1. Substituting the optimized value of τ_1, $(\tau_1)_{min}$, into the equation yields

$$13\alpha_{min}^3-\alpha_{min}^2+\alpha_{min}-1=0 \tag{76}$$

The only real root of this equation may be found by employing the equation for locating the roots of a cubic equation[28]. Applying that equation results in $\alpha_{min}=0.3885$.

Appendix IV. - Quasi-Cusp Transfer Function

The Quasi-Cusp filter accepts an exponentially shaped input pulse and transforms the pulse into the Quasi-Cusp which was defined by Equation (17). In order to determine the transfer function of the filter which makes this transformation, the Z transform of both the input exponential and the output Quasi-Cusp must be found. Starting with the exponential, the time domain representation of an exponential pulse is

$$x(t)=e^{-\frac{t}{\tau}}U(t) \tag{77}$$

After sampling the discrete time version of the exponential may be written as

$$x(n)=e^{-n\frac{\tau_s}{\tau}}U(n) \tag{78}$$

where τ_s is the period of the sampling process. Taking the Z-transform of $x(n)$ results in

$$X(Z)=\frac{1}{1-e^{-\frac{\tau_s}{\tau}}Z^{-1}} \tag{79}$$

Next the Z-transform of the desired output pulse shape should be determined. To perform this task, Equation (17) should first be sampled so that it is in the discrete time domain. The sampling process results in

$$
\begin{aligned}
V(n) = {} & \alpha\tau_s n\left(U(n)-U(n-\frac{T_1}{2})\right)+ \\
& \left((\alpha-1)\frac{T_1\tau_s}{2}+n\tau_s\right)\left(U(n-\frac{T_1}{2})-U(n-T_1)\right)+ \\
& (1+\alpha)\frac{T_1\tau_s}{2}(U(n-T_1)-U(n-T_1-T_2))+ \\
& \left((\alpha+3)\frac{T_1\tau_s}{2}+T_2\tau_s-n\tau_s\right)\left(U(n-T_1-T_2)-U(n-\frac{3}{2}T_1-T_2)\right)+ \\
& (\alpha\tau_s(2T_1+T_2)-\alpha n\tau_s)\left(U(n-\frac{3}{2}T_1-T_2)-U(n-2T_1-T_2)\right)
\end{aligned}
\tag{80}
$$

where T_1 is τ_1/τ_s, T_2 is τ_2/τ_s and $U(n)$ is the unit step function. Finding the Z-transform of this expression requires a few basic transforms, the first of which is the transform of the difference of two time-shifted unit step functions[29]. By employing the time-shift property of Z-transforms, this transform is found to be

$$U(n-a)-U(n-b) \iff \frac{Z^{-a}-Z^{-b}}{1-Z^{-1}} \tag{81}$$

The second basic transform required is the transform of

$$n(U(n-a)-U(n-b)) \tag{82}$$

The transform of this expression is found by employing the differentiation property of Z-transforms[29],

$$nx(n) \iff -Z\frac{dX(Z)}{dZ} \tag{83}$$

Substituting Expression (81), into this transform and simplifying it results in

$$n(U(n-a)-U(n-b)) <=> \frac{aZ^{-a}-(a-1)Z^{-a-1}-bZ^{-b}+(b-1)Z^{-b-1}}{(1-Z^{-1})^2} \tag{84}$$

Using these two transforms, the transform of $v(n)$ is

$$\begin{aligned} V(Z)=&\frac{-\alpha\tau_s\frac{T_1}{2}Z^{-\frac{T_1}{2}}+\alpha\tau_s\left(\frac{T_1}{2}-1\right)Z^{-\frac{T_1}{2}-1}+\alpha\tau_s Z^{-1}}{(1-Z^{-1})^2}+\\ &\frac{(\alpha-1)\frac{T_1}{2}\tau_s Z^{-\frac{T_1}{2}}-(\alpha-1)\frac{T_1}{2}\tau_s Z^{-T_1}}{1-Z^{-1}}+\\ &\frac{\frac{T_1}{2}\tau_s Z^{-\frac{T_1}{2}}-(\frac{T_1}{2}-1)\tau_s Z^{-\frac{T_1}{2}-1}-T_1\tau_s Z^{-T_1}+(T_1-1)\tau_s Z^{-T_1-1}}{(1-Z^{-1})^{-2}}+\\ &\frac{(1+\alpha)\frac{T_1}{2}\tau_s Z^{-T_1}-(1+\alpha)\frac{T_1}{2}\tau_s Z^{-T_1-T_2}}{1-Z^{-1}}+\\ &((\alpha+3)\frac{T_1}{2}+T_2)\tau_s\frac{Z^{-T_2-T_1}-Z^{-\frac{3}{2}T_1-T_2}}{1-Z^{-1}}+\\ &\frac{-\tau_s(T_2+T_1)Z^{-T_2-T_1}+\tau_s(T_2+T_1-1)Z^{-T_2-T_1-1}}{(1-Z^{-1})^2}+\\ &\frac{\tau_s(\frac{3}{2}T_1+T_2)Z^{-T_2-\frac{3}{2}T_1}-\tau_s(\frac{3}{2}T_1+T_2-1)Z^{-T_2-\frac{3}{2}T_1-1}}{(1-Z^{-1})^2}+\\ &\alpha\tau_s(2T_1+T_2)\frac{Z^{-\frac{3}{2}T_1-T_2}-Z^{-T_2-2T_1}}{1-Z^{-1}}+\\ &\frac{-\alpha\tau_s(\frac{3}{2}T_1+T_2)Z^{-\frac{3}{2}T_1-T_2}+\alpha\tau_s(\frac{3}{2}T_1+T_2-1)Z^{-\frac{3}{2}T_1-T_2-1}}{(1-Z^{-1})^2}+\\ &\frac{\alpha\tau_s(2T_1+T_2)Z^{-T_2-2T_1}-\alpha\tau_s(2T_1+T_2-1)Z^{-T_2-2T_1-1}}{(1-Z^{-1})^2} \end{aligned} \tag{85}$$

Next the expression should be simplified by finding a common denominator and collecting terms. After simplification the expression is

$$V(Z)=\frac{\tau_s}{(1-Z^{-1})^2}\left(\alpha Z^{-1}+(1-\alpha)Z^{-\frac{T_1}{2}-1}-Z^{-T_1-1}-Z^{-T_1-T_2-1}+(1-\alpha)Z^{-\frac{3}{2}T_1-T_2-1}+\alpha Z^{-2T_1-T_2-1}\right) \tag{86}$$

Factoring the numerator gives

$$V(Z)=\frac{\tau_s Z^{-1}(1-Z^{-\frac{T_1}{2}})}{(1-Z^{-1})^2}\left(\alpha+Z^{-\frac{T_1}{2}}-Z^{-T_1-T_2}-\alpha Z^{-\frac{3}{2}T_1-T_2}\right) \tag{87}$$

Finally, since the transfer function of a filter is equivalent to the Z-transform of the output signal divided by the Z-transform of the input signal, the transfer function of the Quasi-Cusp filter is

$$H(Z)=\frac{V(Z)}{X(Z)}=\frac{\tau_s Z^{-1}(1-Z^{-\frac{T_1}{2}})}{(1-Z^{-1})^2}\left(\alpha+Z^{-\frac{T_1}{2}}-Z^{-T_1-T_2}-\alpha Z^{-\frac{3}{2}T_1-T_2}\right)\left(1-e^{-\frac{\tau_s}{\tau}}Z^{-1}\right) \tag{88}$$

The Z^{-1} and the τ_s terms may be omitted from the transfer function because they represent pure delay and gain respectively. In this application, the delay through the filter is of no importance and the gain will be adjustable.

Vita

Russell David Bingham began his formal education in the Knox County, Tennessee Public School System. He graduated from Farragut High School in June, 1981. After graduation, he enrolled in the University of Tennessee, Knoxville in September of 1981. He received the Bachelor of Science Degree in Electrical Engineering in June of 1985. In July of 1985, he began full-time employment with EG&G ORTEC as a Project Engineer. He continued attending the University part-time and received a Master of Science in Electrical and Computer Engineering degree from the University of Tennessee, Knoxville in August of 1989. He continued his schooling working toward the Doctor of Philosophy in Electrical Engineering on a part-time basis and received that degree in December, 1996. He is currently employed as a Senior Design Engineer at EG&G ORTEC in Oak Ridge, Tennessee.